Paolo Tufoni

Temporal variability of physico-chemical and biological parameters acquired in a real-time monitoring station in an inner area of Ria Formosa

Master in Marine and Coastal Sciences

Work performed under the supervision of:

José Manuel Quintela de Brito Jacob

Alexandra Maria Francisco Cravo

UNIVERSIDADE DO ALGARVE

FACULDADE DE CIÊNCIAS E TECNOLOGIA

2020

Temporal variability of physico-chemical and biological parameters acquired in a real-time monitoring station in an inner area of Ria Formosa

Declaração de autoria de trabalho

Declaro ser o autor deste trabalho, que é original e inédito. Autores e trabalhos consultados estão devidamente citados no texto e constam da listagem de referências incluída.

I declare to be the author of this work, which is original and unpublished. Authors and works consulted are duly cited in the text and are included in the list of references.

Paolo Tufoni

Copyright

Resumo

As lagoas costeiras estão entre os ambientes mais produtivos da Terra, fornecendo múltiplos serviços ecossistémicos. No entanto, o aumento da pressão humanas, juntamente com as alterações climáticas, podem aumentar os perigos, resultando em alterações da sua dinâmica. Apesar do aumento do número de estudos de processos físicos, químicos e biológicos em lagoas costeiras, ainda é difícil obter conjuntos de dados de séries temporais longas. Neste trabalho, foi efectuada uma análise do conjunto de dados registados em tempo real ao longo de dois anos, por uma estação de monitorização fixa localizada na costa sul de Portugal, numa zona interior da Ria Formosa, onde a pressão humana é maior. O intervalo de amostragem de alta frequência 15 min) permitiu descrever a variabilidade temporal da temperatura, salinidade, oxigénio dissolvido (concentração e saturação), pH, clorofila *a*, e turbidez, a várias escalas temporais, desde a diurnae a semi-diurna, até à quinzenal e à sazonal. Os resultados da análise espectral revelaram que a variabilidade típica dos parâmetros estudados foi induzida principalmente por forças astronómicas, tais como as constituintes principal lunar semi-diurna M2 e lunisolar sinódica quinzenal MSF, mas também por outros factores relacionados com a configuração do sistema, tais como a constituinte lunar quarto-diurna M4 e o componente diurna associada aos efeitos da radiação solar. Além disso, os dados adquiridos permitiram a identificar processos marinhos, e eventos episódicos, desde o desenvolvimento de fitoplâncton, a ocorrências de mesoscala, tais como tempestades, afloramento costeiro e contracorrente costeira. Utilizando uma correlação cruzada entre os dados de vento de hora em hora e as séries temporais de temperatura quase em tempo real, foi possível identificar a alternância entre eventos de afloramento e de contracorrente, ambos suportados pela análise de imagens de satélite. Estes eventos de mesoscala tiveram um impacto importante nos parâmetros da água da Ria Formosa, o que reflectiu a influência das trocas de água através do sistema de múltiplas barras. A estação de monitorização fixa revelou ser uma equipamento eficaz em termos de variação da qualidade da água, permitindo ter uma imagem mais abrangente dos processos e eventos que ocorrem na área da Ria Formosa e que pode representar uma ferramenta muito útil numa perspectiva de gestão ambiental.

Palavras-chave: Lagoa costeira, Ria Formosa, propriedades físicas e biogeoquímicas da água, monitorização em tempo real

Abstract

Coastal lagoons are among the most productive environments on Earth, providing multiple ecosystem services. However, the increase of human pressures, together with climate changes, may increase the hazards resulting in changes of their dynamics. Despite growing of number of studies in physical, chemical, and biological processes in coastal lagoons, long term temporal data sets are still difficult to obtain. In this work analysis of data set recorded in a real-time mode along two years was performed, by a fixed monitoring station located in the south coast of Portugal, in an inner area of Ria Formosa, a sector more influenced by pressures from the surround populations. The high frequency sampling interval permitted to describe the temporal variability of temperature, salinity, dissolved oxygen (concentration and saturation), pH, chlorophyll *a*, and turbidity, at several temporal scales, from diurnal and semidiurnal, to fortnightly (spring tide vs neap tide) and seasonal. The spectral analysis's results revealed that the typical variability of the studied parameters was induced principally by astronomical forces, such as the principal lunar semidiurnal constituent M2, the lunisolar synodic fortnightly constituent MSF, and to other factors related with the system configuration such as the shallow water overtides of principal lunar constituent M4 and the radiational tidal constituent associated with solar radiation effects. Moreover, the data acquired allowed to capture marine processes and episodic events, from phytoplankton growth to mesoscale occurrences, such as storm, coastal upwelling, and countercurrents. Using a cross-correlation between hourly wind data and almost real-time temperature timeseries, it was possible to identify the alternation between upwelling and countercurrent events, both supported by the satellite images analysis. Those mesoscale events had an important impact on Ria Formosa water parameters which reflected the influence of the water exchanges through the multi-inlets system. The fixed monitoring station revealed to be an effective tool in terms of water quality control, enabling to have a more comprehensive picture of the processes and events occuring in the area of Ria Formosa resulting a very useful tool from an environmental management perspective.

Key words: Coastal lagoon, Ria Formosa, physical-and biogeochemical properties of water, Real-time monitoring.

Table of Contents

List of Figures

List of the Tables

1. Introduction

1.1 Importance of coastal lagoon ecosystems

Coastal lagoons are areas of relatively shallow water that have been partly or wholly sealed off from the sea by the formation of coastal sand spits built up above high tide level by wave action (Bird, 1994; Flemming, 2012). These ecosystems occur from micro- to mesotidal coasts (tidal ranges of ~ 0.3–3.5 m), and often showed in macrotidal coast as well (Figure 1.1; from Flemming, 2012). Coastal lagoons and other types of barred coasts are not evenly distributed along the shores of the world (Figure 1.1), the vast majority being associated with low-lying coastal plains (~72%) and river deltas (~28%) (Pilkey, 2003). Moreover, they can occour in the context of global tectonics, 49% of barrier islands are located along trailing-edge coasts, 24% along collision coasts, and 27% along marginal sea coasts (Glaeser, 1978). Furthermore, of those located along trailing-edge coasts, 75% occur along amero-trailing-edge, 19% along afro-trailing-edge, and only 6% along neotrailing-edge coasts (Glaeser, 1978). Coastal lagoons represent about 13% of the world's coastline, and depend considerably upon the link between the terrestrial interface and adjacent coastal waters (Barnes, 1980). The degree of connectivity with the adjacent sea and the intensity of the physical-chemical gradients are fundamental to the functioning of coastal lagoons (Pérez-Ruzafa *et al.*, 2019). In particuar, the connection with the ocean is the most important factor governing the structure and functioning of the resident biotic communities (Smakhtin, 2004). Based on the number of entrance channels (inlets) and, thus, on the degree of water exchange with the adjacent ocean, coastal lagoons are subdivided into (a) choked, (b) restricted, (c) leaky (Kjerve, 1994) and (d) open (Bird, 1994). Coastal lagoons, are naturally stressed ecosystems with frequent environmental disturbances and fluctuactions, and they are considered as physically controlled systems (Barnes, 1980). These ecosystems are important both from the ecological and economic point of view, providing valuable ecosystem services (Newton *et al*., 2013*)*, such as offering ecologically important habitats for fish, shellfish, birds, and supporting diverse human activities (e.g. marine transportation, fishing, tourism, and repository waters for domestic wastewater), providing economic resilience to coastal communities (food security and nutrition, Ryabinin *et al.*, 2019) and protecting them from natural hazards (Rodrigues *et al*., 2017). In Europe, coastal lagoons are particurarly abundant along the coastlines (about 5 %; Barnes, 1980), and cover a wide geographical distribution from the Baltic to the Black Sea (Newton *et al*., 2013). The most

important and studied coastal lagoons in Europe, due to their ecological and economic importance, and, simultaneously, due to their very distinct physical-chemical and morphological characteristics (Newton *et al*., 2013; Rodrigues *et al*., 2017) are: the extensive intertidal areas from the German and Danish Wadden Sea (southern part of the North Sea; Bird, 1994), the Venice lagoon in Italy located on the north Adriatic Sea, Etang de Thau in France and Mar Menor in Spain in the Mediterranean Sea, as many others located along the Atlantic coast of the Iberian peninsula such as Rias Galegas, in Spain and Ria de Aveiro and Ria Formosa in Portugal. Many similarities exist among these coastal lagoons, however there are also the peculiarities exhibited by each system, since they are subjected to different environmental conditions and pressures. These site specific differences are mostly depending, on the the tidal regimes, on the climate, on the presence or absence of some components of the ecosystem, such as the fresh water input, and on different human induced stressor (Newton *et al*., 2013).

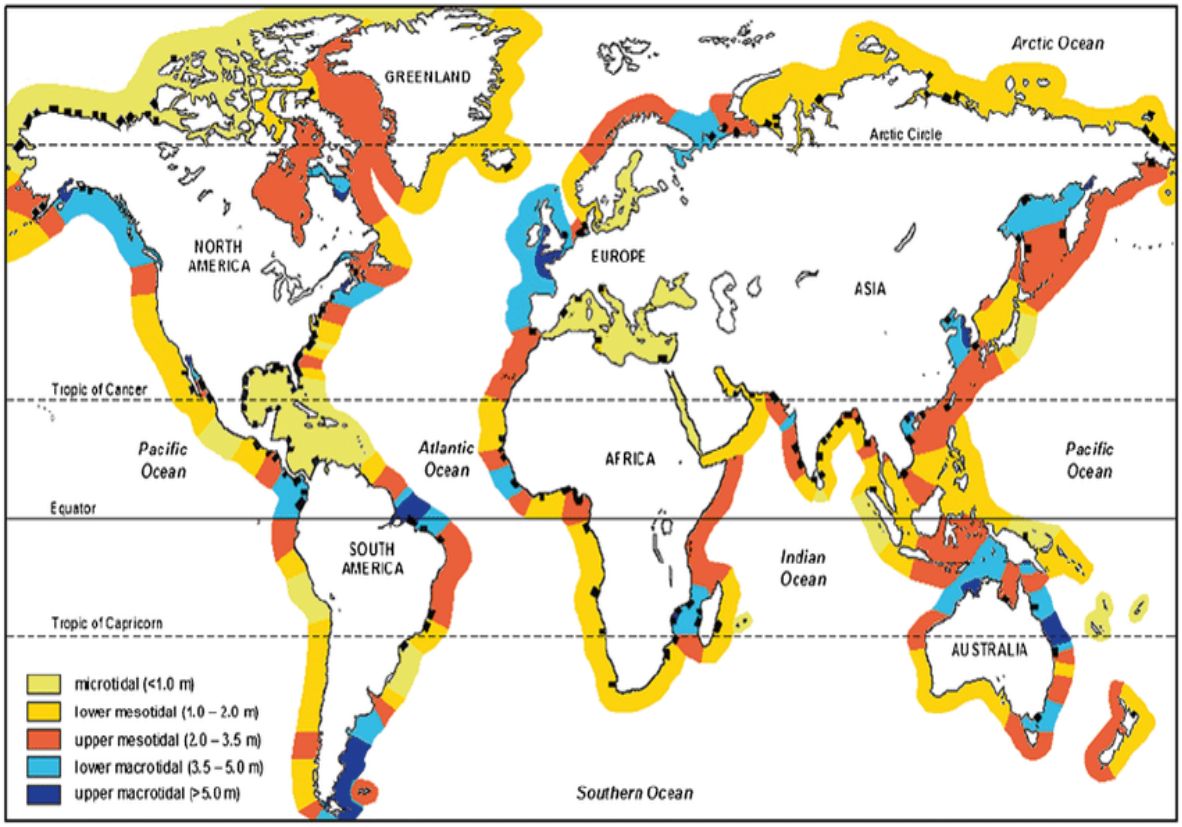

Figure 1.1: Global distribution of coastal barriers backed by tidal flats and/or lagoons (Black square) in relation to tidal regime (from Flemming, 2012).

1.2 Susceptibility and threatens of coastal lagoons associated to climate change

Climate change is impacting the marine ecosystems worldwide, and coastal lagoons are considered to be one of the most fragile marine environments in the face of this threat. Their setting within the coastal environments leave the lagoon especially vulnerable to profound physical and ecological changes (Lloret *et al.,* 2008). Anthony *et al.,* (2009) reported that profound changes are expected in biogeochemical parameters due to climate change, affecting all the ecological and economic services provided by these coastal environments. Moreover, the effects on the ocean waters related to climate change, are amplified in enclosed basins as coastal lagoons (Bird, 1994), which means that the scale of the changes may vary regionally, which will also affect the biogeochemical processes at different magnitude (Raven, 2005). From the increase in water temperature, decrease in dissolved oxygen (DO), increase of CO_2 dissolution and pH decrease leading to acidification issues, increase in appearance of turbid water due to frequent of extreme weather conditions, to the risk of inundation due to sea level rise, the changes in flushing regime and freshwater inputs make climate changes a major concern for coastal oceanographers (Lloret *et al.,* 2008).

1.2.1 Global Warming

The Intergovernmental Panel on Climate Change reported that, as a consequence of Global Warming, the temperature of the world's oceans has increased, and is likely to continue to increase through the next century (IPCC, 2014). Moreover, is stated that, an increase in air temperature of 2-3 ºC could result in the loss of 30% of the coastal lagoon globally due to sea level increase, and millions of coastal inhabitants would be threatened by flooding due to over-wash events (IPCC, 2014). If water temperature and sea level will continue to increase, the worldwide lagoons will be inundated by the seawater, provoking changes in salinity, coastal water circulation (Anthony *et al*., 2009), in the photosynthetic potential and in the primary production, as well as in the concentration of dissolved oxygen and nutrients that will be reduced. Moreover, the physiology of lagoon organisms, species' ranges, and patterns of migration will be affected. In fact, many marine species, live near their threshold of thermal tolerance, at which even small changes in their environments can have large impacts on their existence (Lloret *et al*., 2008).

1.2.2 Reduction in dissolved oxygen (DO)

Recent measurements and model studies have identified a decreasing trend in the concentration of DO in the ocean over the last several decades, driving to the widespread occurrence of reduced dissolved oxygen events (< 2 mg /L O_2, Vaquer-Sunyer and Duarte, 2008). Dissolved oxygen is a key water parameter, severely controlled by temperature changes and by a range of biogeochemical processes. DO is produced in the oceanic surface layer by primary production and is removed in subsurface waters by the respiration of sinking organic matter. Due to global warming, water temperature is expected to increase which would decrease the solubility of dissolved oxygen with the combined effect of water stratification. This would further increase the oxygen demand by respiration of the marine organisms. High rates of respiration cause widespread and recurrent episodes of reduced concentration in DO leading to fish death and system deterioration (D' Avanzo and Kremer, 2004; Vaquer-Sunyer and Duarte, 2008). Reduced dissolved oxygen concentration affects mostly the benthic community, as it leads to important changes in the community structure characterized by a persistent shift in species composition, and an overall decrease in species diversity (Vaquer-Sunyer and Duarte, 2008).

1.2.3 Increase in CO_2 and Ocean Acidification

The oceans are absorbing carbon dioxide (CO_2) from the atmosphere and this is causing chemical changes, making them more acidic (by decreasing the pH of the oceans). Global changes associated with an increase of atmopheric CO_2 will increase their ability to absorb additional CO_2 from the atmosphere, which will affect the rate and scale of global warming. In the past 200 years the oceans have absorbed approximately half of the CO_2 produced by the fossil fuel burning industry production. Calculations based on measurements of the partial pressure of CO_2 on the surface oceans indicate that the uptake of CO_2 has led to a reduction of the pH of surface seawater of 0.1 units, equivalent to a 30% increase in the concentration of hydrogen ions (Raven, 2005). If global emissions of CO_2 from human activities will continue to rise in current trends, the average pH of the oceans could fall by 0.5 units (equivalent to a three fold increase in the concentration of hydrogen ions) by the year 2100 (Raven, 2005). The impacts of ocean acidification on marine organisms and their ecosystems are much less certain but it is likely that, because of their particular physiological attributes, some organisms will be more affected than others, like those having calcium carbonate structures. However, changes

in ocean chemistry, especially rapid modifications such as ocean acidification, could have substantial direct and indirect effects on these organisms and upon the habitats in which they live (Raven, 2005).

1.2.4 Eutrophication and algal blooms

Another consequence of climate change could be the increased nutrients input into coastal areas either from land runoff or upwelling intensification, which could lead to eutrophication processes. Eutrophication processes affect coastal zones through the increase of turbidity due to increased algal bloom events, with the proliferation of floating macroalgae and epiphytes, that could cause oxygen depletion at the sea bottom (Lloret *et al*., 2008). Moreover, harmful algal blooms (HABs), can also proliferate and cause deaths of fishs and contaminate seafood with toxins (Palma *et al.*, 2010, Danchenko *et al* 2019). Alterations of the ecosystem functioning, have been increasing in frequency, magnitude, and duration worldwide due to climate change (Gilbert *et al*., 2014). The quality of coastal waters in many regions of the world has deteriorated in recent years as the human population and activities have increased 50-70% along coastal zones (Pérez-Ruzafa *et al.*, 2019). This increasing pressure may lead to a rise in the discharge of nutrients into coastal systems, which will be aggravated by the expected changes in hydrological regimes, leading to poor water quality, reduced ecosystems health that ultimately will affect all the related social and economic aspects (Newton *et al.*, 2003; Brito *et al.*, 2010).

1.3 The need for monitoring systems

It is essential to have an integration of anthropogenic pressures and the systems' response to the physical and climate drivers, that join sophisticated monitoring networks and advanced modelling systems (Baptista, 2006). The Intergovernmental Oceanographic Commission (IOC) of UNESCO, a specialized organization of the United Nations system for ocean observations, data, service and related capacity development, stress the need for an integrated, interdisciplinary and cross-sectoral approach, as well as enhancing cooperation, coordination and policy coherence, at all levels (Ryabinin *et al.*, 2019). In response to the high variability and impacts on the coastal zones, the assessment of ocean health has reached the status of legal mandate in Europe through the Marine Strategy Framework Directive (*Directive*

2008/56/ECMSFD, 2008) which aims to manage the European seas by using an ecosystem-based approach in order to gain a healthy and productive state (Borja *et al.*, 2013). Without an integrated, coordinated, proactive, cross-sectoral, and science-based approach to coastal and marine management, the resilience of coastal and marine ecosystems and their ability to provide vital services will continue to be reduced (Evans, 2019). The widespread and rapid transformation of coastal lagoon and their services suggest that it is important to assess and to protect these ecosystems. Coastal lagoons are among the most heavily used and threatened natural systems. It is reported that 50% of salt marshes, 35% of mangroves, 30% of coral reefs, and 29% of seagrasses are either lost or degraded worldwide (Babier *et al.*, 2011). This global decrease of coastal lagoons threatens the critical services provided by these ecosystems, specifically coastal protection and coastal freshwater catchment (Babier *et al.*, 2011). The anticipation of the impacts on the coastal zones is mandatory to promote adequate adaptation measures which turns the need for observation imperative. The utilization of ocean observation can provide key information, that can be used and applied to address management and policy, to effectively support the sustainable development of coastal and marine ecosystems (Evans, 2019). Without the knowledge of the current state of the coastal environments, and of the impacts that currently affects these ecosystems, the need for management and the effectiveness of management measures, such as instituting marine protected areas (MPAs), may be missed (Koslow and Couture, 2015).

Developing the knowledge to fill current gaps in ocean observations is an ongoing challenge as reported some years ago by some authors (*e.g.* Tett *et al.*, 2013). Despite the inherent difficulties of achieving real time ocean time series, they are nonetheless essential, given that the oceans are not at equilibrium, but rather continuously varying in response to a poorly understood array of natural and anthropogenic pressures (Koslow and Couture, 2015). The requirement for real-time fixed monitoring stations is clear, given the large number of anthropogenic stressors (Koslow and Couture, 2015). The real time monitoring stations with low sampling intervals (minutes, hours), can capture the details of events not recorded in conventional on-site discrete sampling, which is too limited to adequately address events that occur episodically and/or those that change rapidly, e.g. upwelling, coastal counter-current, hypoxia, water properties associated with biogeochemical cycles. Furthermore, conventional sampling implies a large effort in resources, which is often impractical or cost prohibitive (Cravo *et al*., 2020). This highlights the importance of continuous observations and the need to establish observatories for long term data acquisition. Real time monitoring is being advocated

to advance the knowledge of ecosystem functioning and promising for preservation of water resources (Garel *et al*., 2009). In recent years, several real-time monitoring systems have been developed worldwide as reported by several authors (e.g. Glasgow *et al.*, 2004; Garel *et al.*, 2009; Zhang *et al*., 2017; Cravo et *al*., 2020). However, long-term continuous monitoring tools with high temporal resolution are still generally rarely deployed in estuaries and coastal lagoon in Europe.

1.4 The UBEST project

In the scope of the UBEST project, an online real time monitoring station was installed for the first time in one of the main channels of Ria Formosa coastal lagoon (Cais do Combustível, Faro Harbor) in order to improve the global understanding of the biogeochemical buffering capacity of Ria Formosa.

The UBEST project aimed to investigate the lagoon susceptibility to future scenarios of anthropogenic inputs and climate change, to effectively support the short and long-term management of this ecosystem.

The monitoring station is equipped with an YSI EXO^2 multiparametric probe (deployed in May 2017 and removed in March 2020), that measured with a high frequency (every 15 min) water temperature, conductivity/salinity, pH, dissolved oxygen (DO), turbidity and chlorophyll *a*. Along with that an OBSERMET OMC-045-III data logger was installed, to transmit in real-time the data acquired (Rodrigues *et al*., 2017).

During this period, 4 seasonal field surveys have been conducted at 7 sites along the Ria Formosa. Previous studies using a conventional sampling approach covering several aspects, from the hydrodynamics to the physical, chemical, biological and geological processes or numerical modelling have been already developed in Ria Formosa (e.g. Vila-Concejo *et al*., 2003; Newton *et al*., 2010; Pacheco *et al*., 2010; Alcântara *et al*., 2012; Fabião *et al*., 2016).

The UBEST project provided the first data set in real time from a deployed monitoring station in Ria Formosa, enabling the real-time monitoring of changes in the biogeochemical parameters, crucial for better understanding the intrinsic variability within Ria Formosa and contribute to its protection (Cravo *et al.*, 2020).

1.5 Objectives of the work

The objectives of the present work are:

-To describe the temporal variability of the physico-chemical-biological parameters in one main channel of Ria Formosa coastal lagoon, at distinct timescales, such as semidiurnal, daily, fortnightly, (spring tide *vs* neap tide) and seasonal.

-To highlight the main environmental factors that explained the variability of the studied parameters, along two successive years (July 2017 to June 2019) of high frequency real time data set.

-To show how real time mode long-term monitoring of water characteristics can play a key role in reinforcing research in coastal water helping to support the management of these ecosystems.

2 Material and methods

2.1 General overview and importance of the study area

Ria Formosa is a leaky costal lagoon, complex and highly dynamic located in the south coast of Portugal on the Atlantic coast, but its climate regime is considered Mediterranean, characterized by dry warm summers and humid and moderate winters (Serpa *et al.*, 2005). In the Ria Formosa, the solar radiation is high with annual mean values ranging between 161 and 165 kcal cm-^{2}. The insolation is also high varying between 3000 and 3200 hours per year (Serpa *et al*., 2005).

The lagoon mean water depth is about 3.5 m, tides are semi-diurnal, and the tidal range varies from 0.5 to 3.5 m (mesotidal) (Alcântara *et al.,* 2012). This lagoon has a triangular shape that extends for 55 km in W-E direction and for 6 km in N-S direction is delimited from the adjacent Atlantic Ocean by five sandy barrier islands and two peninsulas (PH&P, 2000a). The connection with the Atlantic Ocean is established by six inlets: Ancão, Faro-Olhão, Armona, Fuzeta, Tavira and Cacela (Falcão and Vale 1990; Cravo *et al*., 2014; Rosa *et al*., 2019*)*.

Offshore wave climate can be considered moderate to high, with annual mean wave heights of about 1 m and peak periods of 8.2 s (Costa *et al.*, 2001; Pacheco *et al.*, 2010), while inside the Ria Formosa the waves are in the order of centimeters (Carrasco *et al.*, 2009). The prevailing winds, about 68% of the total occurrences, are from west, especially during winter (Ceia, 2009). Moreover, SE winds from the Mediterranean are also frequent, particularly during summer (about 25% of the total occurrences; Relvas and Barton, 2002; Garcia *et al.*, 2006; Ceia, 2009). The coastal area near the Ria Formosa is affected by regular upwelling events, related to westerly winds, or advections from the south-western coast. Upwelling events are frequent from April to October, and relaxation of upwelling is usually associated with the development of a warm coastal countercurrent flowing from the Gulf of Cadiz (Relvas and Barton 2002 Garel *et al*., 2016).

Ria Formosa is divided artificially into five water bodies (WB) (Figure 2.1) within the scope of the Water Framework Directive to attain a Good Ecological Status. These are affected by distinct circulation patterns and human pressures, which influence the water properties (Ferreira *et al*., 2005). Ria Formosa-WB1 (4.7 km^{2} – APA, 2015) corresponds to the Ancão basin and to the western end of the lagoon. Ria Formosa-WB2 (33 km^{2}) corresponds to the innermost part of the Ria Formosa, and where the anthropogenic pressures from the Faro and

Olhão cities may be stronger. Ria Formosa-WB3 (30.8 km^2) is characterized by larger exchanges of water through the Faro-Olhão inlet (the major inlet, artificial built in 1929). Ria Formosa-WB4 (10.7 km^2) comprises the Armona and the Fuzeta inlets and is one of the areas with lower anthropogenic pressures (APA, 2012d). Ria Formosa-WB5 (8.8 km^2) corresponds to the area bordered by Tavira and is characterized by lower salinities, justified by the presence of a semi-permanent freshwater source, the Gilão River (Newton and Mudge, 2005) and also include the eastern end of Ria Formosa until Cacela. The coastal water bodies surrounding the Ria Formosa lagoon represent the water bodies CWB.I.6 and CWB.II.7 (APA, 2015). Ria Formosa with high ecological and environmental value, has a large wet area in which one third corresponds to saltmarshes and it is used for spawning and nursery by many species of fish, crustaceans, and bivalves (Falcão and Vale, 1990). This coastal lagoon is recognized as a Natural Park since 1987 (about 18400 ha; Comissão de Coordenação e Desenvolvimento Regional do Algarve CCDRA, 2003) and internationally as a Ramsar site (7PT002, 16000 ha; CCDRA, 2003), being part of the Natura 2000 Network, included in the list of Special Protection Areas (SPAs, PTZPE0017, 23270 ha). Others valuable goods and services are provided by this coastal lagoon, from the social and economic perspectives such as: tourism, fisheries, aquaculture, industrial development, ports and marinas, sand and salt extraction (about 50% of the national salt production), and coastal engineering as artificial inlets (Falcão and Vale, 2003; Newton *et al*., 2003; Duarte *et al*., 2007; Jacob *et al*., 2014).

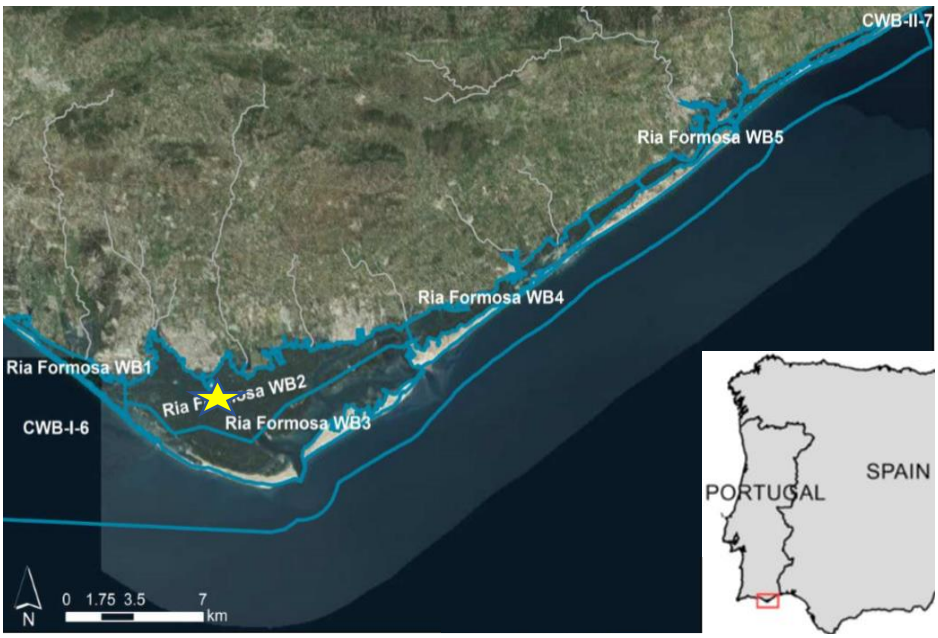

Figure 2.1: Ria Formosa Water Bodies (the star represents the location of the study area) (adapted from Ferreira *et al*., 2005).

2.2 Hydrodynamics

The hydrodynamic knowledge and characterization of the water circulation inside the lagoon and the exchange with the coastal through the multi-inlets system of Ria Formosa are crucial to understand the variability of the physico-chemical properties of the water. This lagoon, can be divided into three different hydrodynamic sectors (Salles *et al.*, 2005): (a) the eastern sector, that includes only the Cacela inlet; (b) the central sector consisting of the Fuzeta and Tavira inlets; and (c) the western sector with the Ancão, Faro-Olhão and Armona inlets. The inlets of the western sector of Ria Formosa show a high hydrodynamic interconnectivity representing 90% of the total tidal prism in the lagoon and the main contribution for the water renewal and water circulation (Salles *et al.*, 2005; Pacheco, *et al.*, 2010). The oceanic conditions propagate into Ria Formosa mainly with the tide, which is the main factor that control the hydrodynamic inside the system (Salles *et al.*, 2005; Dias *et al.* 2009; Jacob and Cravo, 2019). Moreover, the hydrodynamic is influenced additionally by the wind and the atmospheric pressure which combination of these environmental factors produces important changes in the hydrodynamic of this system, at different temporal and space scales (Jacob *et al.*, 2014; Fabião *et al.*, 2016). Dias *et al.* (2009) investigated the tidal propagation inside Ria Formosa, reporting the predominance of astronomical forces such as the principal lunar semidiurnal constituent M2, and the lunar diurnal constituent K1. Other important constituents reported are the Lunisolar synodic fortnightly constituent MSF, and the shallow water overtides of principal lunar constituent M4 and M6. The shallow water over-tides are higher inside the lagoon than in the inlets zone, suggesting a high tidal distortion in the interior area (Dias *et al.*, 2009). Along a MSF period caused by the various combinations of lunar (M2) and solar semidiurnal (S2) tides, the tidal currents are stronger in spring tide decreasing the residence time of the water, while in neap tide the currents are weaker and the residence time increases (Dias *et al.*, 2009). In general, the maximum values for the tidal current velocities at the main inlets are around 2 m/s, higher when compared to the channels, where they are $\leq$ 0.8 m/s (Valença *et al.*, 2011; Cravo *et al.*, 2014; Fabião *et al.*, 2016) demonstrating that the tidal velocity decreases towards the inner zones of the lagoon (Dias *et al.*, 2009; Brito *et al.*, 2010). The circulation of the water inside Ria Formosa depends also on morphological factors, such as the morphology and cross-sectional area of the channels and the bathymetry (Pacheco *et al.*, 2010; Jacob *et al.*, 2013, 2014). Changes in any of these factors can globally modify the hydrodynamic regime in the lagoon, affecting directly the physico-chemical parameters in the system and, consequently, the biogeochemical processes (Fabião *et al.*, 2016).

2.3 Location of study area and deployment of the multiparametric probe

The monitoring station was installed on May 2017 and maintained until March 2020 by the National Laboratory of Civil Engineer (LNEC) and the University of Algarve, within the scope of the project UBEST-"Understanding the biogeochemical buffering capacity of estuaries relative to climate change and anthropogenic inputs" (PTDC/AAG MAA/6899/2014). The water quality monitoring station was located in the Ria Formosa in the Cais do Combustível of the Port of Faro (37º00'9.92'' N, 7º55'16.28'' W) (Figure 2.2), which is an old and disabled fuel dock under the administration of the APS-Ports of Sines and the Algarve Authority.

Figure 2.2: Location of the monitoring station at the Cais do Combustível (Port of Faro) indicated by the yellow star (37º00'9.92'' N, 7º55'16.28'' W).

The Port of Faro is in the Faro channel on the western sector of Ria Formosa encompassed by Ria Formosa-WB2 (where the hydrodynamic conditions are less intense, in a sector more influenced by anthropogenic pressures from the Faro and Olhão populations). The selection of the monitoring station took also into consideration other criteria, such as the access to essential infrastructures (e.g. GSM/GPRS connectivity), the ability to obtain permission to install the equipment and the protection from vandalism (Rodrigues *et al*., 2017).

2.3.1 Multiparametric Probe Equipment

The water quality online monitoring station was equipped with an YSI EXO^2 multiparameter probe (Figure 2.3). The multiparameter probe was in operation from May 26, 2017 to March 12, 2020, while the online data transmission system started on June 29, 2017. This probe

includes sensors to measure water temperature (ºC), conductivity (µS/cm)/salinity, dissolved oxygen (DO) (mg/L and O_2 %), turbidity (NTU), chlorophyll *a* (Chl *a*) (µg/L) and pH. It has a diameter of 7.62 cm, a length of 71.10 cm, and weight about 3.60 kg. The probe is also equipped with a copper-alloy sensor guard and an anti-fouling wiper to reduce the biofouling in the sensors, and to protect the data quality. The range, accuracy and resolution of the sensors are reported in Table 2.1. Data were measured continuously at the monitoring station with 15 minutes intervals and were transmitted hourly through the internet, from the remote site to LNEC's premises, using the FTP protocol, producing a new ***csv*** formatted file encompassing the data sampled/acquired in that period.

Table 2.1: Specifications of the sensors (range and accuracy/resolution) reported by the manufacturer.

Parameter	Range	Accuracy	Resolution
Temperature (ºC)	-5.50	± 0.2	-
Conductivity (µS/cm)	0-100,000	± 1% of reading or 2 (µS/cm)	-
DO (mg/L; %)	0-50; 0-500	For 0-20 mg/L= ±1% of reading or 0.1 mg/L, 20-50 mg/L = ±5% of reading, 0-200%= ±1 % of reading or 1% air saturation, 200-500% = ± 5% of reading	-
pH	0-14	± 0.1 within ± 10 ºC of calibration temperature, ± 0.2 for entire temperature range	-
Chlorophyll *a* (µg/L)	0-400	-	0.01
Turbidity (NTU)	0-4000	For 0-999 = 0.3 or ± 2% of reading, for 1000-4000 = ± 5% of reading	-

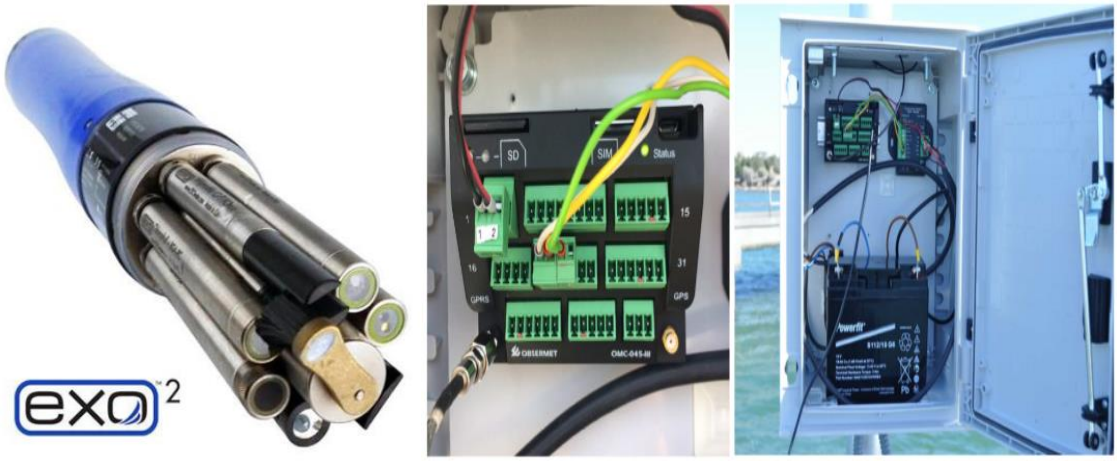

Figure 2.3: left - the multiparametric probe YSI EXO^2 (http: www.ysi.com; www.EXOwater.com); right - OBSERMET OMC-045-III data logger.

Data acquisition and transmission (wireless) was performed using an OBSERMET OMC-045-III data logger (Figure 2.3), which includes a GSM/GPRS modem. The Data transmitted were stored in a data repository developed for the UBEST project, soon accessible in the web platform (http://portal-ubest.lnec.pt/ubest/). This multiparametric probe was supported and protected by a PVC tube, while the data logger was protected by an environmental shelter (Figure 2.3; Figure 2.4). The power supply to the operation of the multiparametric probe and of the data logger was provided by a solar panel. At the beginning (June and July 2017), the turbidity parameter was not installed in the probe.

Figure 2.4: PVC tube for the support and protection of the probe (37º00’9.92 N, 7º55’16.28’W).

2.3.2 Maintenance of the equipment

Maintenance procedures were established and implemented to guarantee the continuous acquisition and the data quality (Rodrigues *et al*., 2017). At the monitoring station, these procedures were performed by the members of the University of Algarve's team with the support of APS-Port of Faro, which provided the access to the place where the probe was installed. Two levels of maintenance procedures were considered: periodic cleaning, verification, visual inspection with manual cleaning of the probe, and calibration of sensors. These procedures were performed with a weekly to fortnightly periodicity during the first two months of the probe's functioning to ensure the quality of the acquired data. After this period, these procedures were performed monthly (Rodrigues *et al*., 2017). For safety reasons at least two technicians were required. Out-of-schedule supplementary procedures for inspecting the probe were undertaken when needed (e.g. lack of communication from the probe, observation of out of the range measurements, after storms and bad weather events). During the first month of operation of the probe five maintenance visits were performed in June 2017. During these visits, the visual inspection of the probes and supporting structures was performed (Rodrigues *et al*., 2017). Measured conductivity, pH and turbidity were verified using several calibration solutions. Conductivity was calibrated against a standard solution (1-point) of 50000 µS/cm, pH by 2 different standard solutions (2-point calibration: pH 7, 10) and turbidity by 2 standard solutions (2-point calibration): distilled water (0 NTU) and 12.7 NTU. Dissolved oxygen was calibrated at 100% air saturation each visit (1-point calibration) and checked sometimes with the Winkler methods. Chlorophyll *a* was calibrated during the first day of deployment, at 1-point (0 µg/L) based on distilled water, while on the June 23, 2017 a 2-point calibration was performed using distilled water (0 µg/L) and the results of a laboratory analysis of a water sample collected *in situ*. As expected, the results of calibrations suggested a good performance of the sensors (Rodrigues *et al*., 2017). After each maintenance, the optical sensors which measure turbidity and Chl *a* data usually showed little variation in the values (< 0.1), and adjustments of these time series were needed to avoid this error. The time series acquired by the multiparametric probe contains some gaps due to several reasons. A long gap period without pH data was identified, from 05/09/2018 to the 1/06/2019. Moreover, two shorter periods of data lost are present in the records: i) one month for all parameters, from 13/11/2018 to 15/12/2018, due to lacks of recording data on the probe memory and communication with the data logger; and ii) three months of salinity data, from 09/02/2019 to 15/05/2019, due to

conductivity sensor malfunctioning, which also affected the calculation of DO saturation percentage.

2.4 Data Analysis

2.4.1 Data processing

Water temperature, salinity, DO, pH, chlorophyll *a* and turbidity data acquired every 15 min, for 2 years between July 2017 and June 2019, represent almost 67000 observations, which reflect both short to long term temporal scales (from hourly to anual) of processes occurring in the study area. All the analysis were conducted using MATLAB.

With the help of the graphical representation, unrealistic values mainly in the chlorophyll *a* and turbidity time series, were identified and removed. These values were for both parameters, lower than 0 (µg/L or NTU), and above 10 (µg/L or NTU). Moreover, the missing values (e.g. three missed values on the salinity data and four in DO sat), were filled with interpolated values using linear interpolation.

Basic statistical analysis, such as the individual of maximum, minimum, median, and 10% and 90% percentiles were applied on the time series of the studied parameters. In order to analyze and characterize carefully the temporal variability of the studied parameters, the statistical analysis were performed on the raw-data for temperature, salinity, DO, pH, while for chlorophyll *a* and turbidity, the analysis were performed after removing the unrealistic values.

After these preprocessing step, the record mean and trend were identified and removed from each time series for filtering, spectral analysis and cross-correlation computation purposes. The trend was identified through a linear regression curve fitting to the time series and then removed in order to avoid the distortion of the low-frequency components which could consequently compromise the quality of the analysis results.

In addition, for the sake of improving visualization in graphical presentation, the high frequencies events were removed from the original time series using a 6^{th}-order low-pass Butterworth filter. The cut-off frequency used was 0.25 cycle per day (cpd). In general, a good filter should be able to effectively remove all unwanted frequency signals leaving the remaining frequency components unchanged and not changing the phase. The Butterworth filter produces

zero phase shift and its amplitude is attenuated by a factor of two at the cut-off frequency (Emery and Thomson, 2001).

2.4.2 Spectral Analysis

The identification and interpretation of the periodic components of a time series are crucial to understand the dynamics of the underlying oceanographic mechanism. Spectral analysis is a frequency domain statistical method enabled to find the "hidden" signals buried in the measurements noise distinguishing between typical/non-typical behavior of the studied parameters, and to identify the constituents that can be considered as deterministic for the study. A complete description of the system includes a list of dominant cycles at precise frequency and an estimation of their relative importance or magnitude. Different methods exist to determine the spectral density function from a timeseries, but in general the Fast Fourier Transform (FFT) is the most used. Joseph Fourier (in the 1800's) demonstrated that almost any function can be represented as a linear combination of an infinite number of harmonic oscillations. A natural time series can be defined as well as a linear combination of periodic or quasi-periodic components that are superimposed on a long-term trend and random high-frequency noise (Emery and Thomson, 2001). The basic assumption in spectral analysis is that the time series can be considered to be a sum of sines and cosines with all frequencies. The spectral analysis is widely used in the analysis of noise-like signals because it provides a frequency decomposition in harmonics, which can be studied separately (Emery and Thomson, 2001).

Spectral analysis is very useful for determining, for instance, tidal components in a time series of sea surface height, or deciding if variations are seasonal or interannual. The frequency (f) of these oscillations is typically expressed in terms of the number of cycles per unit time, and their contributions on the variance are reported in terms of energy per unit time and are represented in the periodogram (Emery and Thomson, 2001). Moreover, periodic influences in consequence to the approximately regular cycles in the weather are detectable in the periodogram (Zaytsev and Cervantes-Duarte, 2018) such as the solar annual and the solar diurnal cycles, usually found in region where the diurnal heating cycle is strong. The physic of the solar components or radiational tides is related more directly to the solar radiation while their gravitational input is weak (Pugh, 1987).

The periodogram enables to pinpoint the peak of those frequencies that are important for the characterization of the time series making possible to determine the dominant patterns of variation and their driving agents. For this reason, the time series should span at least a few repeated cycles of the time scale of interest (Emery and Thomson, 2001), since long term measurements has more properties representative of the time series, providing greater resolution, and making possible to identify a greater number of constituents which may be independently determined (Aubrey and Speer, 1985). However, in choosing the time/space sampling interval it is important to have some idea of the inherent time/space scale of the process under investigation.

The existence of trends in a time series must be assessed before spectral analysis. If the trend is not removed, the results are likely to be dominated by this variation making any other effects difficult or impossible to observe (Goela *et al*., 2016). Moreover, regarding the slope of the spectra showed in the periodogram, it might indicate the effect of turbulent processes or not, depending on the angle of the slope, as suggested by Platt (1972).

In result of some gaps in the time series of pH, salinity, and DO (%), it was decided to analyze a shorten period than the original one. Anyway, for the purpose of spectral analysis, this choice did not compromise the results of these parameters, since when more than one year of measurements are recorded with extreme high frequency, allowing to distinguish the principal constituents that caused variation in the studied parameters from the meteorologically forced background noise.

2.4.3 Correlation between variables

Time series have several fundamental statistical properties that help to characterize the temporal variability of the series and make it easier to compare one timeseries against another. Perhaps the easiest way to present the correlation between timeseries is in the form of a scatter plot where the dots represent individual XY pairs. A scatterplot is a type of data display that shows the relationship between two numerical variables. Each member of the dataset gets plotted as a point whose coordinates relates to its values for the two variables. The scatterplots contain a linear regression curve fitting, which is a straight line drawn through the centre of the data points that best represents the trend of the data. The correlations have properties depending on the sign and strength. Regarding the sign, it could be positive, meaning that the variables

move in the same direction, and as one variable increases/decreases the other variable also increases/decreases, while the relation is negative when the variables move in opposite directions and as one variable increases/decreases, the other variable decreases/increases. The strength of a correlation indicates how strong the relationship between the two variables is. The strength is determined by r, the numerical value of the correlation (coefficient of correlation). A correlation of |1|, whether it is +1 or -1, is a perfect correlation, while 0 mean no correlation (Emery and Thomson, 2001). The relationships between variables were explored using the Pearson correlation coefficient at a significant level of 95%. The significance of the coefficient of correlation is dependent on the degrees of freedom (number of observations - 2).

The cross-covariance function is used to describe the covariability of two given time series, that may have different lenght but the same time duration. The variability of two random variables is computed as the averaged sum of the cross product of the variations from the respective means of the two variables (Emery and Thomson, 2001). The cross-covariance is useful in aligning two time series, delaying one in respect to the other, as its peak (maximum or minimum in the graphical representation) occurs at the lag at which the two time series are best correlated (Emery and Thomson, 2001). The practical importance of cross-covariance function is that it can compare maximum values and identify the time lag that vary between zero and half of the total time and it can be positive and negative between two timeseries (Chatfield, 2004). There are many situations where several variables are simultaneously recorded that exhibit dependence, such as the wind field and temperature.

Therefore, a cross-correlation was used, as several authors before, to examine and measure the relationship between the upwelling events, based on the alongshore (y-direction) component of coastal wind velocity, and the sea surface temperature (SST) (e.g. Benazzouz *et al*., 2014; Gonzalez-Nuevo *et al*., 2014, Goela *et al*., 2016). The wind component along the coast since, following the Ekman's theory, its the responsible for the existence of coastal divergence or convergence. According to this theory, there will be divergence at the southern coast of Portugal (W-E oriented coastline) if the wind stress acting on the sea surface is oriented eastwards (e.g upwelling), and convergence (e.g. downwelling) if the stress is westwards. Another important indication for upwelling is, the difference between the nearshore sea surface temperature which is colder than the one observed offshore, while it get warmer during coastal convergence associated with the instauration of the countercurrent flow (Relvas and Barton 2002; Garel *et al*., 2016).

In addition, to visualize and analyse the wind time series, the "stick plot" was used, where each stick (vector) corresponds to a measured wind speed and wind direction at the specified time (Emery and Thomson, 2001). To simplify the identification of upwelling and countercurrent along the period of study, the wind stick plot was divided by year, 2017/2018 and 2018/2019. To allow the identification of these events, high frequency signals, such as semidiurnal and diurnal, the wind (west-east components) and temperature timeseries were filtered with a Butterworth filter, using a cut off frequency of 36 hours.

Moreover, before the wind stick plot and cross covariance function analysis, as said before, the mean and trend were removed to avoid errors in the results. Hourly meteorological data from Faro airport meteorological station, including winds (intensity and direction), were provided by IPMA (http://www.ipma.pt.html). Due to lack of measurements, the wind data for the first semester of 2019 are from Olhão, 3 km away from the sampling site.

Simultaneously, to confirm upwelling and countercurrents ancillary level 3 (L3) satellite data regarding Sea Surface Temperature (SST) and chlorophyll *a* concentration composed of 8 days (average) with 4 km resolution (OceanColor Nasa; https:// oceancolor.gsfc.nasa.gov/) were analyzed using MIRONE software (Luis, 2007). In order to have an accurate analysis the satellite images were reinterpolated using a bicubic interpolation. The L3 satellite images widely used by the scientific community (e.g. Benazzouz *et al*., 2014) helped to evaluate the influences of oceanographic processes occurring in the adjacent coastal ocean on the temporal variability of the studied parameters.

3 Results

3.1 Oceanographic settings and mesoscale events analyses

The two years measurement of water temperature inside Ria Formosa complemented with wind intensity and direction data provide the results of the cross covariance function (Figure 3.1) allowing to identify a series of mesoscale events associated with the meteorological conditions occurred in the adjacent coastal ocean. The cross-covariance function results showed a negative correlation between temperature and wind direction, with a negative coefficent of - 0.12150. It is observed a delay correspond to a time lag of 72 h before the wind stress induces water cooling (Figure 3.1).

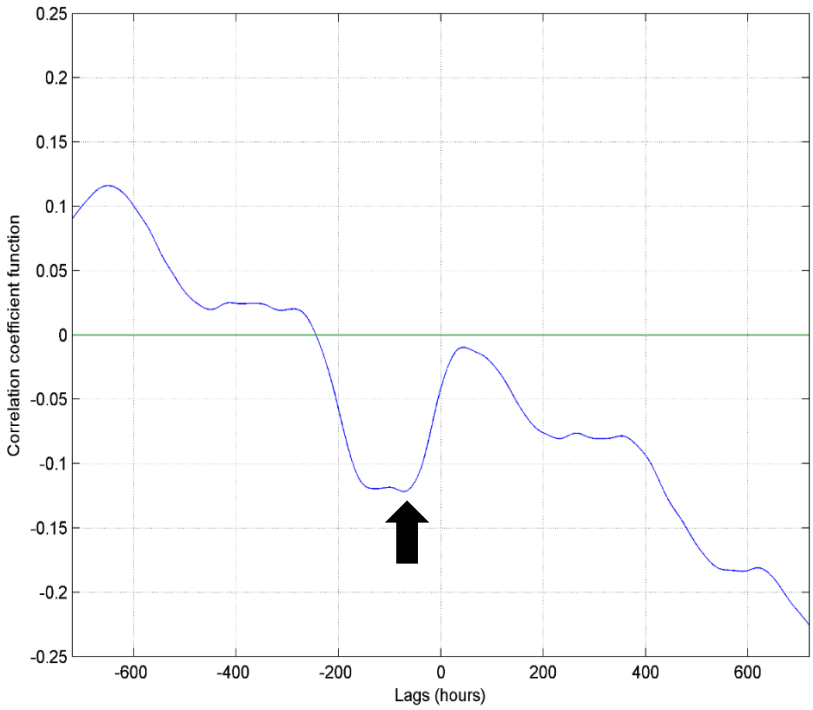

Figure 3.1: Cross-Covariance function between temperature and alongshore component of wind velocity filtered timeseries; the arrow indicates the relative minimum, corresponding to a time lag of 72h.

Several mesoscale events were found, 12 coastal upwelling events and 12 countercurrent events were identified in the first year of measurement (Figure 3.2 A), while in the second year 10 coastal upwelling events and 11 countercurrent (Figure 3.2 B) were detected. Among the identified events, 3 of the most significant of each type were selected to be supported by Sea Surface Temperature (SST) and chlorophyll *a* satellite imagery. The upwelling events were

identified trough the acronym UP-1 for the first event, UP-2 for the second, and UP-3 for the third event identified, while the acronym used on the identification of the countercurrent is CC-1, CC-2, CC-3 (Figure 3.2 and Table 3.1).

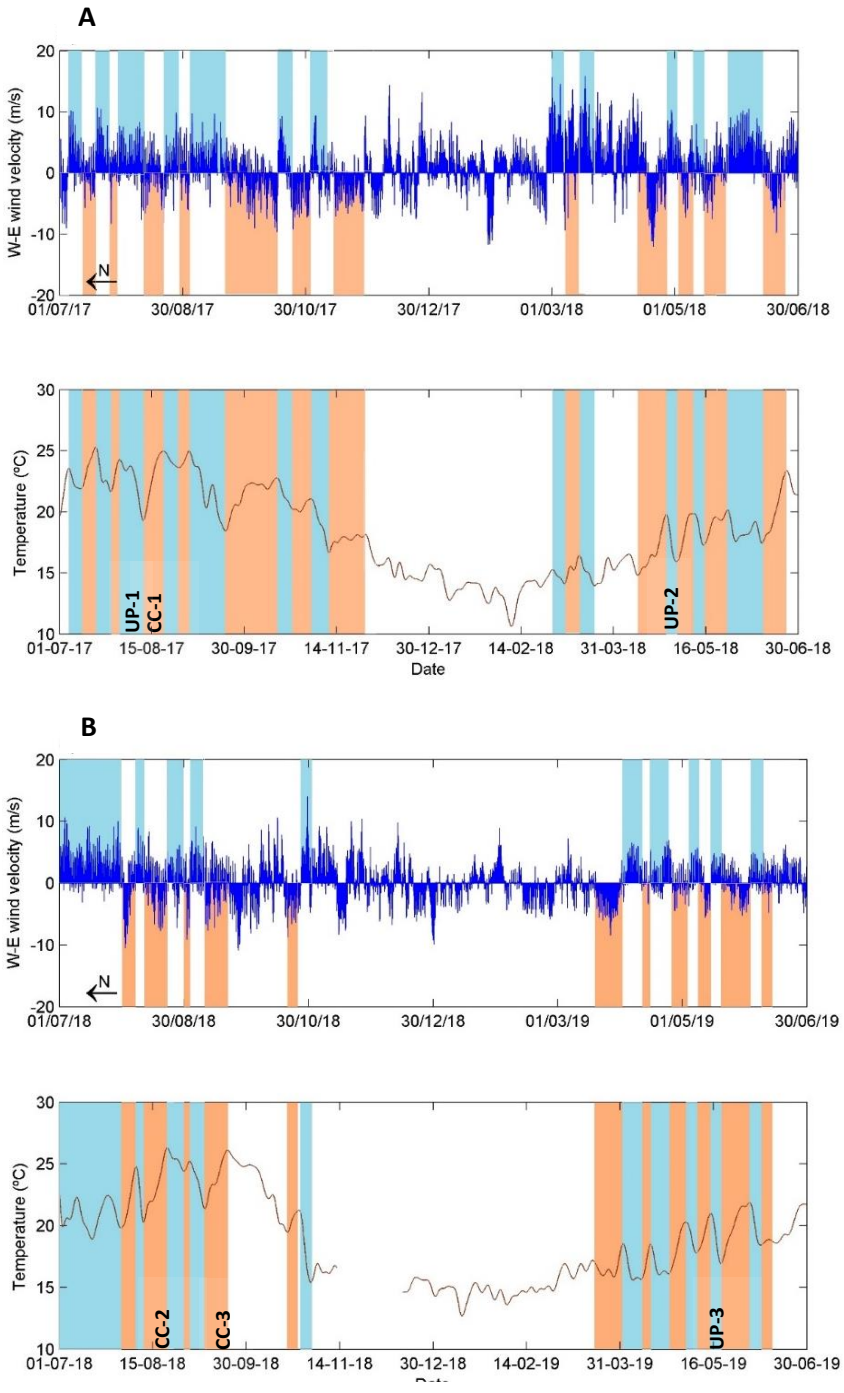

Figure 3.2: Identification and characterization of the mesoscale oceanic occurrences: A) during the first year of real time measurements; B) during the second year of real time measurement. The blue area represents the upwelling associated with the westerlies and drop in water temperature, while the red area is representing the coastal countercurrent associated with the easterlies and the increase in water temperature.

Table 3.1: Identification of the mesoscale events.

Mesoscale event	Start	End
UP-1	28/07/2017	12/08/2017
UP-2	01/05/2018	08/05/2018
UP-3	17/05/2019	24/05/2019
CC-1	13/08/2017	28/08/2017
CC-2	13/08/2018	20/08/2018
CC-3	29/08/2018	05/09/2018

From the analysis of the wind stick plot (Figure 3.2) and satellite images it is observed an alternation between upwelling and countercurrent along the period of study that generated an oscillation between cold and warm water (Figure 3.3 3.4). The mean west wind intensity, leading to upwelling, was around 10 m/s (Figures 3.2). It induces coastal water displacement to the offshore, with the advection of deeper colder water. As Figure 3.8 shows, UP-3 occurred when wind intensity is observed to be < 10 m/s (Figure 3.2 B), reflecting that upwelling continued to occur also when west wind had low intensity (Figure 3.2). Generally, the range of SST observed in the satellite images, during the upwelling events in front of Ria Formosa, is *ca.* 16-18 ºC.

The shifts in water temperature and afterwards in Chl *a* (Figures 3.3, 3.4), occurred more frequently during the spring to summer period (Figure 3.2).

The satellite images show that in front of Ria Formosa, the values of Chl *a* during upwelling were mainly > 2 µg/L (Figures 3.3, 3.5, 3.8).

Regarding the warm countercurrents, that are observed recirculating from the Gulf of Cadiz to the south coast of Portugal, these are amplified when the east wind starts to blow with intensity > 5 m/s and can even reach the Cape São Vicente, if the wind is stronger (Figure 3.2). When the warm countercurrent was observed, the values of Chl *a* decreased and reached the minimum *ca*. 0.1-0.5 µg/L, while the water temperature increased, ranging from 20 to 26 ºC (Figures 3.4, 3.6, 3.7).

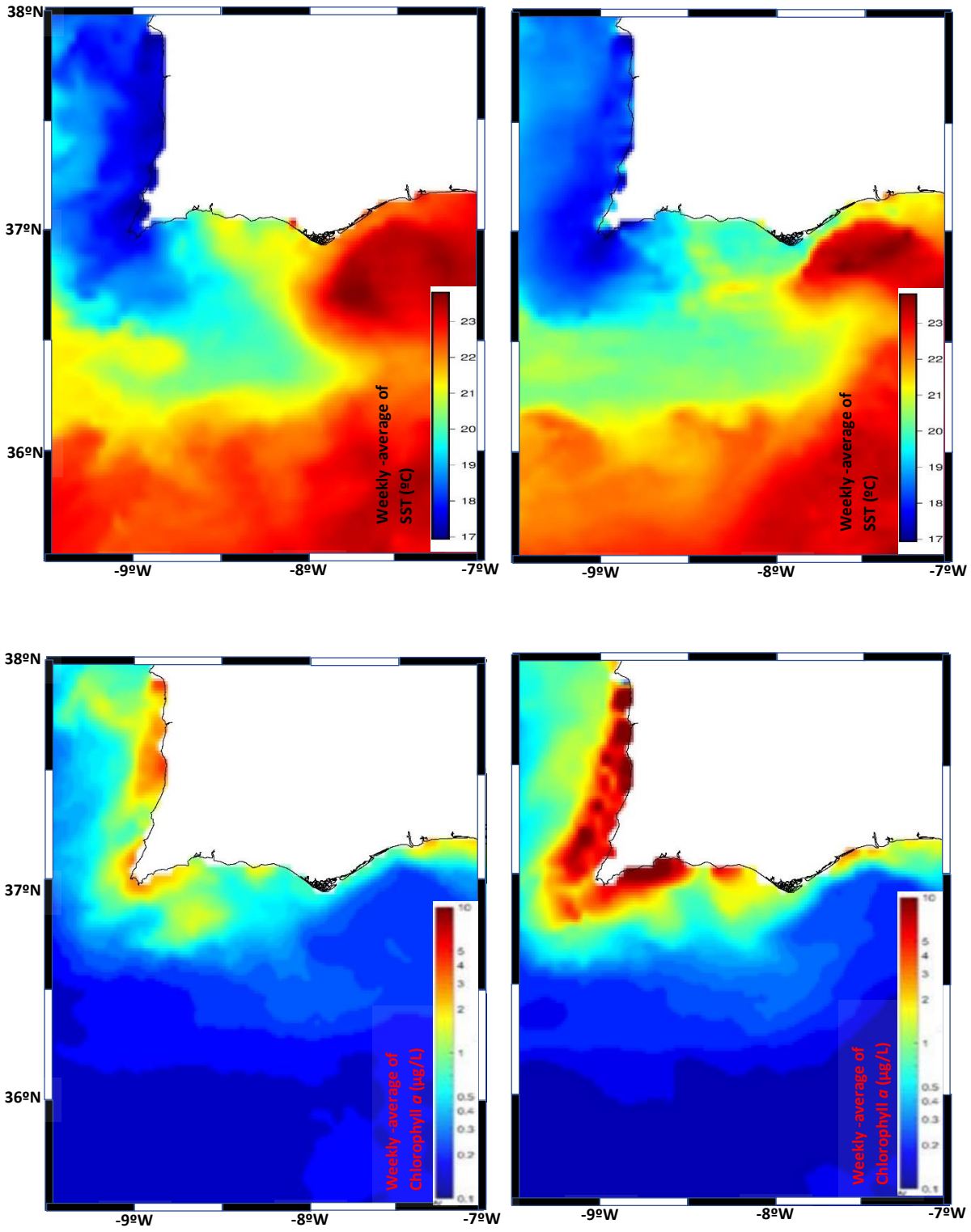

Figure 3.3: Satellite images of the south coast of Portugal. UP-1, up) weekly average of Sea Surface Temperature (SST), and bottom) weekly average of chlorophyll *a* concentration, corresponding to the period at left between, 28 July and 4 August and at right, between 5 and 12 August 2017.

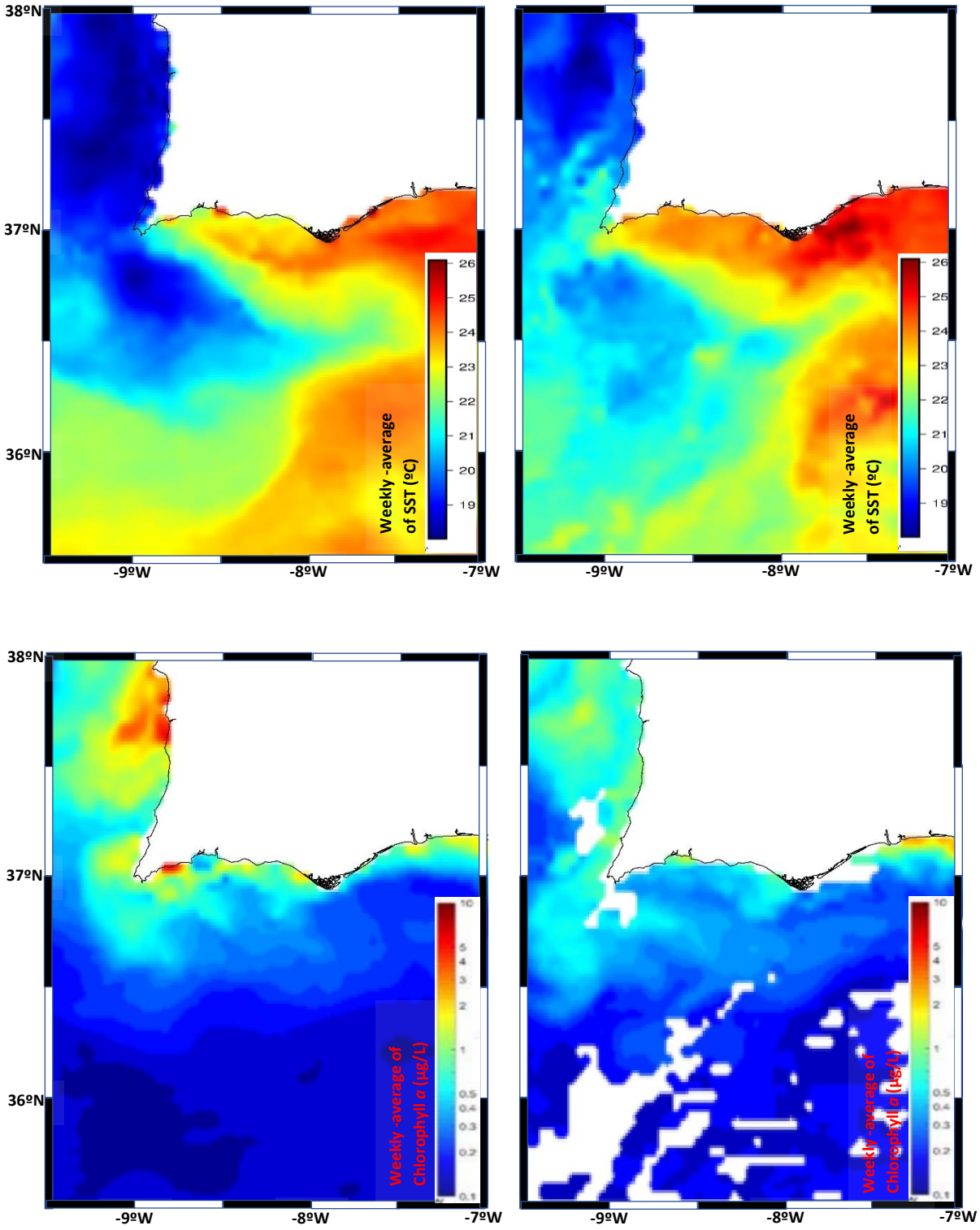

Figure 3.4: Satellite images of the south coast of Portugal. CC-1, up) weekly average of Sea Surface Temperature (SST), and bottom) weekly average of chlorophyll *a* concentration, corresponding to the period at left between, 13 August and 20 August and at right, between 21 and 28 August 2017.

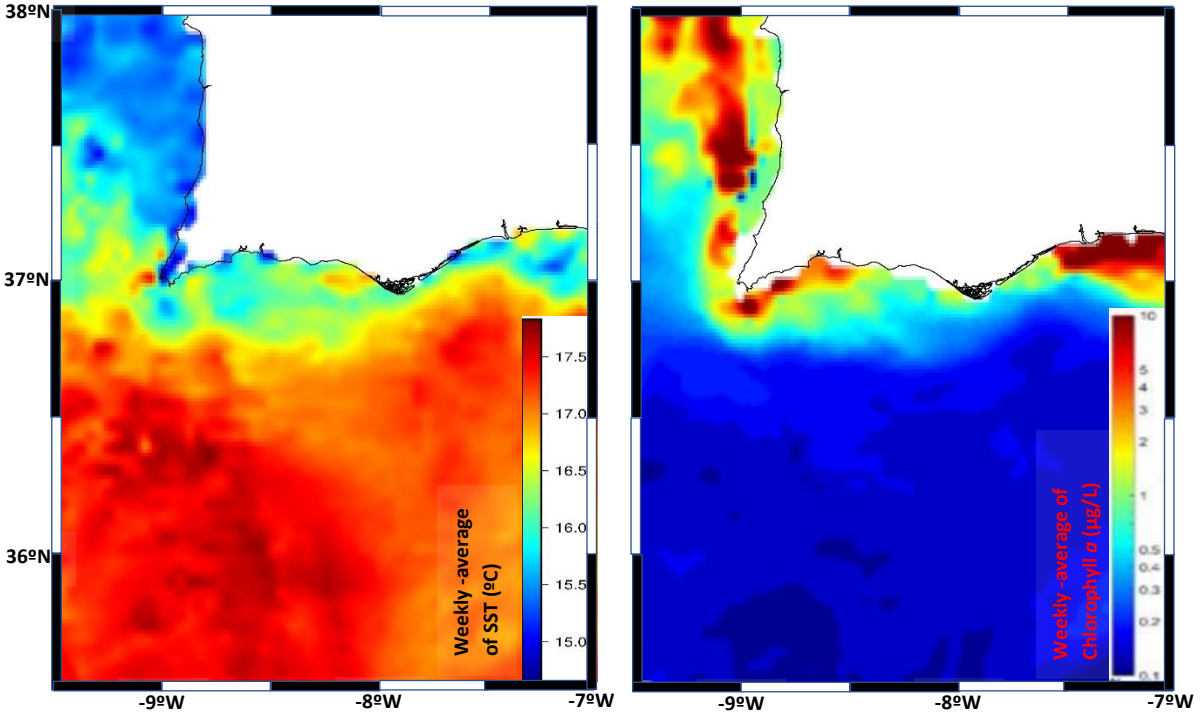

Figure 3.5: Satellite images of the south coast of Portugal. UP-2, left) weekly average of Sea Surface Temperature (SST), and right) weekly average of chlorophyll *a* concentration, corresponding to the period to the period between 1 and 8 May 2018.

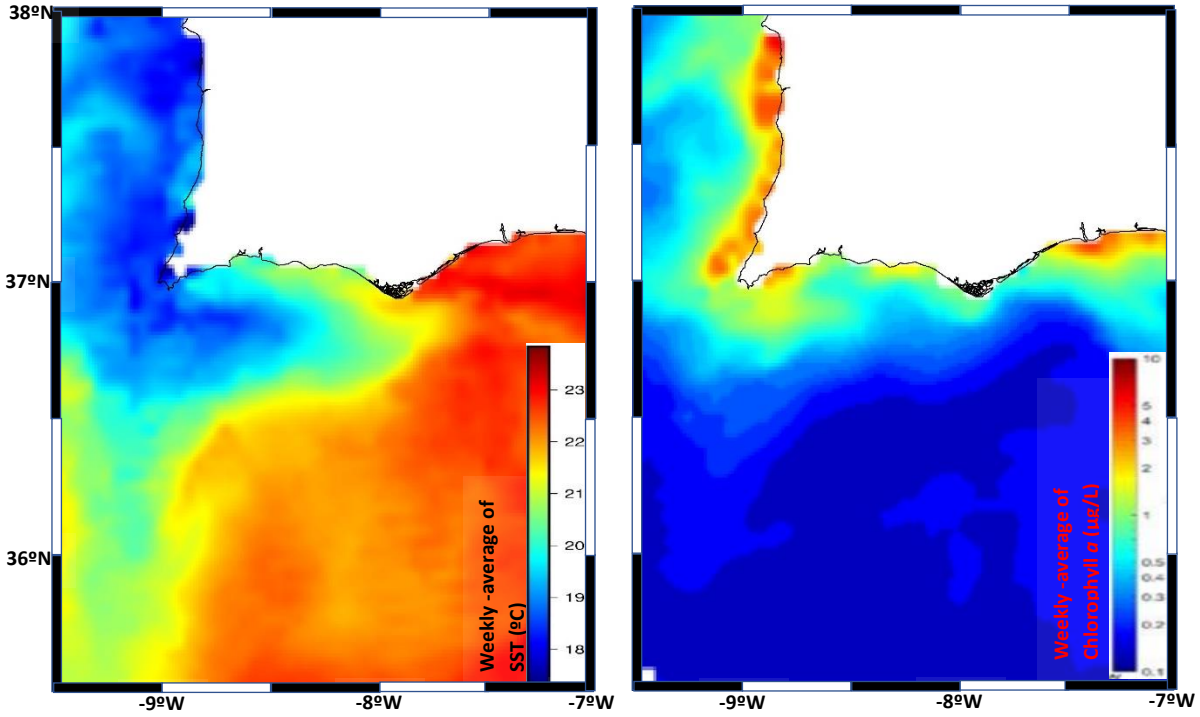

Figure 3.6: Satellite images of the south coast of Portugal. CC-2, left) weekly average of Sea Surface Temperature (SST), and right) weekly average of chlorophyll *a* concentration, corresponding to the period between 13 August and 20 August 2018.

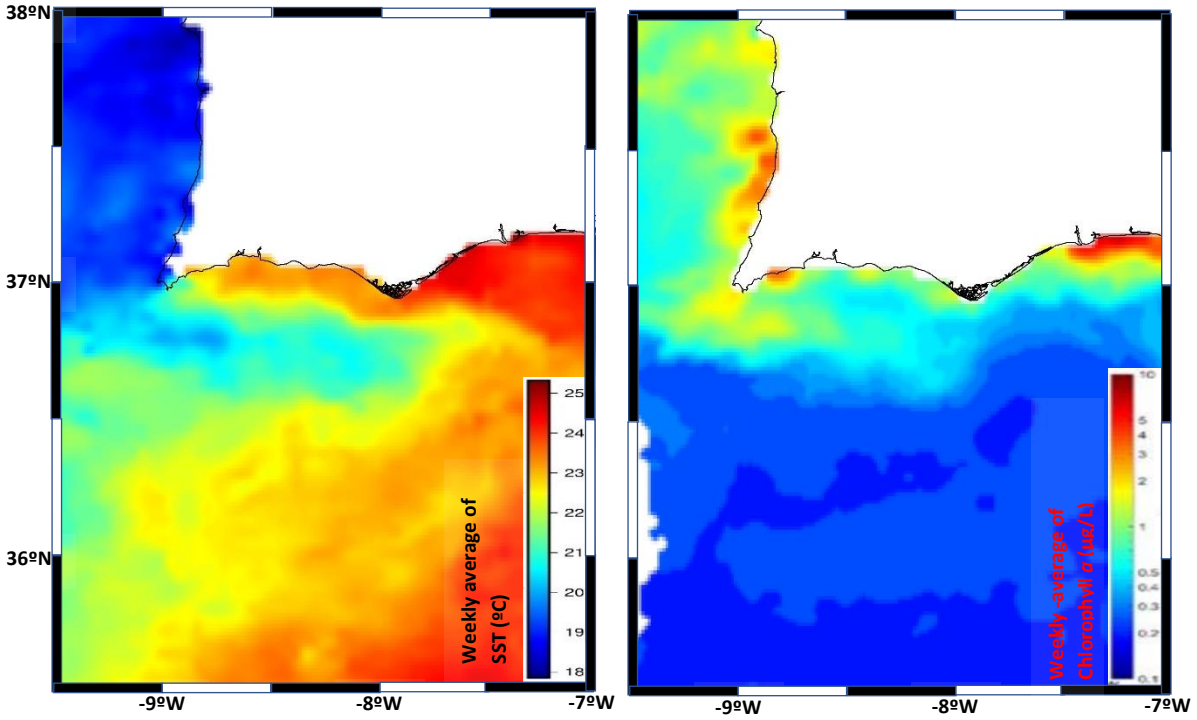

Figure 3.7: Satellite images of the south coast of Portugal. CC-3, left) weekly average of Sea Surface Temperature (SST), and right) weekly average of chlorophyll *a* concentration, corresponding to the period between 29 of August and 05 of September 2018.
0

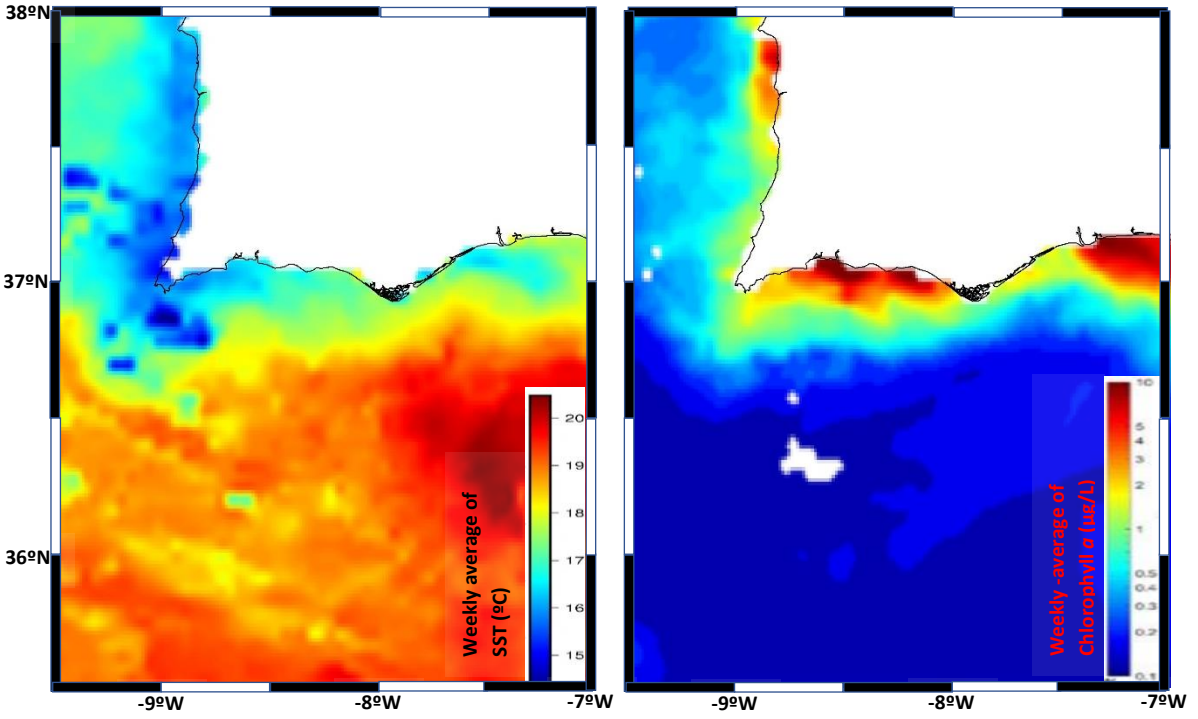

Figure 3.8: Satellite images of the south coast of Portugal. UP-3, left) weekly average of Sea Surface Temperature (SST), and right) weekly average of chlorophyll *a* concentration, corresponding to the period between 17 and 24 May 2019.

3.2 Temporal variability at various scales for water temperature, salinity, pH, dissolved oxygen, turbidity, and chlorophyll *a*

3.2.1 Seasonal and interannual pattern of variation

The temporal variability of the studied parameters along two years of real time measurements, from 1/07/2017 to 30/06/2019 was explored through basic statistical analysis, and the results are reported in Table 3.2. To carefully describe the datasets, gaps in the timeseries (which were mainly present in the second year of measurement), were not included in the analysis. The filtering process helped the identification of the general pattern of variation of the timeseries along the period of study, since high frequency events were cut-off. The raw timeseries and the filtered timeseries of the studied parameters are showed in Annex 1 and from Figures 3.9 to 3.12 respectively.

Table 3.2: Result of the basic statistical analysis conducted on the raw timeseries of the studied parameters along two years of real time measurements from 1/07/2017 to 30/06/2019.

	Temperature (ºC)	Salinity	DO (mg/L) - (%)	pH	Chlorophyll *a* (µg/L)	Turbidity (NTU)
Mean	18.61	36.24	7.13 – 91.82	8.08	0.74	1.13
Median	18.16	36.27	7.22 – 92.61	8.08	0.45	0.91
Minimum	9.88	33.21	1.89 – 28.01	7.74	0.01	0
Maximum	27.85	37.36	10.88 – 136.51	8.33	10	10
Percentiles						
10%	14.25	35.83	5.71 – 79.42	8.00	0.070	0.20
90%	23.95	36.69	8.40 – 103.13	8.18	1.66	2.16

The pattern of variability for temperature timeseries (Annex 1 A, Figure 3.9 A) was similar between the two years of measurements, with highest values observed in summer months (June, July, August) and lowest values in winter months (December, January, February). For both

summers (2017-2018), mean values were around 23 ºC, and the maximum value was recorded on 22 of august 2018, when the water temperature attained 27.85 °C. The winter 2017/2018 attained the minimum value of 9.88 °C (on 9 of February 2018), while the minimum in winter 2018/2019 was about 11.56 ºC (13 of January 2019), almost 2º C warmer than in the winter 2017/2018. Despite that, the mean values for both winter periods were similar, around 14.5º C. Moreover, during the winter period the variability of water temperature (9.88-18.41 ºC) was relatively smaller when compared with the amplitude recorded during summer period (15.46-27.85 ºC). Intermediate temperatures were observed from March to May, corresponding to the spring period (mean spring 2018, 17.45 ºC and mean spring 2019, 18.8 ºC) and from September to November, corresponding to the autumn (mean autumn 2017, 19.95 ºC and mean autumn 2018, 19.70 ºC). The temperature timeseries showed a median (18.16 ºC), 0.5 ºC lower than the mean (18.61 ºC), with the 10^{th} percentile 14.25 ºC and the 90^{th} percentile of 23.95 ºC (Table 3.2).

The salinity mean value for the studied period was 36.24, very similar to the median value (36.27), while the 10^{th} percentile was 35.83 and the 90^{th} percentile 36.69 (Table 3.2). In general, salinity showed a relatively low variability along the period of study (except during spring 2018) (Annex 1 B, Figure 3.9 B), with the highest values attained during the summer and the lowest during the winter (35.4; on 11 of Jannuary). During the summer 2017 the salinity achieved a maximum value of 37.36 (on 6 of July 2017) (Table 3.2). Along the time, salinity starts to decrease from Autumn 2017, continuing through the winter 2017/2018 (range 35.5-36). Moreover, in the spring 2018 an important decrease in salinity was detected, when the lowest values ranged around 34, and when the minimum of 33.21 (on day 1^{th} of March) was recorded. Starting from late May 2018, the salinity increased again till the first days of October 2018 (37.4; on day 5). Unfortunatly, from 09/02/2019 till 15/05/2019 the multiparametric probe stopped sending the salinity data for an unknown reason and a gap in the timeseries is observed.

In the case of DO in concentration (mg/L) (Annex 1 C, Figure 3.10 C), it was observed a large range of variability along the period of study. The highest values were recorded in winter/spring, with the maximum value observed in spring 2019 (10.88 mg/L, 3 of May) (Table 3.2) when DO ranged between 3.51-10.88 mg/L, while in spring 2018 the DO ranged between 3.46-9.92 mg/L. The lowest values of DO were recorded in summer 2017 and summer 2018. The minimum concentration was recorded in summer 2018 (1.89 mg/L; on 20 of August, Table 3.2) when DO ranged between 1.89-8.44 mg/L, while in summer 2017 DO ranged between 3.08-8.87 mg/L. Moreover, in spring and in summer the DO had a wider range of variability

than in the winter 2017/2018 and in the winter 2018/2019 (6.24-9.08 mg/L and 4.51-9.92 mg/L, respectively). The median value for DO (7.22 mg/L) is close to the mean (7.13 mg/L), while the 10th percentile is 5.71 mg/L and the 90th percentile is 8.40 mg/L (Table 3.2). Regarding the DO in saturation, it follows the seasonal pattern described above for DO concentration. The DO saturation showed close mean and median values, slightly lower than 100% of saturation (92% and 93%, respectively) (Annex 1 D, Figure 3.10 D). The 10th percentile for dissolved oxygen timeseries was 79% and the 90th percentile was 103% (Table 3.2). Important variations are observed in summer 2018, when the DO reached the maximum value of 137 % (on 21 of June) and the minimum value of 28% (on 21 of August).

The pH timeseries (Annex 1 E, Figure 3.11 E), generally showed a small range of variation. The mean and median values were the same along the period of study (8.08), the 90th percentile was 8.18 and the 10th percentile was 8.00 (Table 3.2). It is observed a general decreased in pH along the time, from the begining of the measurements (summer 2017) until the beginning of the autumn 2017. However, the minimum pH values were recorded mostly in summer (7.84 and 7.74 recorded on 29 of September 2017, and on 6 of August 2018 respectively), while a maximum value of 8.33 was recorded during autumn 2017 (on 15 of November). During the winter 2017/2018 pH showed intermediate values. Due to an unknown reason, the multiparametric probe stopped to send data from september 2018 until the end of the period of study, as mentioned in Material and Methods chapter, and, unfortunatly, only one year of measurements was recorded for this parameter.

Chlorophyll *a* was highly variable along the period of study. The chlorophyll *a* 10th percentile was 0.070 µg/L and the 90th was 1.66 µg/L; with the mean value of 0.74 µg/L and median about 0.45 µg/L (Table 3.2). The Chl *a* ranged between a minimum of zero, especially in spring (2018 and 2019) to a maximum of 10 µg/L (Annex 1 F, Figure 3.11 F) when the phytoplankton biomass expressed by the Chl *a* concentration was above the 90th percentile, in summer (2017) and in autumn (2018) (Annex 1 F). Generally, during both summers (2017 and 2018) Chl *a* was highly variable, but with lower concentrations than the values found in autumn and spring (Figure 3.11 F).

Regarding turbidity (Annex 1 G, Figure 3.12 G), it was found that this parameter had not a specific temporal pattern of distribution between years. In this context, turbidity ranged between 0 NTU and 10 NTU, while the mean was 1.13 NTU close to the median that was 0.91 NTU. The 10th percentile was 0.20 NTU and the 90th percentile was 2.16 NTU (Table 3.2).

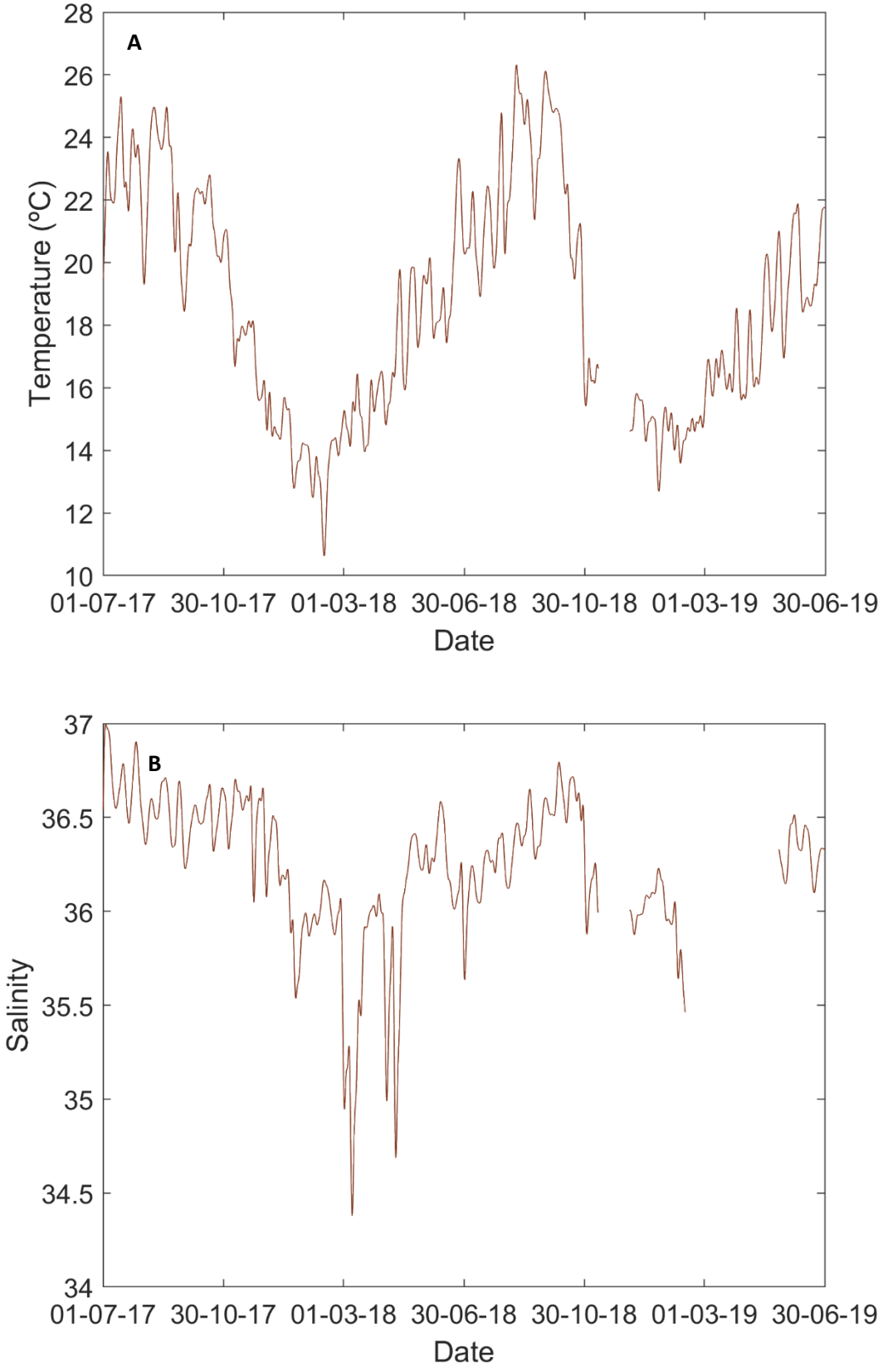

Figure 3.9: Filtered timeseries with 6th-order low-pass Butterworth filter, the cut-off frequency equal to 0.25 (cpd). A) temperature timeseries B) salinity timeseries.

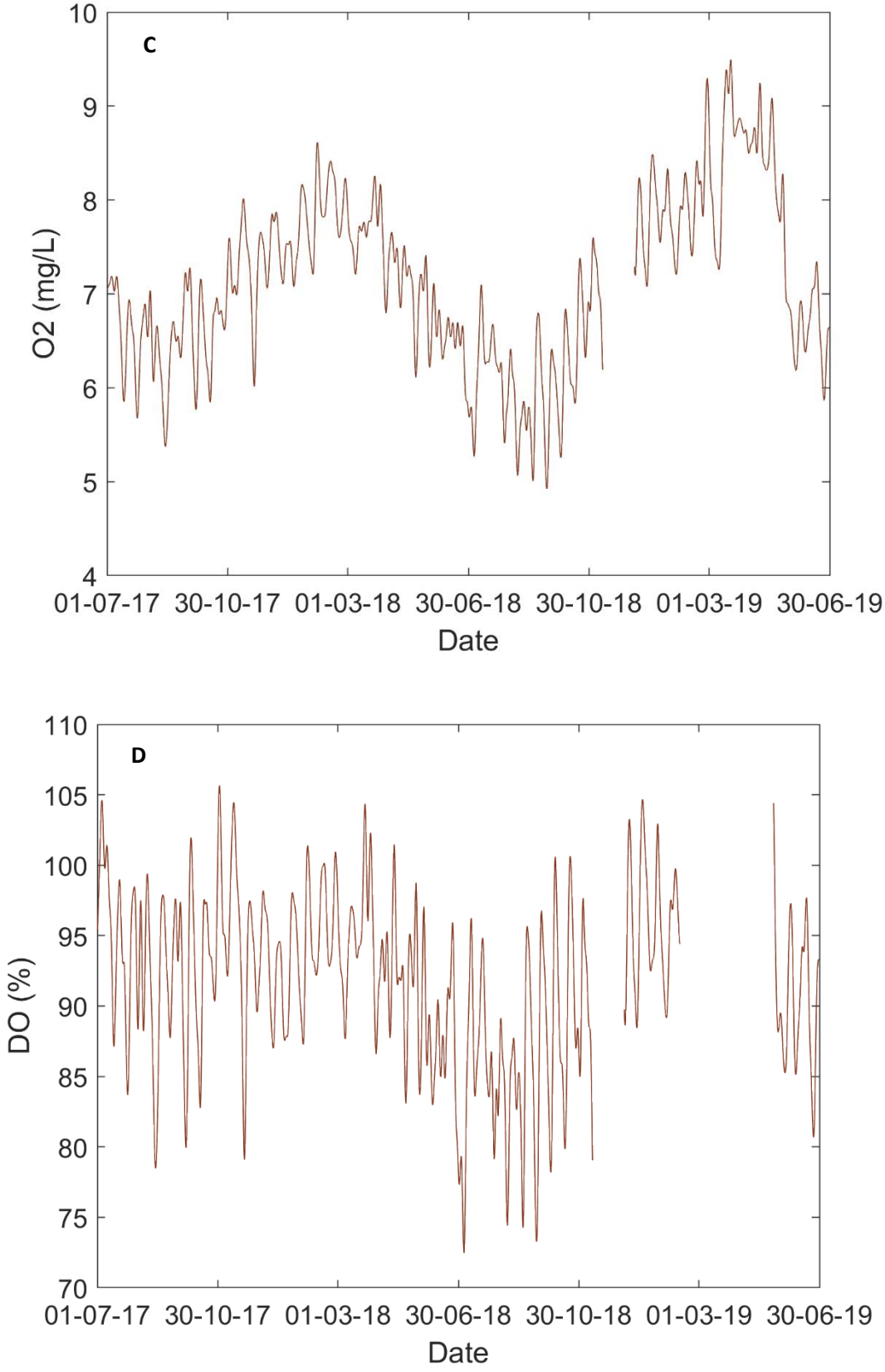

Figure 3.10: Filtered timeseries with 6th-order low-pass Butterworth filter, the cut-off frequency equal to 0.25 (cpd). C) DO in concentration D) DO in saturation timeseries.

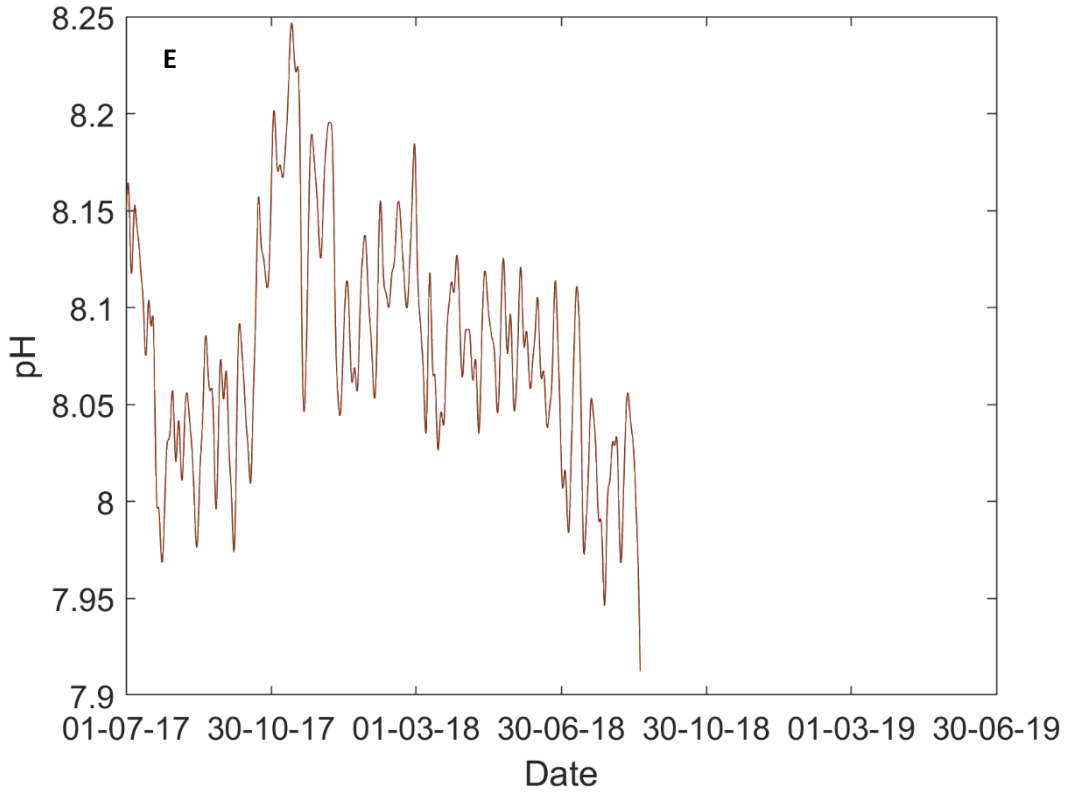

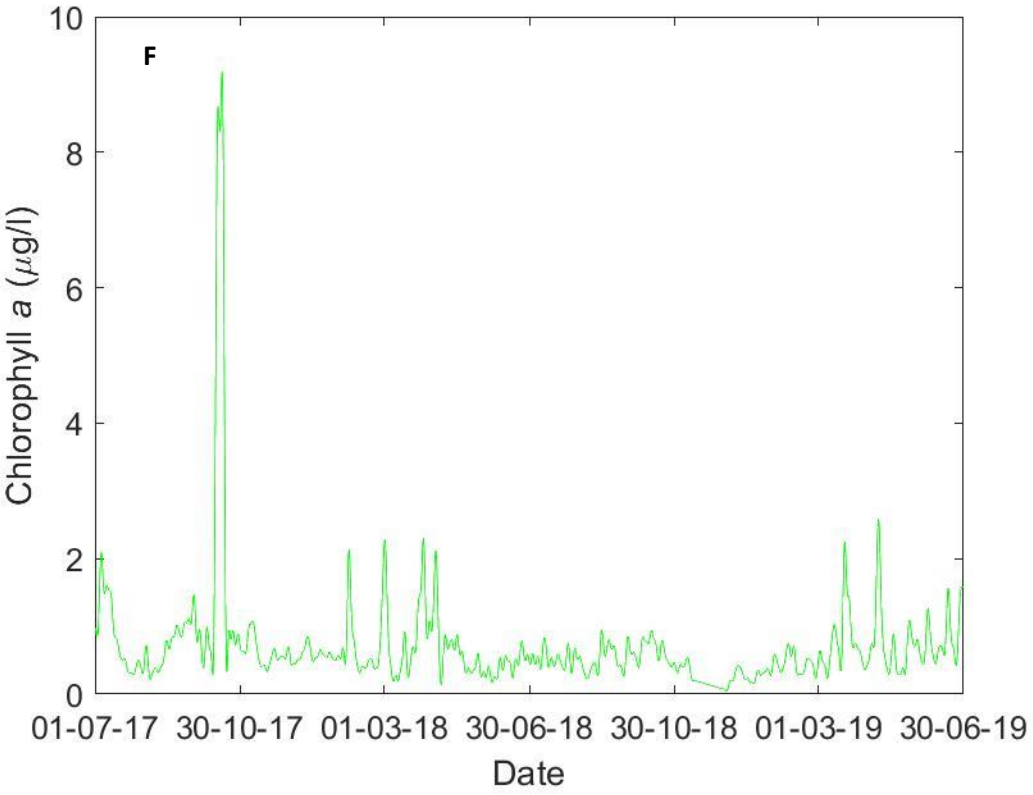

Figure 3.11: Filtered timeseries with 6th-order low-pass Butterworth filter, the cut-off frequency equal to 0.25 (cpd). E) pH timeseries F) chlorophyll *a* timeseries.

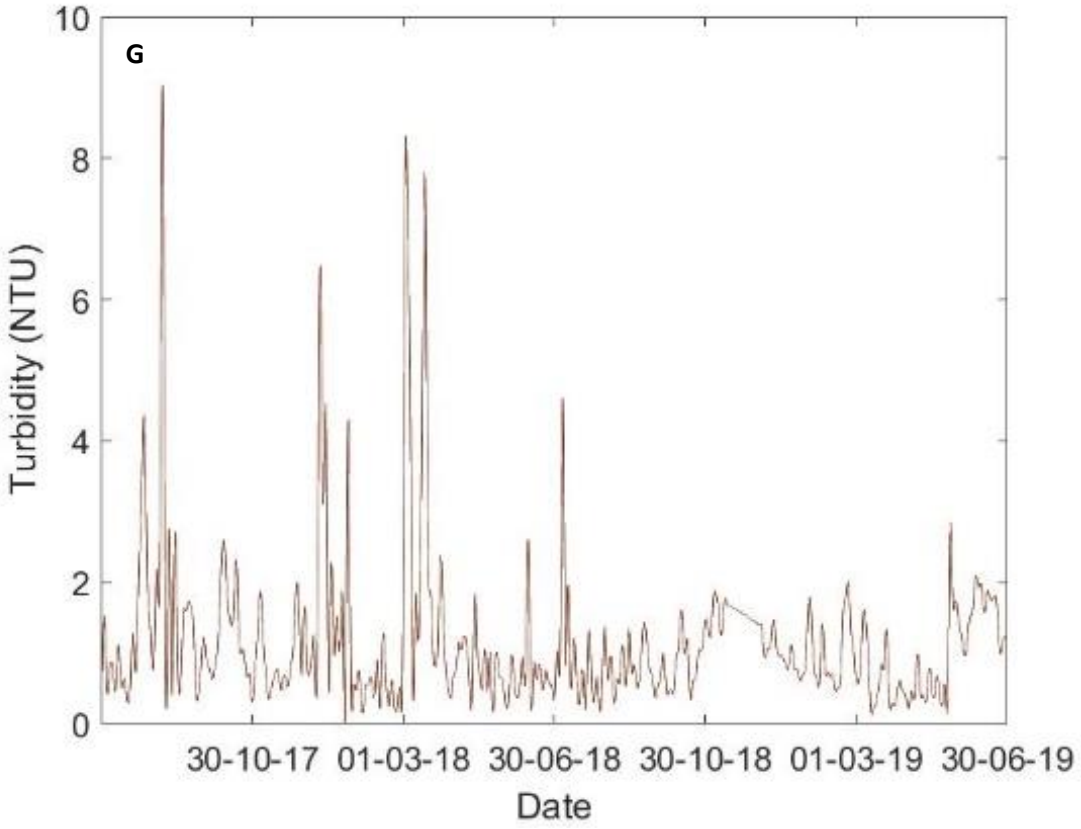

Figure 3.12: Filtered timeseries with 6th-order low-pass Butterworth filter, the cut-off frequency equal to 0.25 (cpd). G) Turbidity timeseries.

3.2.2 Spectral Analysis

The main variations of temperature, salinity, DO, pH, chlorophyll *a* and turbidity resulted from the tides induced by astronomical forces, such as the principal lunar semidiurnal constituent M2, the diurnal lunar constituent K1, and the lunisolar synodic fortnightly constituent MSF. Moreover, variations related to other factors which were primarily associated by the system configuration are observed, such as the shallow water overtides of principal lunar constituent M4 and the radiational tidal constituent S1, associated with solar radiation effects, although distinct peaks were not always obvious (Figures 3.13; 3.14).

At a lowest frequency, temperature (Figure 3.13 A), and DO (Figure 3.13 C) signals showed a marked peak corresponding to a period of 365 days (solar annual). Despite that, on the periodograms of the other studied parameters the solar annual radiation effect (SA) was not observed, and, in general, significant peaks in spectral density energy at frequencies lower than the fortnightly tidal component were not present.

At a fortnight scale (MSF) it was observed a strong variation for all the studied parameters. With frequency around 0.067 cpd and period of 14.6 days, the MSF had the strongest signal, compared to the other analysed timescales, for turbidity (Figure 3.14 G), DO % (Figure 3.13 D) and pH (Figure 3.14 E), and the second strongest signal for the rest of the studied parameters.

At a daily scale, the variation caused by the solar radiation S1 with 1 cpd (24 h) and by the lunar diurnal constituent K1, are observed to be important, as it is showed in the periodograms of the studied parameters. The strongest variance due to the diurnal cycle solar radiation effect (S1) is observed particularly in the chlorophyll *a* (Figure 3.14 F) and DO periodograms (Figures 3.13 C, D).

Moreover, at solar radiation frequency (S1), it was found a peak in spectral density energy for temperature (Figure 3.13 A), while the solar diurnal radiation is observed to influence salinity with low magnitude (Figure 3.13 B). In addition, the diurnal tidal component K1 is observed to have influence in all the studied parameters, but in particular in the DO (Figure 3.13 C, D), pH (Figure 3.14 E) and turbidity (Figure 3.14 G) variation. Therefore, this component is observed to have a secondary role in the diurnal variation, and it is observed always with lower magnitude than the solar diurnal cycle.

On a semidiurnal time scale, with 1.930 cpd, the principal lunar semidiurnal component, M2, was the main factor of variation for the salinity (Figure 3.13 B) and for temperature (Figure 3.13 A). For these two parameters the M2 peak was more pronounced than the peaks associated to the solar diurnal cycle and MSF. Moreover, variations of pH (Figure 3.14 E) and turbidity (Figure 3.14 G) were observed at semidiurnal time scale, but with lower spectral density energy than that corresponding to MSF. Regarding the DO (mg/L), it is observed to be more affected by the solar diurnal variation (S1) than by the semidiurnal (M2). However, in general, the variation was nearly equal in magnitude (Figure 3.13 C), while the DO expressed in percentage of saturation depended more on the effect of the semidiurnal component (Figure 3.13 D). In addition, for all the studied parameters a variation induced by the overtide M4, with a frequency of 3.864 cpd, was observed. The M4 caused changes especially in temperature (Figure 3.13 A), salinity (Figure 3.13 B), DO (Figure 3.13 C) and turbidity (Figure 3.14 G), but, in general, with less contribution than the diurnal solar cycle (except salinity), K1 (except temperature, salinity, Chl *a* and turbidity) and MSF. Moreover, for the periodograms of the studied parameters, another constituent can be observed, such as the M6. The signal of the M6 was observed in

almost all the periodograms, but was not taken into account on the temporal characterization, due to the scarce influence on the variance of the parameters. Furthermore, an unknow peak, with a frequency of aproximately 3 cpd, was observed in some periodograms (e.g temperature, DO). However, this signal represents also a lower contribution than the M4 and K1.

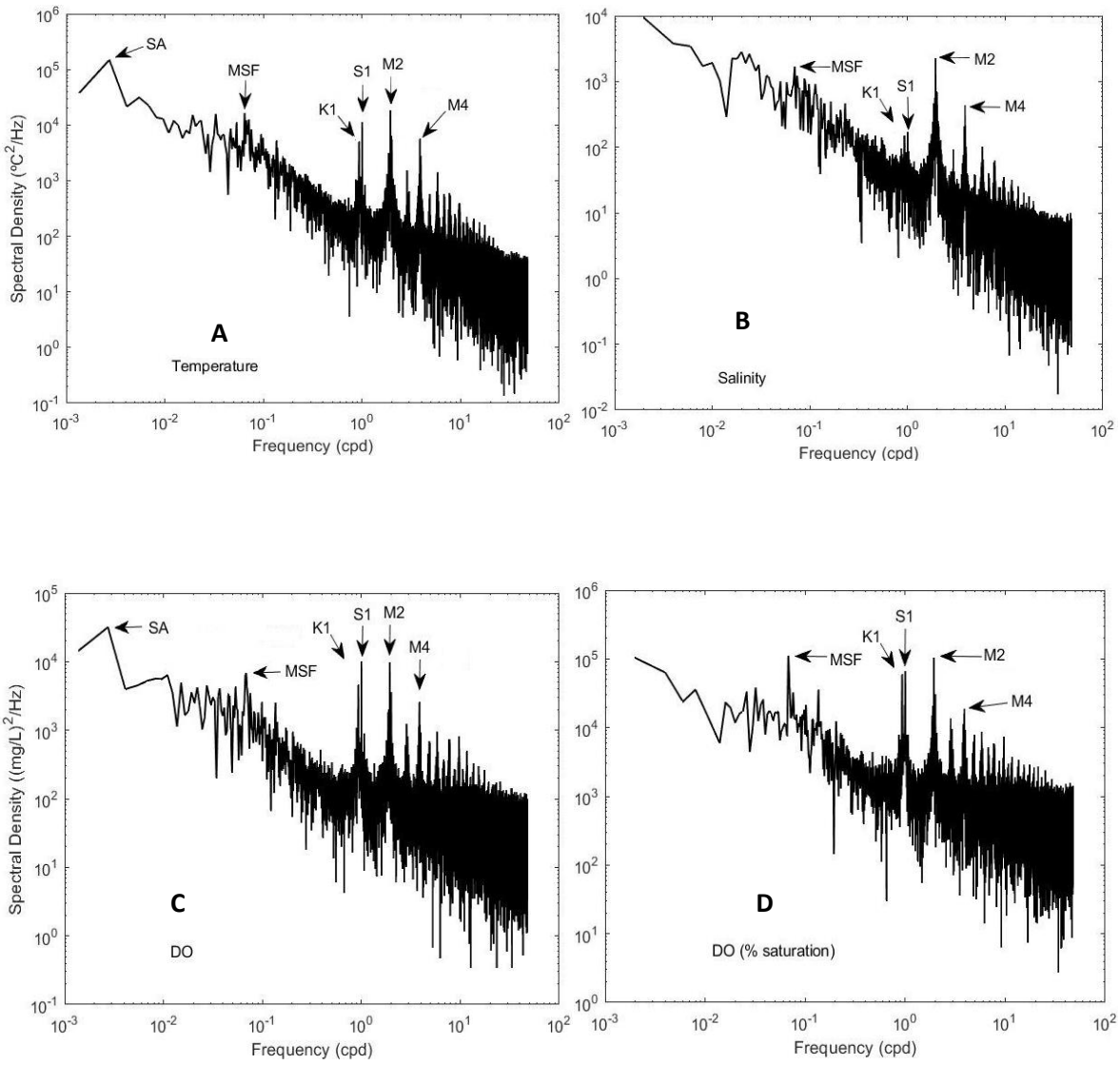

Figure 3.13: Periodograms of the studied parameters, with the arrows indicating the main constituents that cause the variation on the studied parameter: Fortnight, - MSF, Diurnal - K1 Semidiurnal M2, over-tide M4, Solar annual SA and Solar diurnal cycle S1. A) Temperature, B) Salinity, C) DO in concentration D) DO in saturation.

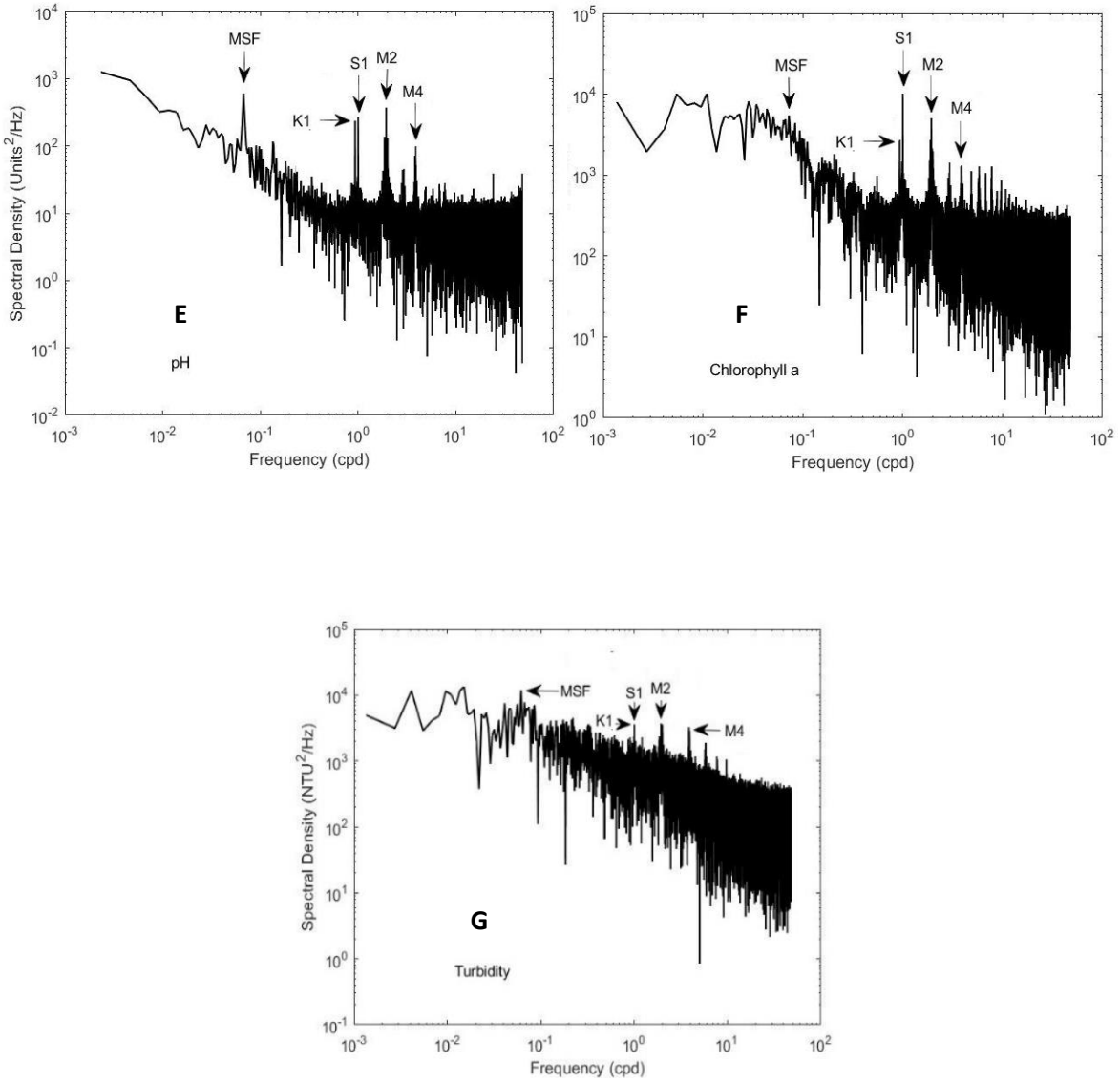

Figure 3.14: Periodograms of the studied parameters, with the arrows indicating the main constituents that cause the variation on the studied parameter: Fortnight,- MSF, Diurnal - K1 Semidiurnal M2, over-tide M4, Solar annual SA and Solar diurnal cycle S1. E) pH, F) chlorophyll *a*, G) Turbidity.

3.2.3 Pattern of variation at fortnightly scale (Spring tide *vs*. Neap tide)

The period analysed to characterize the parameters studied on a fortnightly scale is approximately one month, from 27 of April to 24 of May 2018. The tidal tables were provided by the Hydrographic Institute of Portugal (https://www.hidrografico.pt/m.mare) (Tables 3.3).

Table 3.3: Fortnightly tidal cycle.

Tide/ name	Amplitude	Start and end of the maximal tidal excursion
Spring ST1	*ca*. 3 m	28/04/2018 02:14 30/04/2018 21:47
Neap NT1	*ca.* 1 m	06/05/2018 00:54 08/05/2018 22:11
Spring ST2	*ca*. 3 m	14/05/2018 02:27 16/05/2018 22:08
Neap NT2	*ca.* 1.5 m	21/05/2018 13:55 23/05/2018 16:39

At fortnightly, temperature (mean value 18.51 ºC) ranged from lowest values recorded, during the spring tidal condition (15.36 ºC on 29 of April during ST1, and 15.31 ºC on 15 of May during ST2; Figure 3.15 A), while the highest values were recorded at neap tidal condition (20.75 ºC on 7 of May during NT1, and 20.83 ºC on 22 of May during NT2; Figure 3.15 A). However, temperature maximum (21.57 ºC on 27 of April) and minimum (14.94 ºC on 2 of May) are not coinciding with the maximal tidal excursion. Salinity (Figure 3.15 B) was relatively constant along the considered period with values around the mean (36.24). Neverthless, salinity reached lowest values during spring tidal condition (36.09 on 29 of April during ST1 and 36.46 on 16 of May during ST2; Figure 3.15 B) and highest values during neap tidal condition (36.50 on 7 of May during NT1 and 36.50 on 23 of May NT2; Figure 3.15 B). As for temperature, maximum (36.72 on 13 of May) and minimum (35.35 on 27 of May) of salinity are not coinciding with maximal tidal excursion.

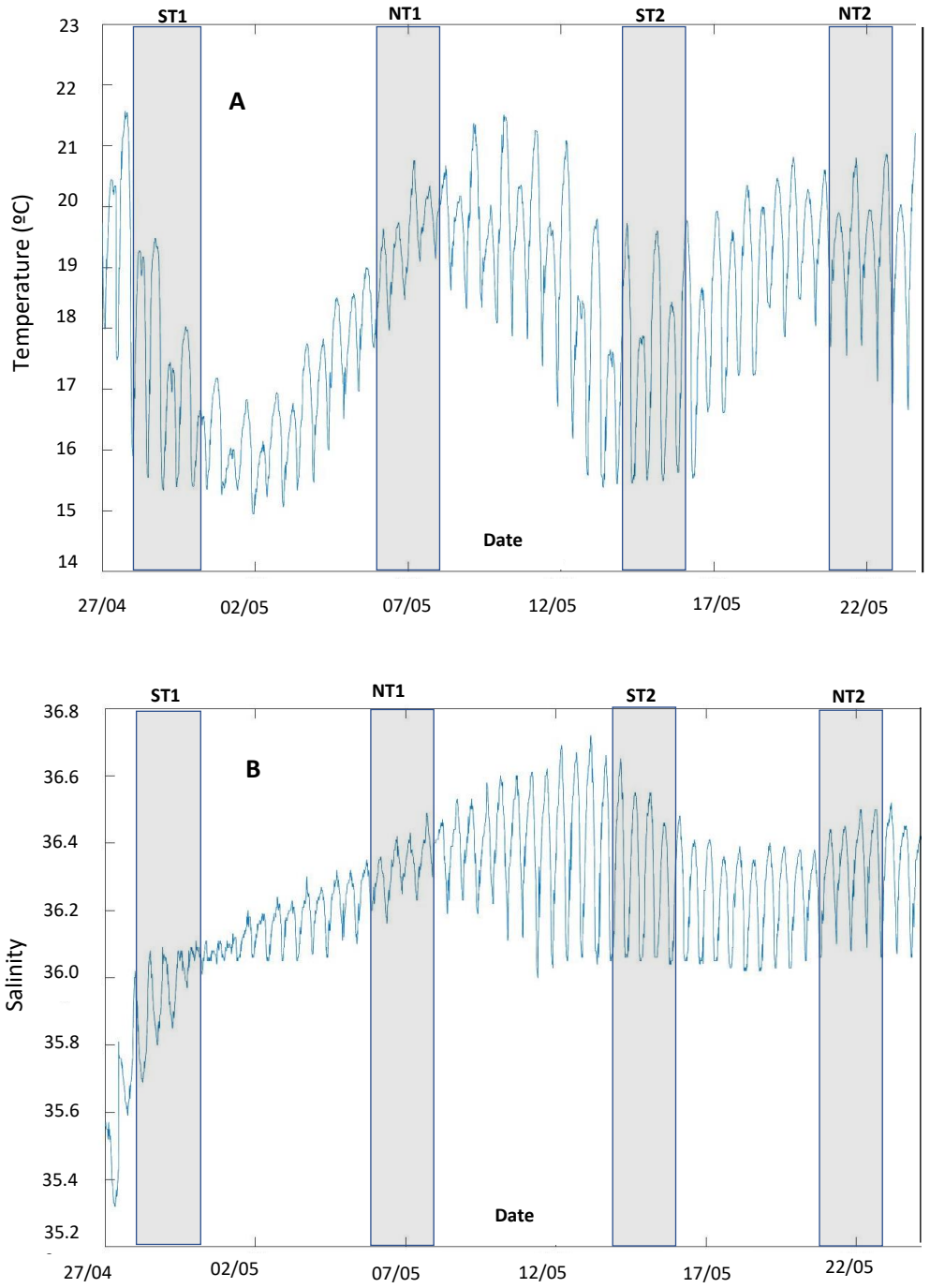

Figure 3.15: Variation of the studied parameters at fortnight time scale in spring 2018. ST (spring tide) NT (neap tide). A) Temperature raw timeseries, B) Salinity raw timeseries.

The DO mean concentration was 6.91 mg/L its observed with highest values during spring tidal condition (8.12 mg/L on 28 of April during ST1, and 7.93 mg/L on 15 of May during ST2; Figure 3.16 C) and with lowest values concentrated during the neap tidal condition (3.57 mg/L on 8 of May during NT1, and 4.54 mg/ L on 21 of May NT2; Figure 3.16 C). Moreover, the minimum of DO coincided with the maximal tidal excursion NT1, while the maximum value (8.92 on 18 of May) is showed after the ST2. The DO mean saturation in oxygen was 91% its

observed with highest values during spring tidal condition (110.40 % on 28 of April during ST1 and 105.90% on 15 of May during ST2; Figure 3.16 D) and with lowest values during the neap tidal condition (48.64 % on 8 of May during NT1, and 61.69 % on 21 of May during NT2; Figure 3.16 D). The minimum of DO coincided with the maximal tidal excursion NT1, while the maximum value (116.50 % on 18 of May) is showed after the ST2.

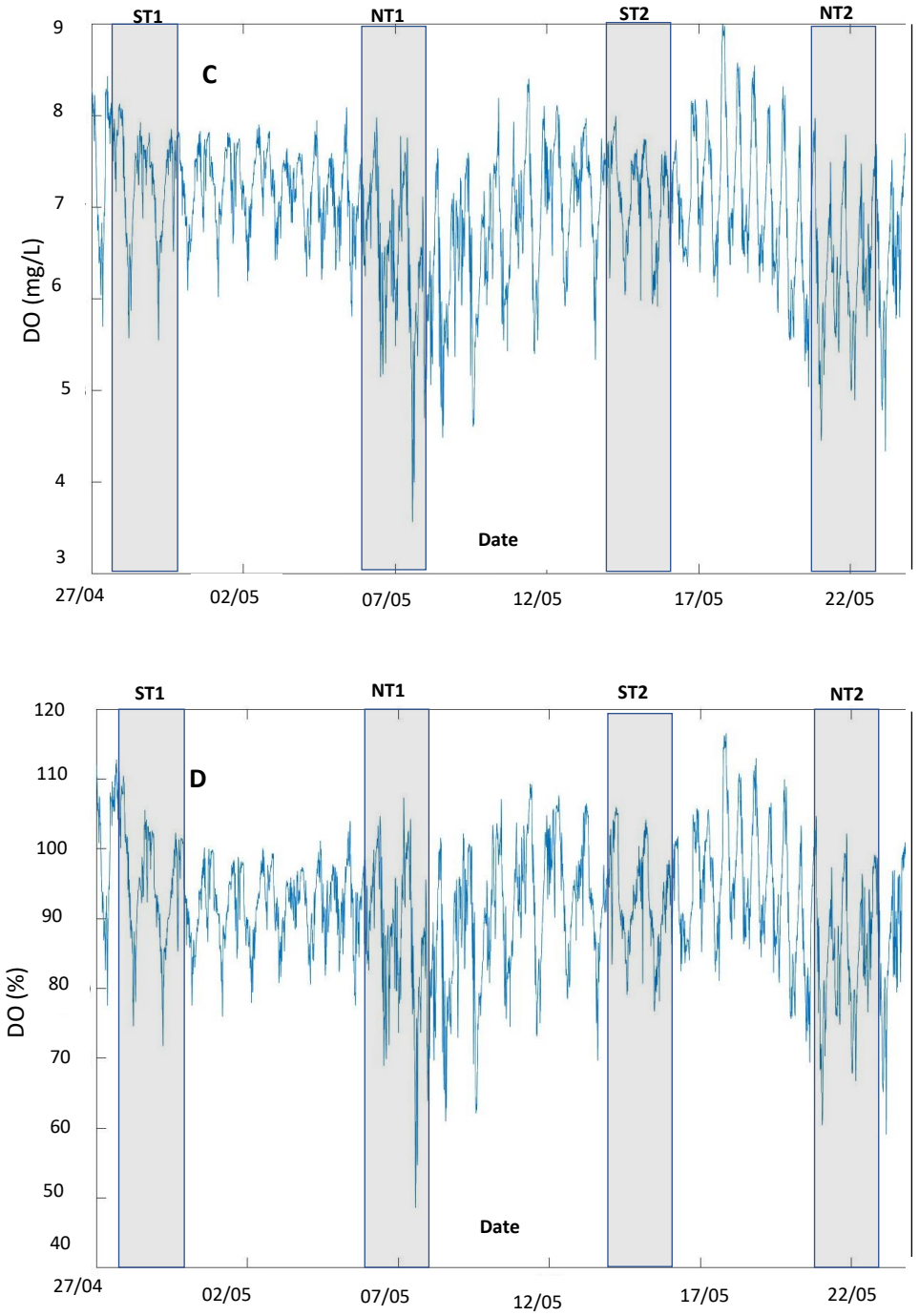

Figure 3.16: Variation of the studied parameters at fortnight time scale in spring 2018. ST (spring tide) NT (neap tide). C) Concentration in DO raw timeseries, D) Saturation in DO raw timeseries.

The pH (mean value 8.09) is observed quite constant at fortnightly. However its depicted with highest values during the spring tidal condition (8.21 on 28 of April during ST1, and 8.00 on 15 of May during ST2; Figure 3.17 E), and lowest values during the neap tidal condition (7.84 on 8 of May during NT1; and 7.91 on 21 of May during NT2; Figure 3.17 E). The pH maximum and minimum approximately coincided with the maximal tidal excursion. However, as for the DO, on day 18 of May after ST2, the pH showed another maximum (8.21).

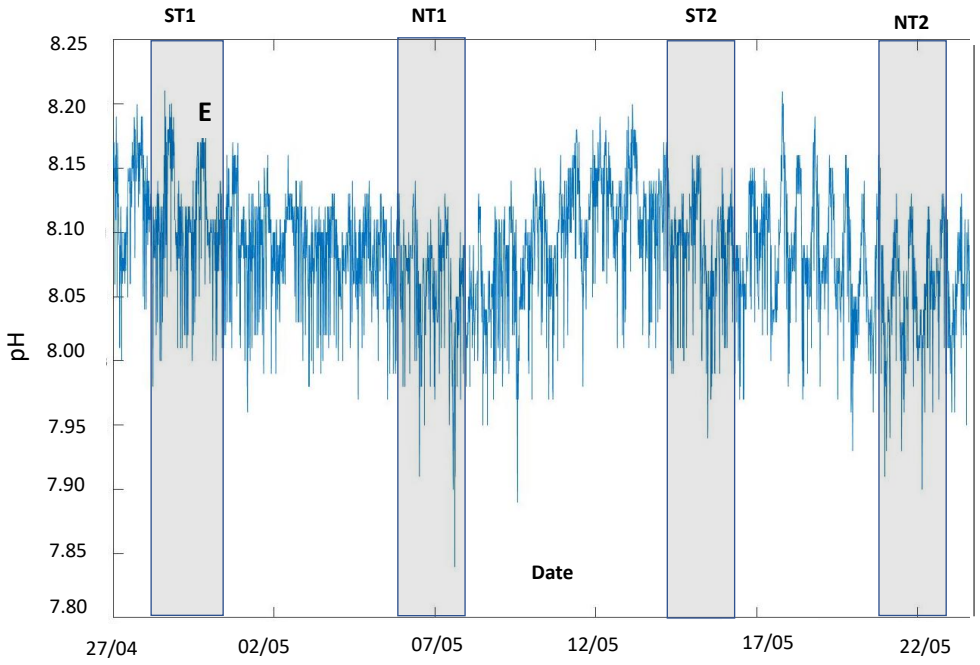

Figure 3.17: Variation of the studied parameters at fortnight time scale in spring 2018. ST (spring tide) NT (neap tide). E) pH raw timeseries.

The chlorophyll *a* (Figure 3.18 F), and turbidity (Figure 3.18 G) are observed highly variable at fortnightly. Regarding Chl *a* (mean value 0.63 µg/L) showed the highest concentration during the spring tidal condition (4.72 µg/L on 28 of April during ST1, and 4.35 µg/L on 15 of May ST2; Figure 3.18 F), and the lowest concentration during neap tidal condition (3.14 µg/L on 7 of May NT1, and 3.57 µg/L on 21 of May during NT2; Figure 3.18 F). Neverthless maximum concentration are observed one or two days after the maximal tidal excursion when Chl *a* atteined values of 6.38 µg/L on 1 of May after ST1 and 6.76 µg/L on 18 of May after ST2; (Figure 3.18 F). Over the fortnightly period, turbidity (mean value of 0.75 NTU) showed highest values during spring tidal condition (7.79 NTU on 29 of April during ST1, and 5.69 NTU on 14 of May during ST2; Figure 3.18 G), and the lowest values during neap tidal

condition (0.55 NTU on 7 of May during NT1 and 0.51 NTU on 21 of May during NT2; Figure 3.18 G). Moreover, a significant peak is observed on 18 of May (two days after ST2) when turbidity was 8.08 NTU.

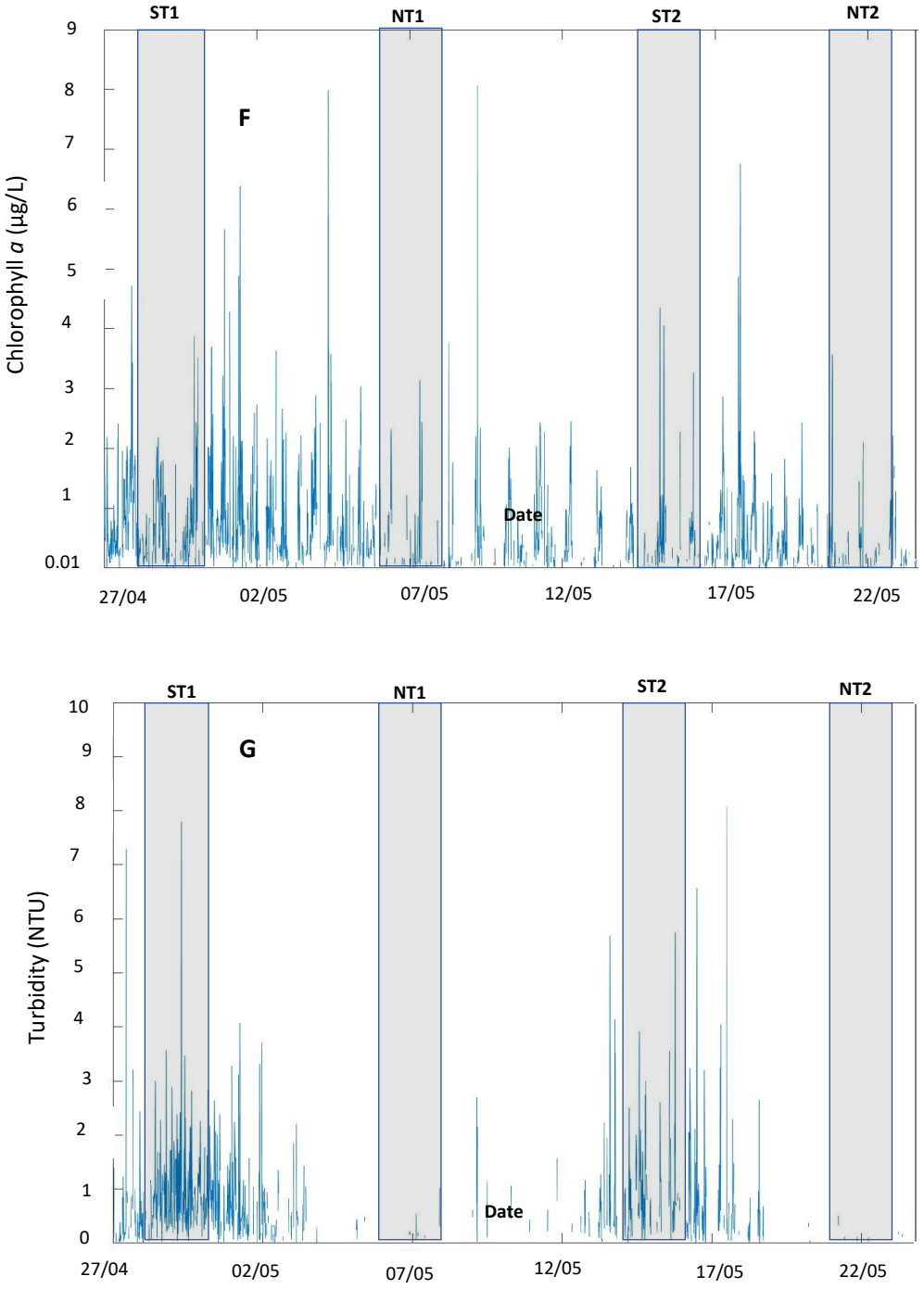

Figure 3.18: Variation of the studied parameters at fortnight time scale in spring 2018. ST (spring tide) NT (neap tide). F) Chlorophyll *a* raw timeseries, G) Turbidity raw timeseries.

3.2.4 Daily variations in Spring and Neap tide conditions

To describe the daily variation of the studied parameters, the semidiurnal tidal cycle was analyzed at spring and neap tide, respectively. The tidal tables were provided by the Hydrographic Institute of Portugal (https://www.hidrografico.pt/m.mare) (Tables 3.4 and 3.5).

Table 3.4: Semidiurnal tidal cycle during spring tide.

Water level/Name	Tide height	Hour
High water / HW1	3.4 m	03:36
Low water / LW1	0.6 m	09:30
High water / HW2	3.4 m	15:54
Low water / LW2	0.6 m	21:47

Table 3.5: Semidiurnal tidal cycle during neap tide

Water level/Name	Tide height	Hour
Low water / LW1	1.5 m	03:15
High water / HW1	2.4 m	09:43
Low water / LW2	1.6 m	15:35
High water / HW2	2.6 m	22:11

Daily variation of water temperature during spring tidal conditions (mean of 16.38 ºC) ranged from a minimum of 15.40 (at 04:15) and 15.35 ºC (at 15:30) recorded during the high water (HW1 and HW2; Figure 3.8 A) to higher values of 16.65 ºC (at 9:45) and 17.18 ºC (at 23:15) observed during the low water (LW1 and LW2; Figure 3.19 A), when a maximum of 17.86 ºC was recorded (at 00:15). The temperature daily pattern of variation, during the neap tidal condition is similar to the one observed during spring tidal conditions (Figure 3.19 A1). Neverthless, the temperature during the neap tidal condition was higher (mean value of 19.90 ºC) and was observed range from a minimum value of 19.15 ºC (at 10:15) and 18.63 ºC (at 22:45) after the high water (HW1 and HW2; Figure 3.19 A1), to maximum of 20.34 ºC (at 05:30) and 20.67 ºC (at 18:30) after the low water (LW1 and LW2; Figure 3.19 A1). Moreover,

at spring tidal condition temperature showed maximum and minimum values approximately coinciding with the peak of the tide (low water and high water respectively), while at neap tidal condition temperature is observed to have an evident delay of about one hour after the peak.

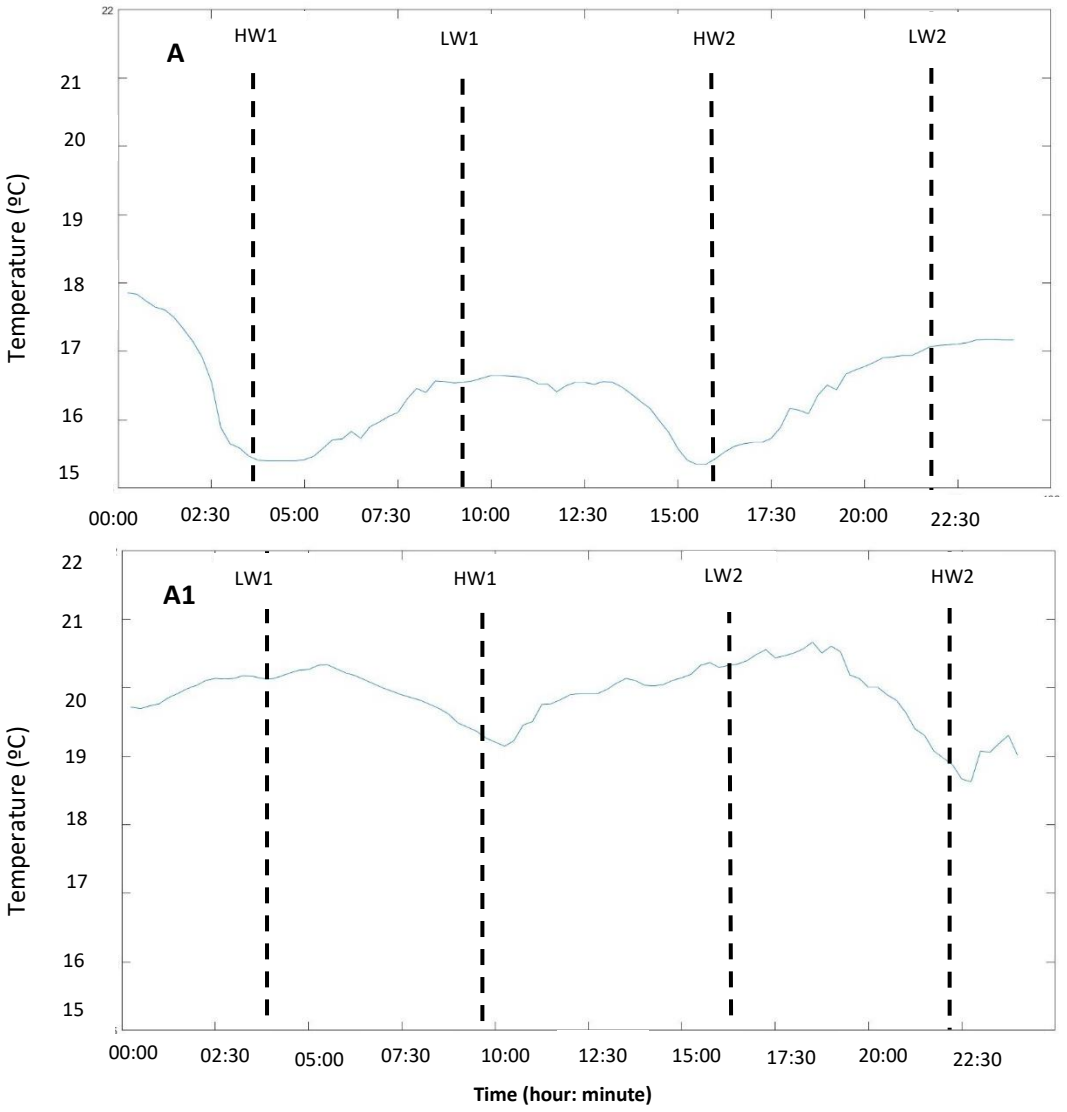

Figure 3.19: Variation of the temperature (ºC) raw timeseries along a semidiurnal tidal cycle in spring 2018, during: A) Spring tide, A1) Neap tide. (HW, high water; LW, low water).

The salinity at spring tidal condition had a minimum value of 36.01 (at 10:45) and 36.04 (at 22:45) after low water (LW1 and LW2; Figure 3.20 B), to maximum value of 36.11 (at 05:30 observed after HW1, and 36.11 (at 14:45) before the HW2 (Figure 3.20 B). The daily variation for salinity, during the neap tidal conditions, (Figure 3.20 B1), had a mean value (36.38) slightly higher than during spring tidal (36.07) (Figure 3.20 B). During neap tidal condition, the salinity showed minimum value of 36.3 (at 10:15) and 36.19 (at 22:30) after the high water

(HW1 and HW2; Figure 3.20 B1), while maximum value of 36.49 (at 05:15) and 36.47 (at 18:30) after low water (LW1 and LW2; Figure 3.20 B1). Moreover, as for the temperature, salinity showed maximum and minimum delayed in relation to the peaks of the tide, both at spring and at neap tidal condition, but in general this delay is more evident at neap tide.

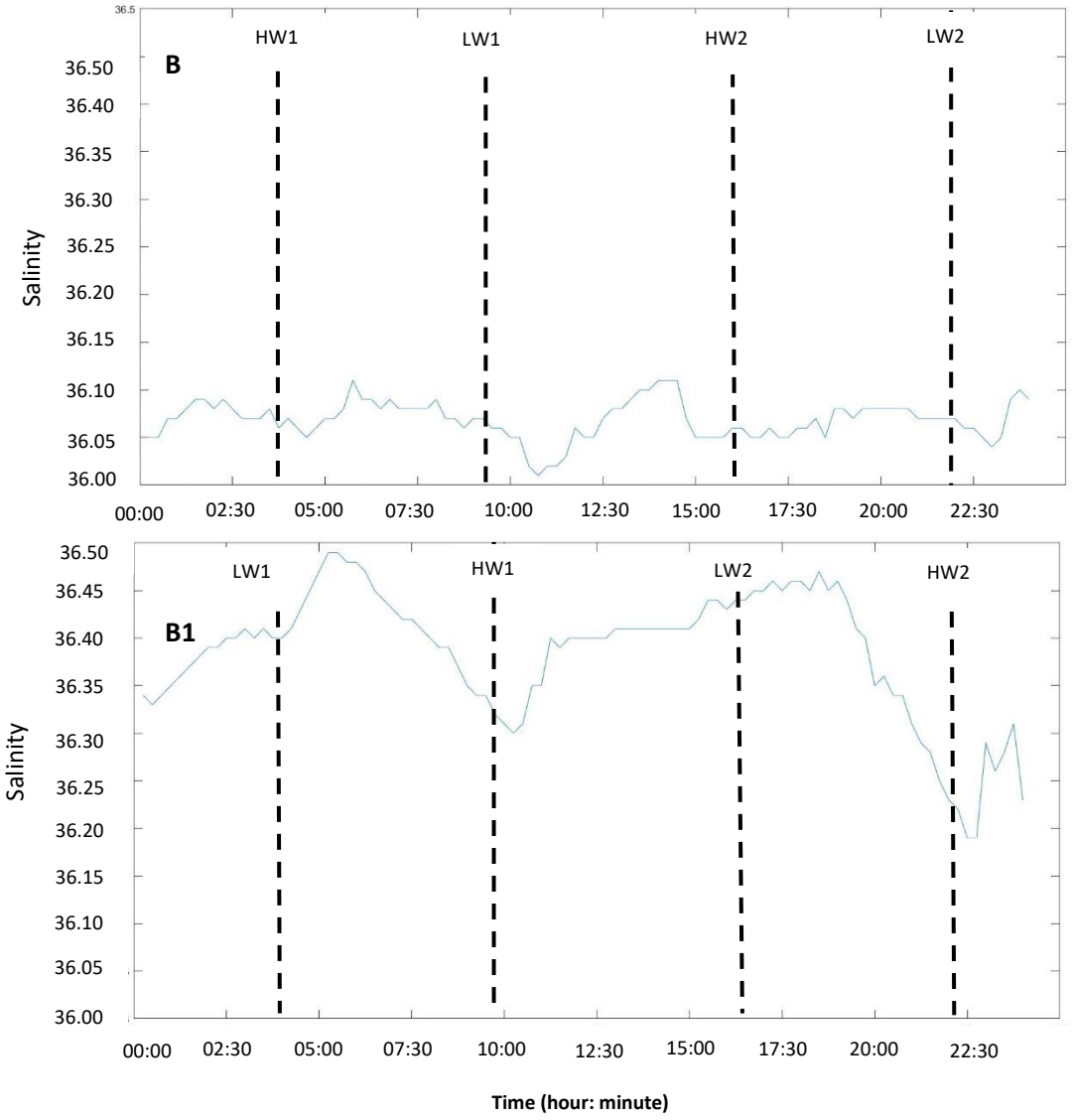

Figure 3.20: Variation of salinity raw timeseries along a semidiurnal tidal cycle in spring 2018. B) Spring tide, B1) Neap tide. (HW, high water; LW, low water).

At spring tidal conditions, the DO minimum mean concentration was 7.21 mg/L with minimum of 6.09 mg/L (at 09:00) and 6.73 mg/L (at 22:15) oserved during the low water (LW1 and LW2; Figure 3.21 C) while a maximum of 7.51 mg/L (at 02:45) is observed before HW1, and 7.83 mg/L (at 19:30) is depicted after HW2 (Figure 3.21 C). Moreover, is observed a offset in the pattern of semidiurnal variation, and the maximum and minimum values of DO delayed

respect the tidal peaks. The mean DO is observed with lower concentration during the neap tidal condition (mean value 5.97 mg/L) than during spring tidal condition. At neap tidal condition, DO minimum of 3.57 mg/L (at 02:00) and 5.06 mg/L (at 17:15) are observed during the low water (LW1 and LW2; Figure 3.21 C1), while the DO maximum of 7.11 mg/L (at 10:30) and 7.64 mg/L (at 22:45) are observed during the high water (HW1 and HW2; Figure 3.21 C1). Despite that, a minimum is observed *ca.* two hours after the HW1 (at 12:00) when DO atteined 4.70 mg/L.

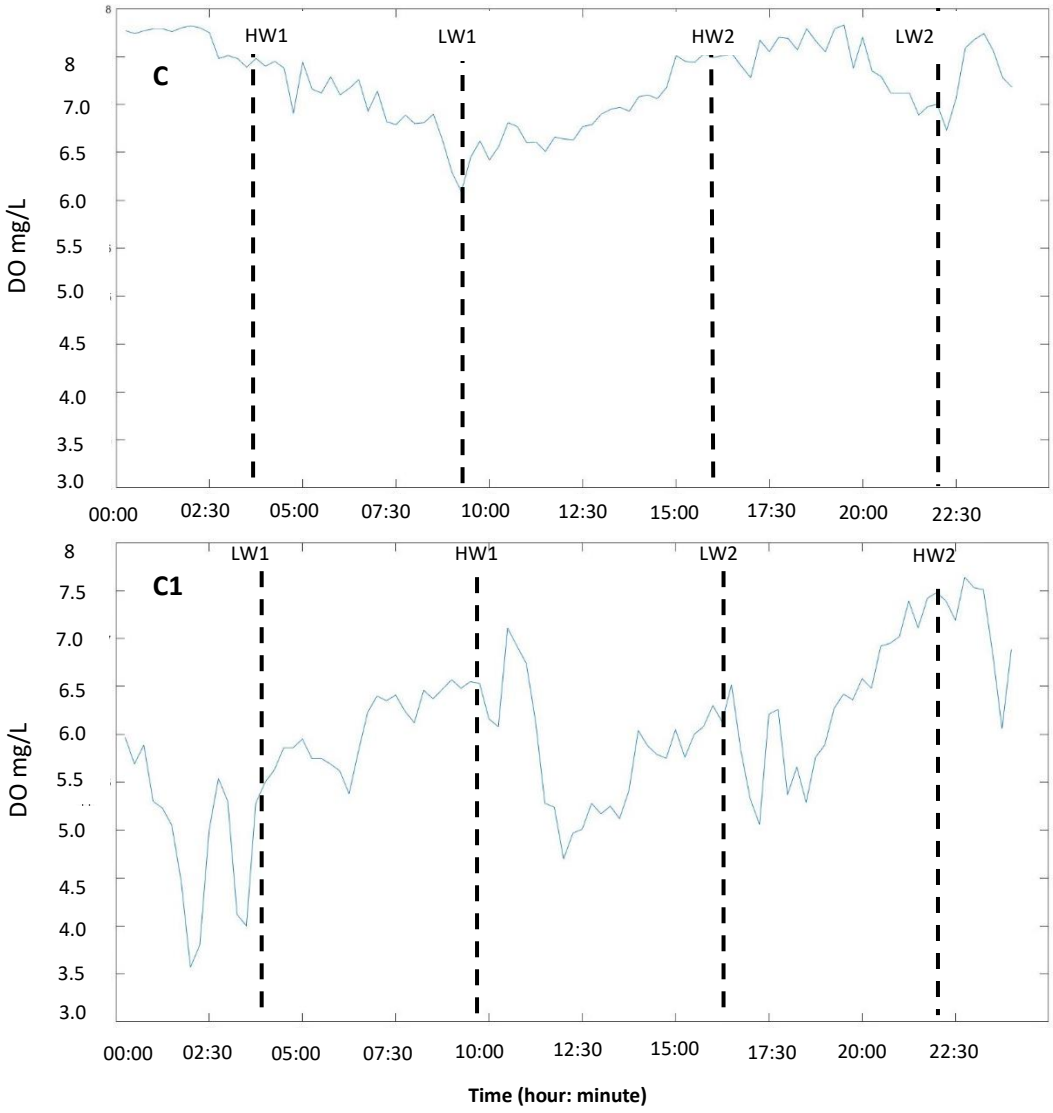

Figure 3.21: Variation of DO (mg/L) raw timeseries along a semidiurnal tidal cycle in spring 2018. C) Spring tide, C1) Neap tide. (HW, high water; LW, low water).

During the spring tidal condition DO in saturation (mean value 91.71 %) had minimum of 77.61 % (at 09:00) and 86.71 % (at 22:15) observed during the low water (LW1 and LW2;

Figure 3.22 D) while maximum was 101.04 % (at 00:45) before the HW1 and 94.26% (at 16:15) approximatley coinciding with the HW2 (Figure 3.22 D). Moreover, one hour after LW2 the saturation in DO is observed atteined the value of *ca.* 100% (at 23:00). As for the DO in concentration a offset was observed in the pattern of semidiurnal variation, and the maximum and minimum values of DO in saturation delayed respect the tidal peaks.

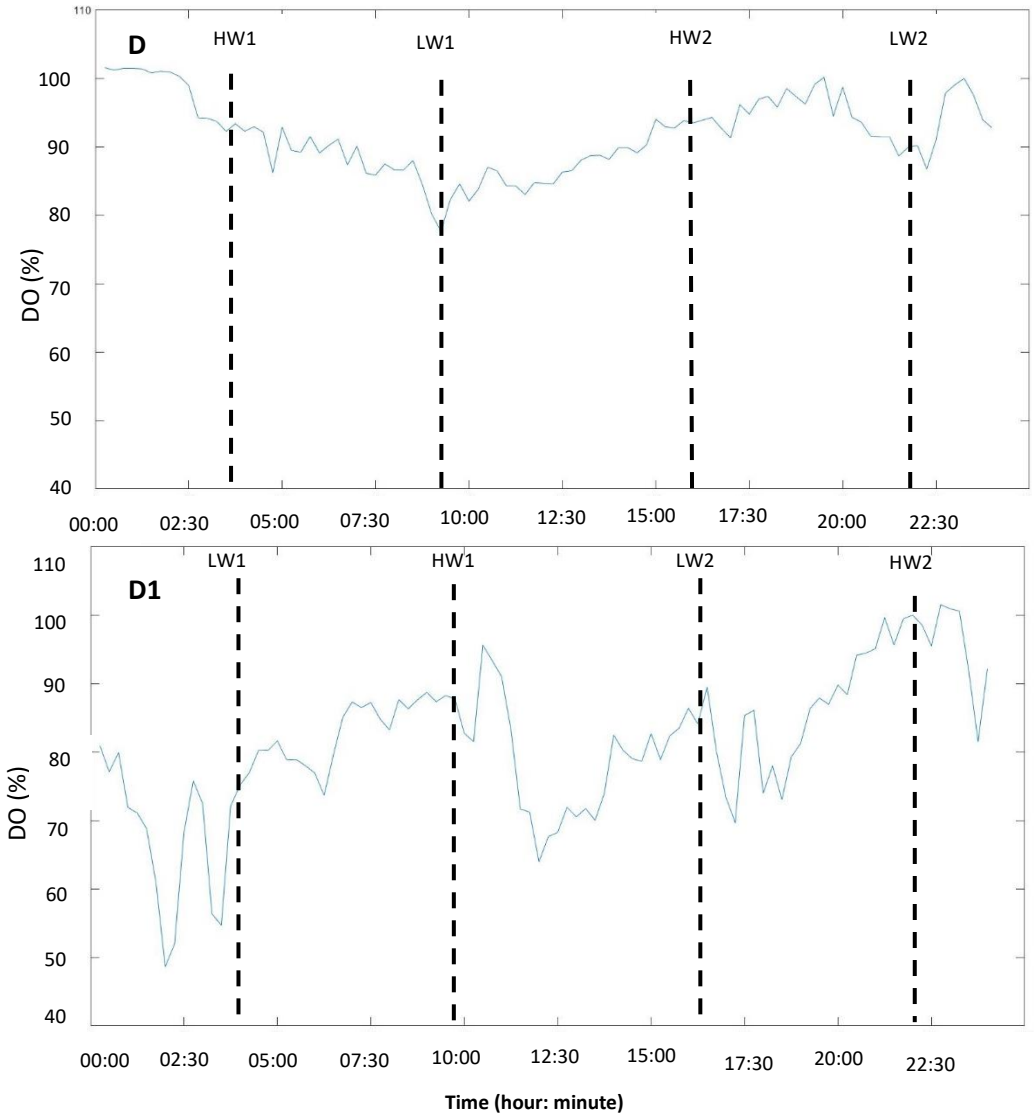

Figure 3.22: Variation of DO (%) raw timeseries along a semidiurnal tidal cycle in spring 2018, during: D) Spring tide, D1) Neap tide. (HW, high water; LW, low water).

The mean saturation in DO during the neap tidal condition was 81.18% with minimum of 48.64 % (at 02:00) and 69.69 % (at 17:15) observed during the low water (LW1 and LW2; Figure 3.22 D1). As for the DO in concentration a minimum is observed two hours after the HW1 (at 12:00) when the saturation in DO was 63.93% (Figures 3.22 D1). Maximum DO of 95.55 %

(at 10:30) and 101.50 % (at 22:45) were observed after the high water (HW1 and HW2; Figure 3.22 D1). Regarding pH, at spring tidal conditions its showed with minimum of 8.00 (at 10:00) and 8.01 (at 22:15) during the low water (LW1 and LW2; Figure 3.23 E) and maximum of 8.18 (at 02:00) and 8.17 (at 23:00) during the high water (HW1 and HW2; Figure 3.23 E). The mean value of pH at spring tidal condition (8.10) was sligthly higher than the one observed at neap tidal condition (8.04). At neap tidal condition pH ranged between minimum of 7.84 (at 03:15) and 7.98 (at 15:15) during the low water (LW1 and LW2; Figure 3.23 E1) and maximum of 8.09 (at 09:45) and 8.13 (at 21:45) during the high water (HW1, HW2; Figure 3.23 E1). Moreover, no significant offset between the tidal peaks and pH values is observed at both spring and neap tidal conditions.

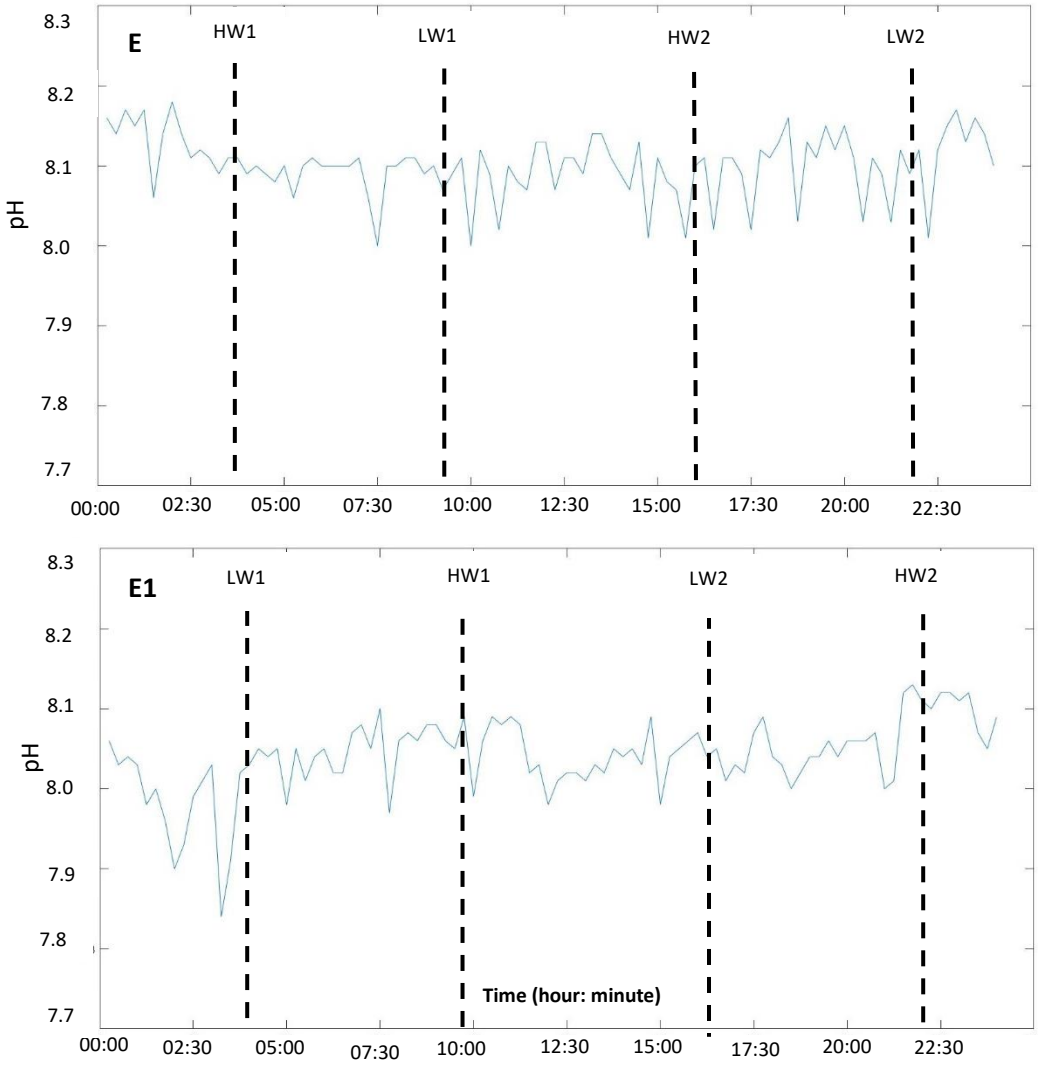

Figure 3.23: Variation of the pH raw timeseries along a semidiurnal tidal cycle in spring 2018, during: up) Spring tide, bottom) Neap tide. (HW, high water; LW, low

Daily variations in chlorophyll *a* concentration are observed in spring tidal conditions, with the minimum of 0.13 µg/L (at 09:30) and 0.17 µg/L (at 9:30) during the low water (LW1 and LW2; Figure 3.24 F) and maximum of 3.88 µg/L (at 03:45) and 3.70 µg/L (at 17:45) after the high water (HW1 and HW2; Figure 3.24 F). The Chl *a* mean value at spring tidal condition was 1.08 µg/L. Moreover, a delay (about two hours) is observed between the highest Chl *a* values and the peaks of the high tide (e.g. HW2). During neap tidal condition, daily variation in Chl *a* concentration showed values below the zero which were considered unrealistic as stated in Material and Methods.

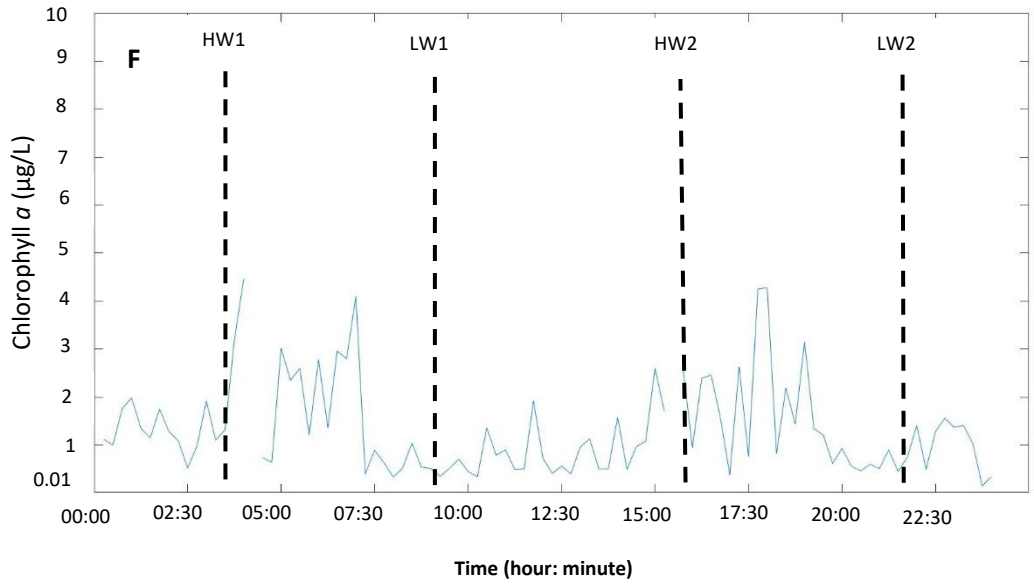

Figure 3.24: Variation of chlorophyll *a* (µg/L) along a semidiurnal tidal cycle in spring 2018: F) Spring tide. (HW, high water; LW, low water).

With a mean value of 0.95 NTU, the turbidity is showed highly variable at spring tidal condition (Figure 3.25 G), with approximately the same pattern of variation for the low water (LW1, LW2) and for the high water (HW1, HW2). However, the highest values are oserved during the HW1 (2.26 NTU; at 03:00), LW1 (2.84 NTU; at 09:30) and HW2 (2.64 NTU; at 14:45) while the lowest values are observed during the LW2 (1.06 NTU; at 22:45). A delay between the tidal peaks and turbidity maximum/minimum is observed (about one hour). As for Chl *a* during neap tide, daily variation in water transparency showed values below the zero which were considered unrealistic.

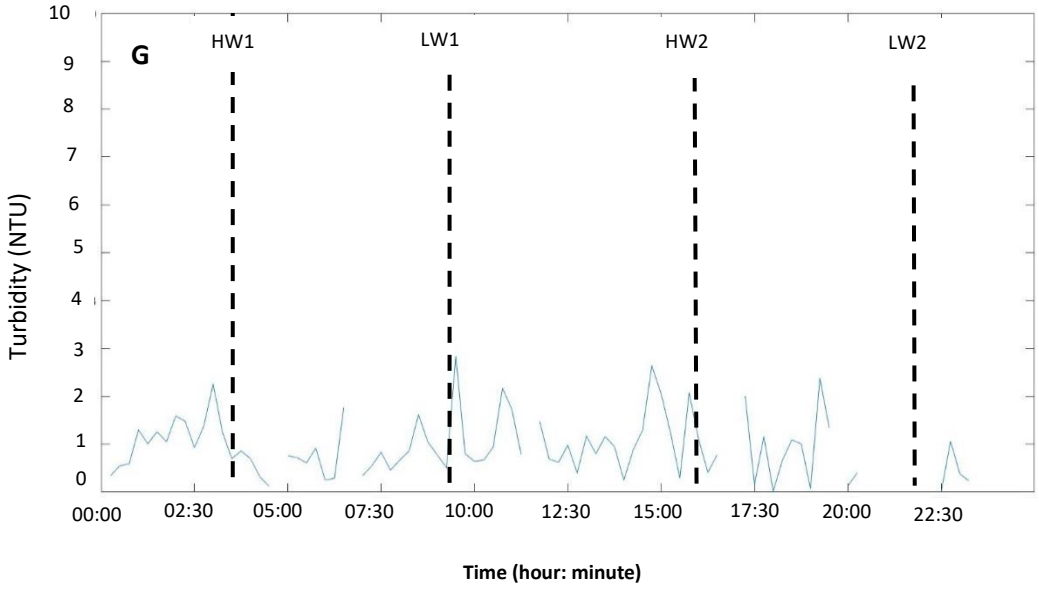

Figure 3.25: Variation of turbidity (NTU) along a semidiurnal tidal cycle in spring 2018: G) Spring tide. (HW, high water; LW, low water).

3.3 Relationship between variables

With the aim to characterize in detail the relationships between variables, all the *Nan* values, as well as the unrealistic values and the gaps were removed from the timeseries. Most of the parameters recorded by the multiparametric probe during the two years of measurements were correlated, since the parameters were dependent from each other and the number of observations were very high. Only the more significant relations in terms of physical-chemical and biological processes were analysed resulting with a total of 13 significant relationship observed ($p \leq 0.05$). Regarding temperature it is observed significantly negative correlated with DO (Figure 3.26 A), and pH (Figure 3.26 B) while it is depicted positive correlated with salinity (Figure 3.26 C) and chlorophyll *a* (Figure 3.26 D). As mentioned in literature, the increase in water temperature leads to an increase in salinity and to a decrease in the DO solubility. The reduced solubility in DO induced by rises in temperature leads to a significant pH decrease (Figure 3.27 H), not only due to the reduced availability of DO in the system, but also because in warmer period the respiration also increase coupled with increase the ability of water to ionise and form more hydrogen ions. Moreover, the positive relationship observed between temperature and chlorophyll *a* is indicating that more intense phytoplankton growth occured during warmer periods, leading to an increased in chlorophyll *a* as a proxy of phytoplankton biomass. In the case of chlorophyll *a* it is observed significantly positive correlated with pH (Figure 3.26 E), salinity (Figure 3.26 F), and in particular with DO (Figure 3.27 G), as a consequence of the increase of the photosynthesis process which leads to an increase in DO and pH. In addition, the positive relation between Chl *a* and salinity may be indicating import from the adjacent coastal Ocean. Dissolved Oxygen is found also positive correlated with turbidity (Figure 3.27 J) and negative correlated with salinity. These releationships are pointing that particulate matter in the water column is associate with phytoplankton biomass, as expressed by the positive correlation between chlorophyll *a* and turbidity (Figure 3.27 K), and as said before that during the warmer period the DO decrease while the salinity increase. Turbidity resulted negatively correlated with salinity (Figure 3.27 M) indicating a decrease in water transparency due to the introduction of debris associated to land run off after heavy precipitations which lead to a salinity decrease (but also to an increase of chlorophyll *a* confirming the positive relation with salinity). Moreover, turbidity was negative correlated with pH (Figure 3.28 N) showing that turbid water which contain organic matter leads to a pH decrease, but also that turbid water doesn't let the light penetrate which can limited the

photosyntesys process, the phytoplankton growth, and consequently as said before the availability of DO in the system, leading to a pH decrease.

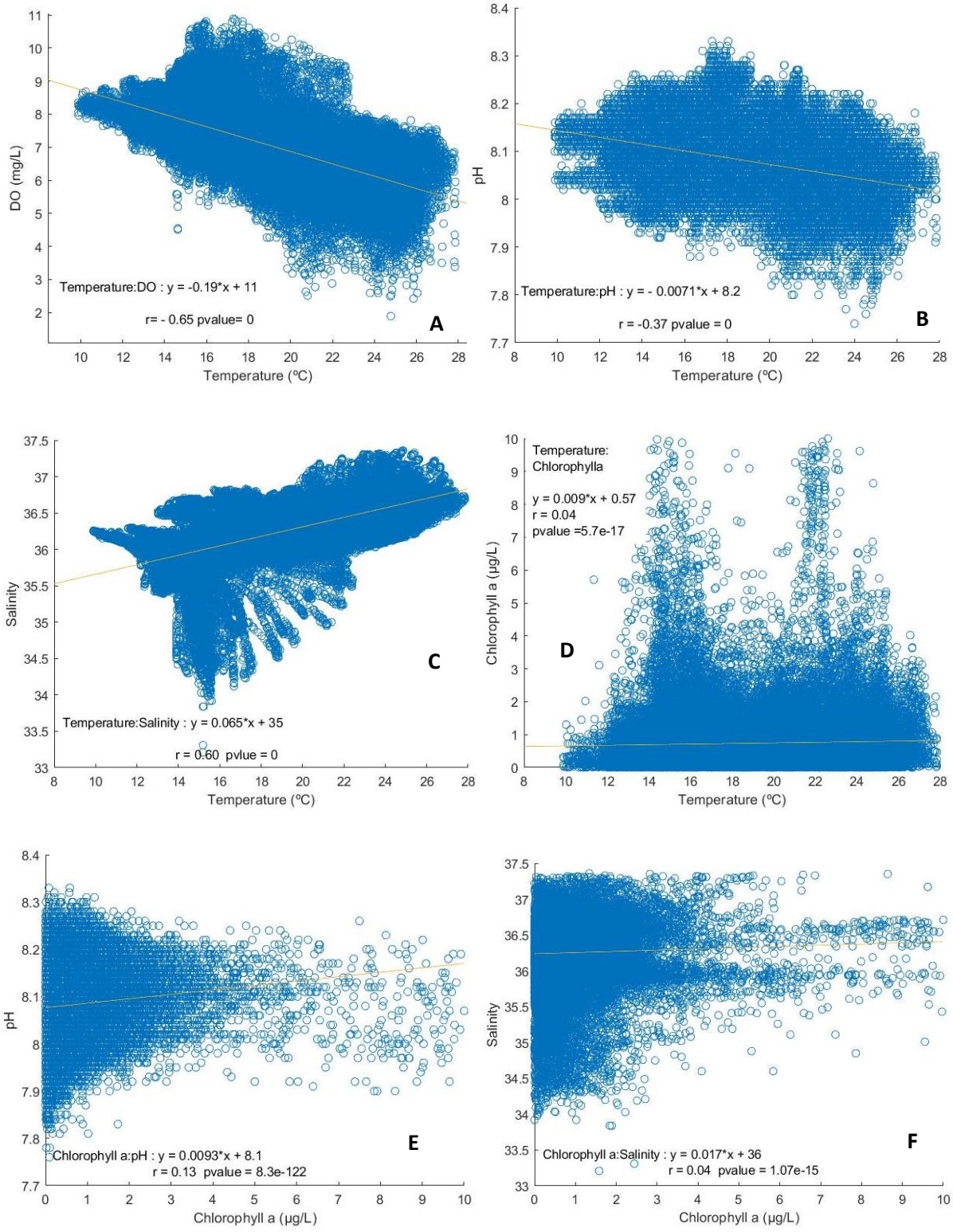

Figure 3.26: Significant relationship between variables; in each plot is indicated the equation of the linear fit, the r and p values.

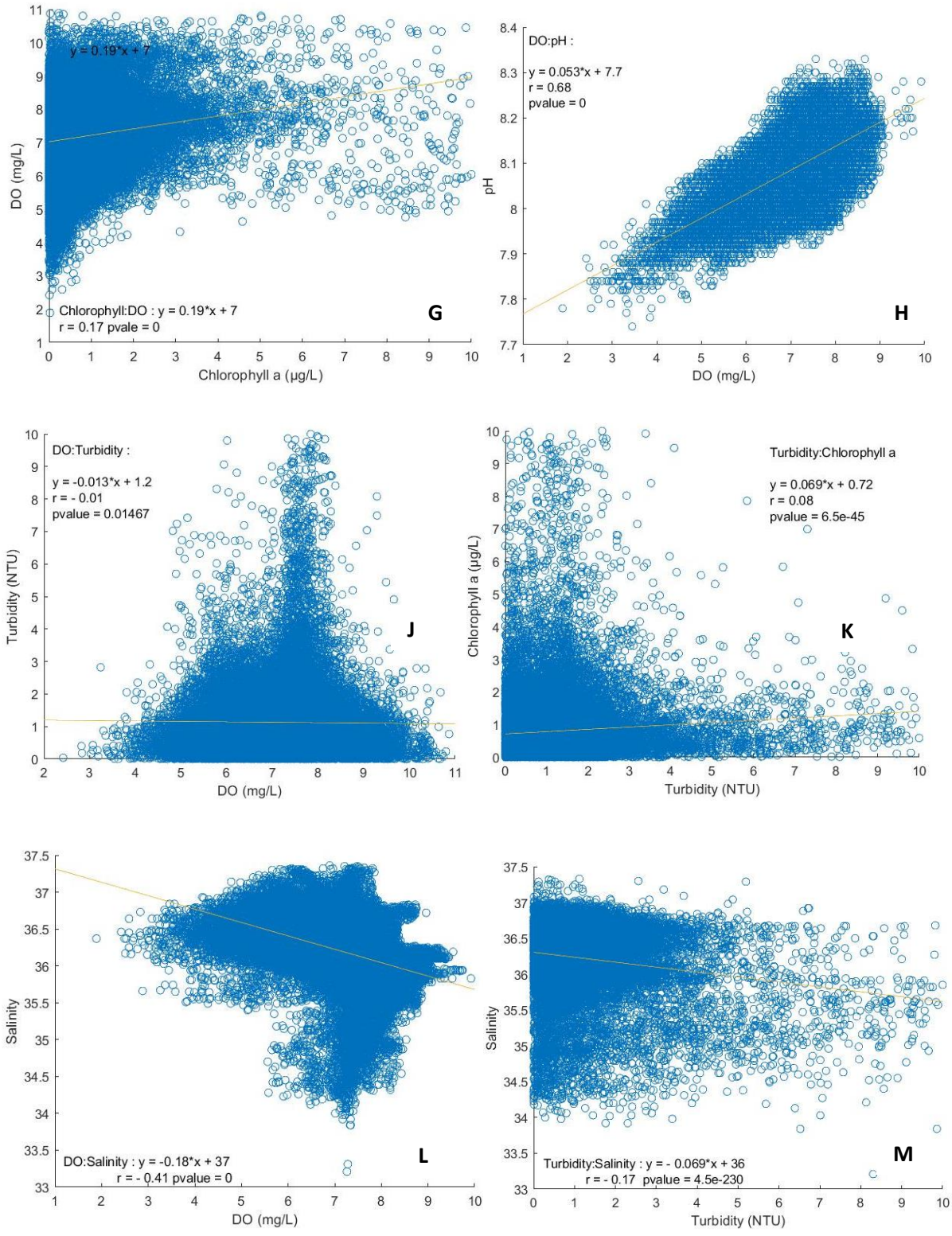

Figure 3.27: Significant relationship between variables; in each plot is indicated the equation of the linear fit, the r and p values.

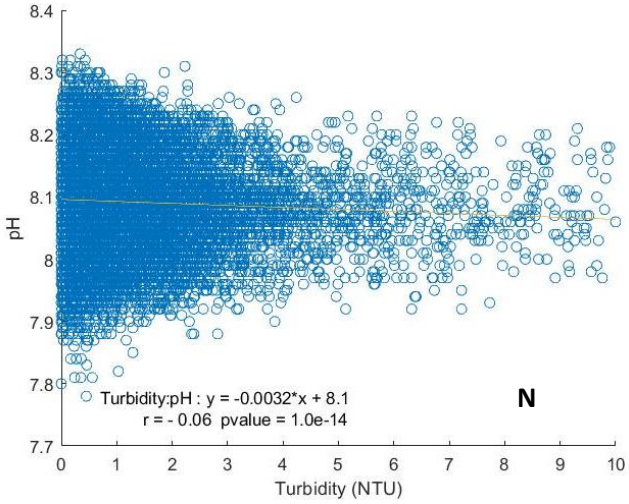

Figure 3.28: Significant relationship between variables; in each plot is indicated the equation of the linear fit, the r and p values.

4. Discussion

4.1 Oceanographic and meteorological conditions

The Ria Formosa is an ecosystem in permanent connection with the adjacent ocean through its inlets, representing a dynamic and variable coastal lagoon, where the interplaying of biogeochemical processes in the lagoon with the ocean are pivotal for the system functioning (Alcântara *et al.*, 2012). The mesoscale events occurring along the coast may superimpose the tidal processes (Rosa *et al*., 2019) revealing the importance of the fully awareness about these occurences on the coast to better understand the temporal variability of the physical, chemical and biological parameters.

The result of the cross covariance function (Figure 3.1) showed a negative correlation between the temperature and the West-East wind component. Only the West-East components of the wind time series were used, because they are the ones that induce the alternation between upwelling (Fiúza, 1982; Relvas and Barton, 2002, Loureiro *et al*., 2005; Cardeira *et al*., 2013) and inshore countercurrent (and the associated downwelling) in the coastline with West-East orientation on the south coast of Portugal (Relvas and Barton 2002; Garcia *et al.*, 2006; Garel *et al*., 2016). The cross-covariance function (Figure 3.1) confirmed that wind with the West component (positive) leads to a decrease in water temperature (Figure 3.2). Moreover, the cross covariance function showed that there is a mean delay of 3 days (72 h), before the wind leads the oceanic water to cool due to an upwelling event. This lag is in accordance to Fiúza *et al.* (1982) that reported a time lag from 1 to 2.5 days. This difference of 0.5 day could be explained by the different considered study areas, coastal waters along the Portuguese coast in the former case, and an inner area of Ria Formosa, as in the present study. With this knowledge, it was possible to identify a total of 22 coastal upwelling events, and 23 countercurrent events during the two years of real time monitoring (Figure 3.2).

The satellite data of level 3 (L3), showed that the upwelling (UP-1, UP-2, UP-3; Figures 3.3, 3.5, 3.8) and countercurrent (CC-1, CC-2, CC-3; Figures 3.4, 3.6, 3.7) influenced both the SST values and chlorophyll *a* concentration. The upwelling events, also supported by the wind stick plot (Figure 3.2), were observed mainly during spring (2018, 2019) and late summer (2017, 2018), corresponding to a period between March and October as reported by other authors (Fiúza *et al.* 1982; Relvas and Barton 2002; Rosa *et al*., 2019).

For instance, the event UP-1 (Figure 3.3) originated in the West coast of Portugal, and extended eastwards along the shelf of the southern coast after being forced by northerly winds, as reported byFiuza *et al.*(1982) led to a decrease in the SST of *ca.* 3º C in front of Ria Formosa, and afterwards to an increase in Chl *a,* which attained values of *ca.* 2 µg/L. This is a common situation in consequence of persistent upwelling in the West coast of Portugal, mainly observed in summer (Relvas and Barton, 2002). Moreover, during the events UP-2 and UP- 3 (Figures 3.5, 3.8) generated by westerlies (*ca.* 10 m/s; Figure 3.2) colder coastal water was observed to be extended along the entire south coast while the warm coastal water circulating from Gulf of Cadiz was pushed offshore, as reported by Relvas and Barton (2002). During these events, the water attained minimal values of *ca.* 15 ºC.

The UP-3 event (Figure 3.8) which occurred under persistent but low wind intensity (< 10 m/s; Figure 3.2) from the begin of April 2018, and particularly in May 2018, showed that upwelling continued to occur during a period of wind relaxation as reported by Relvas and Barton (2002). Moreover, coinciding with UP-3, chlorophyll *a* reached the highest values in the proximal coastal area compared to the other analyzed upwelling events (Figures 3.3, 3.5, 3.8) confirming that the wind intensity along the UP-3 was low, able to allow the phytoplankton growth. The wind, responsible for the rising of upwelling water from deeper levels (due to the vertical motion) is a factor which may influence the surface water stability and consequently the Chl *a* concentration (Ketchum, 1954; Valiela *et al*., 1997; Wilkerson *et al*., 2006). Therefore, after upwelling (Figures 3.3, 3.5, 3.8), and under optimal conditions of light and nutrients availability, chlorophyll *a* showed higher concentration in the proximal area (>10 µg/L) than in front of Ria Formosa (*ca.* 2 µg/L; Figures 3.3, 3.5, 3.8), in a range typically found in the Ria Formosa with a delay of few days (Cravo *et al*., 2014). It has been reported that coastal upwelling can leave a fingerprint inside Ria Formosa, such as lower water temperature and higher concentration in Chl *a* (Cravo *et al*., 2014). This phenomena was found to be extended at least *ca.* 6 km upstream from the main inlets, setting up its biological productivity (Alcântara *et al.*, 2012; Cravo *et al.*, 2013b, 2014, 2019).

Under periods of wind relaxation and predominantly under easterlies (Figure 3.2), the warm counter current was observed (Figures 3.4, 3.6. 3.7) that significantly influence water temperature and chlorophyll *a* concentration, as frequently reported by other authors for the Gulf of Cadiz region (Garcia *et al.*, 2006; Garel *et al.* 2016). This was responsible for the temperature increase in front of Ria Formosa, where the maximum values attained *ca.* 25 ºC, values confirmed by the satellite images (Figures 3.4, 3.6, 3.7). The westward countercurrent

did not promote the phytoplankton growth, since these warm waters usually are impoverished in nutrients and considered oligotrophic, leading to a general decrease of the biological productivity (Navarro *et al.*, 2006; Rosa *et al.*, 2016), inducing a decrease in Chl *a* concentration as it was observed during CC-1 CC-2 and CC-3 (Figures 3.4, 3.6, 3.7) when the lowest values ranged between *ca.* 0.1-0.5 µg/L.

In addition, the contribution and intensity of the meteorological conditions, mainly the precipitation showed to have a key role on the variability of the studied parameters. For instance, the average precipitation occurred was particularly intense in March 2018 (Annex 2). It was reported that under events of higher freshwater contribution, a strong chemical gradient may occur in this system, which is not observed beyond the region where the coastal and oceanic waters interact (Cardeira *et al*., 2013). However, under weak river discharges, such as during spring and summer months, in coastal waters the biogeochemical characteristics are governed mainly by seasonal processes and/or pulses of upwelling and relaxation events (Relvas and Barton, 2002; Sanchez *et al*., 2006; Garel *et al*., 2016).

4.2 Seasonal variability of temperature, salinity, DO, pH, Chl *a* and turbidity

The temporal variation of water temperature depicted a marked seasonal cycle, as expected in a shallow water system such as Ria Formosa. It attained minimum values during winter and maximum values during summer, clearly reflecting the variation of the annual variation of solar radiation (Figure 3.9 A, Annex 1 A, Table 3.2), like reported by Barbosa (2010). Moreover, from the results of the spectral analysis of temperature and DO (Figures 3.13 A, C) a peak in spectral density of energy was observed associated with the solar annual variation. At a seasonal scale, this variation had the strongest signal in the temperature and dissolved oxygen periodograms (due to the negative relationship with temperature; Figure 3.26 A). With a defined frequency of 365 days, the solar annual variation effect was pointed out; clearly visible either in the filtered or raw time series (Figures 3.9 A; 3.10 C and Annex 1 A and C).

The range in temperature presented in this work, 9.88-27.85 ºC (Table 3.2), did not exhibit a generalized warming trend but similar values to those reported in historic datasets such as CEPASA (1980); Newton (1995); Alcântara *et al*. (2012), Brito *et al*. (2012). The highest oscillation in water observed in spring (from *ca.* 15 ºC to *ca*. 21 ºC) and in summer (from *ca.* 15 ºC to *ca*. 27 ºC) was associated with the alternation between upwelling and countercurrent

as found by Relvas and Barton (2002) and by Garel *et al.* (2016). Due to reduced freshwater inputs and elevated tidal exchanges, the lagoon is basically euryhaline (S~36; Table 3.2), and major salinity decreases are associated with heavy rainfall events, like during the storm period in March 2018 (total precipitation of 118 mm, IPMA, Annex 2) when the salinity minimum (*ca.* 33, Table 3.2; Figure 3.9 B) was recorded. The same evidence was already pointed out by other authors (Newton and Mudge 2003; Mudge *et al.*, 2008). Neverthless, salinity seasonal variability was closely related to water (and atmospheric) temperature, as it is confirmed by the strong positive correlations between those two parameters (Figure 3.26 C). The highest salinity values were recorded during the warmest period, when evaporative processes can be more relevant probably starting in late spring, with a continuos increase along the summer, when more saline water was formed, as reported by Newton and Mudge (2003). The maximum value (> 37; Table 3.2) was recorded around the beginning of the measurements on July 2017 (Figure 3.9 B, Annex 1 B), confirming that salinity attained the highest values in summer (Rosa *et al*., 2019).

The range of DO was typical for this system (Falcão and Vale, 2003; Newton and Mudge, 2003; Barbosa, 2010) and DO seasonal variability (Figures 3.10 C, D) mostly depended on the temperature and salinity variation, confirmed by the two negative relationships with DO (Figure 3.26 A, and 3.27 L). The lowest values were found in summer (August 2018 1.89 mg/L; Table 3.2), due to the reduced solubility of oxygen in warm water along with intensified metabolic and respiration processes, when DO ranged from 8.87 mg/L down to 1.89 mg/L. The low concentrations of oxygen observed during summer could also be explained by high rates of bacterial degradation as reported by Pereira *et al.* (2007) in the western sector of Ria Formosa. The highest values were observed in winter/spring when the water attained a maximum in spring (10.88 mg/L May 2018). This high variability during spring reflected the DO interplay between the dominant physical, chemical and biological processes. During spring the biological productivity is usually more intense along with more frequent upwelling events (Relvas and Barton, 2002) and light availability (Barbosa, 2010), with consequent intensification of the photosynthetic process. This fact also leads to an increase in the pH (due to CO_2 removal), as confirmed by the positive correlation between the concentration of DO, pH and the phytoplankton active biomass, expressed by the clorophyll *a* concentration (Figures 3.26 E and 3.27 G, H).

Along the entire period of study a small range of variation of pH values was observed (7.74-8.33; Figure 3.11 E, Annex 1 E), typical of coastal waters, and in agreement with the hystorical

observations (Valença *et al.,* 2011; Alcântara *et al.,* 2012). In general, the pH timeseries showed a pattern similar that of the DO variation at seasonal scale, with an increase from autumn (maximum value 8.33 November 2017), continuing through the winter (2017/2018) until the spring (2018), while it showed a general decrease in summer (2017), as explained before. The pH was observed to have a strong positive correlation with DO (Figure 3.27 H), and a negative relation with water temperature (Figure 3.26 B) and turbidity (Figure 3.28 N), showing that warm and turbid water (during summer) leads to a reduced light penetration and a decrease of the photosynthetic rates (DO availability) and consequently of the pH (Cravo *et al*., 2020) or that turbid water enriched in organic matter leads to a pH decrease.

Regarding Chl *a* and turbidity, since these parameters are measured by fluorescence sensors they can easily suffer interference from other fluorescent compounds, as suspended solids (including humic substances) occurring after runoff due to precipitation (Garel *et al*., 2009). This may explain why these parameters had some extremely high values (Annex 1 H and J). Those values were considered unrealistic and removed from the data set, as described in Material and methods chapter.

High variability of Chl *a* was observed at seasonal or even inter-annual scales, as confirmed in several studies (Falcão and Vale, 2003; Newton and Mudge, 2003; Loureiro *et al.*, 2005, 2006; Brito *et al.*, 2010, 2012; Alcântara *et al*., 2012; Cravo *et al.*, 2014). In this work the chlorophyll *a* concentration range (Table 3.2) is in agreement with historical datasets, where chlorophyll *a* ranged from 0 to values >12 µg/L between 1967 and 2013 (Brito *et al*., 2012; Rodrigues *et al*., 2017). Close the monitoring station, the phytoplankton growth followed the availability of light, temperature and nutrients, since the Chl *a* showed highest values, particularly during spring and summer (as expressed by the positive relationship between Chl *a* and temperature; Figure 3.26 D) like reported by a study of Barbosa (2010). Maximum values in chlorophyll *a* of *ca.* 10 µg/L can be considered high and typical of algal bloom periods, since average values close to the Ria Formosa inlets are generally < 2 µg/L as mentioned before and concentration typical of an upwelling event can get *ca.* 5 µg/L (Brito *et al.*, 2012). This suggests that under upwelling conditions there is fertilization of the Ria Formosa due to an import of Chl *a* from the adjacent ocean to the lagoon (Brito *et al.*, 2012, Cravo *et al.,* 2014) which can be supported by the positive relation between Chl *a* and salinity (Figure 3.26 F). An increase in Chl *a* (Figure 3.11 F) was also observed after a period of heavy precipitation in spring that may derived to some extent from agricultural runoff to Ria Formosa that will increase the availability of nutrients after organic matter remineralization, as previously reported by Newton *et al.* (2003)

and Bebianno (1995). Chlorophyll *a* also showed a generalized interannual declining trend during autumn and winter. This decline may be eventually related to the winter cooling tendency and decrease in light. The relatively low concentrations of chlorophyll *a* observed in the Ria Formosa (usually < 2 µg/L) can also be associated with the shellfish communities, organisms that can remove part of the primary producers from the water column by filtration (Brito, *et al*., 2012) or by the nutrients absorption in the salt marsh sediment on the intertidal area (Serpa *et al.,* 2007; Sousa *et al.,* 2010).

Turbidity was highly variable at a seasonal scale, often following the pattern of Chl *a* variability as confirmed by the direct relationship between those parameters (Figure 3.27 K). The turbid water was not only related to algal bloom events (Koch, 2001) which increased the concentration of Chl *a*, but also due to the transport of allochthonous suspended solids (debris included organic matter, DOM; Erena *et al.*, 2019) during rainfall events (Figure 3.12 G, Annex 2). It is observed after period of storms in spring 2018 (minimum of salinity) and confirmed by the negative relation with salinity (Figure 3.27 M). However, in the present work the turbidity values were mostly observed < 5 NTU (Table 3.2), typical of clean coastal waters, as it is confirmed in a study by Barbosa (2010), where the euphotic zone during most occasions (99%) was extended up to the bottom.

4.3 Diurnal, semidiurnal, and fortnightly variability

In Ria Formosa the water parameters are strongly influenced, not only at a seasonal and interannual scale, but also due to the effect of shorter temporal scales such at diurnal, semidiurnal and fortnighlty scales (Dias and Sousa; 2009). This is can be observed through high frequency observations, as it was the case with data acquisition every 15 min by the multiparametric probe installed in the Ria Formosa for more than two years, usually not possible when conventional water sampling strategies are applied. The solar diurnal cycle revealed to be an important constituent upon the variability of the studied parameters (Figures 3.13; 3.14). For instance, phytoplankton growth echoed by chlorophyll *a* concentration is controlled by the availability of light during the diurnal solar cycle, what can be seen in Figure 3.14 F, and confirmed in several studies (e.g. Alvarez, 2004; Cloern and Dufford 2005; Gasol *et al.* 2008).

It is important to remark the fact that, at daily scale, the diurnal solar radiation was observed to affect the temperature, chlorophyll *a*, DO, and pH with higher magnitude than the diurnal lunar tidal constituent. Temperature and DO presented a strong diurnal component depending on the daily insulation (Figures 3.13 A, C), as it was also confirmed by Garel and Ferreira (2011), through measurements acquired by a monitoring station at the Guadiana low estuary. For temperature, it means that the water get warmer during the day and cooler during the night period. Chlorophyll *a*, DO and to some extent pH also present a daily variation (also confirmed by the established significant relationships), due to their dependence on solar radiation controling photosynthesis reflected in higher chlorophyll *a* concentrations during the day, like reported for Ria Formosa by Barbosa (2010) and indirectly by respiration, showing lower oxygen concentration and generally lower pH during the night (when respiration is predominant).

Ria Formosa as a semidiurnal mesotidal system, without important contribution of freshwater, that experiences intense mass exchanges with the sea (40–75%) during each semi-diurnal tidal cycle (Falcão and Vale 2003) making this system well mixed (Alcântara *et al*., 2012), with higher water renewal than the microtidal coastal lagoons from the Mediterranean basin, where the tidal influence is reduced (Newton and Mudge, 2003; Cañedo-Argüelles *et al*., 2012). The semidiurnal tidal cycle evidently influenced temperature, salinity, DO in concentration and pH (Figures 3.13 A, B, C D and 3.14 E), as well as Chl *a* and turbidity (Figures 3.14 F, G). This effect was already pointed out by several authors, not only for this ecosystem (e.g. Falcão and Vale, 1990, 1998, 2003; Newton and Mudge, 2003; Loureiro *et al*., 2006; Pereira *et al*., 2007; Cravo *et al*., 2014, 2015), but also for other important estuarine system on the south coast of Portugal, at the Guadiana low estuary (Garel and Ferreira, 2011). Temperature and salinity showed lowest values during the high water and highest values during the low water (Figures 3.19 A, A1; and 3.20 B, B1), as reported by Loureiro *et al*. (2006) in the western sector of Ria Formosa. It suggests that the influence of freshwater is relatively low, not sufficiently high to decrease the salinity during ebb. Even, as this is a shallow system, at high water the volume of water coming from the ocean is high enough to slightly decrease the temperature and salinity (Figures 3.19 A, A1; and 3.20 B, B1), as reported by Newton and Mudge (2003).

Regarding DO, pH and Chl *a* (Figures 3.21 C, C1; 3.22 D, D1; 3.23 E, E1 and 3.24 F) these parameters had the highest values during the high water and lowest values during the low water, while turbidity showed to be highly variable along the tidal cycles (Figure 3.25 G). The lowest DO and pH values at low water during the night reflect the effect of the restriction of mixing

and circulation in a period when the presence or availability of organic matter can be stronger in a much shallow water column. The same trend has been found by several authors in Ria Formosa (e.g Machás and Santos, 1999; Newton *et al*., 2003; Mudge *et al*., 2007; Serpa *et al*., 2007; Gamito, 2008, Cravo *et al*., 2020).

It is reported that low values of Chl *a* at low water can also lead to an export to the coastal ocean waters (Falcão and Vale, 2003) or by a general nutrients impoverishment after their consumption limiting afterwards phytoplankton growth (Brito *et al.*, 2012). During the high water, the DO increase can be associated with the inflow of oxygenated water coming from the ocean with lower concentration in organic matter. Moreover, high concentration in Chl *a* at high water can indicate an import from the Ocean to the lagoon, leading to an increase of DO and, indirectly, to an increase of the pH by the reasons already indicated. This suggests a fertilization of Ria Formosa, impacting the water characteristics (Cravo *et al.*, 2013b; Cravo *et al.*, 2014) such as pH, DO but also turbidity due to their positive relationships, also found by Cravo *et al*. (2020). Furthermore, during the high water at night the recording of high DO (Figures 3.21 C, and 3.22 D) and Chl *a* concentration (Figure 3.24 F) values could be associated with a period of upwelling, when there was a decrease of temperature (Figure 13.19 A).

In addition, due to the response of Ria Formosa to the semidiurnal tidal forcing, at the monitoring station it was observed the overtide M4. The generation of M4 is local and depended on factors such bottom friction and channels cross-sectional area and complexity (Aubrey and Speer, 1985; Salles *et al*., 2005). In shallow areas, such where the monitoring station was located there were a strong attenuation of M2 tidal constituent while the M4, resulted amplified inducing tidal asymmetry (Dias and Sousa, 2009). Due to these factors, the semidiurnal tidal wave has a phase delay of 1.2 hours, from the Faro Inlet to Faro city (Dias and Sousa, 2009), which influences also the values of the water parameters (Figures 3.19, 3.20, 3.21, 3.22). The M4 influenced the magnitude of variation of all the studied parameters, but in general with smaller contribuition than the effect of the semidiurnal or the fortnight tidal constituents (Figures 3.13, 3.14), as confirmed either by Dias and Sousa (2009) in the western sector of Ria Formosa or by Garel and Ferreira (2011) in the estuarine system of Guadiana low estuary. The delay in the phase of the tidal wave induced by non-tidal factors was also observed during the spring and neap tidal condition, when a offset of few days were depicted between the maximum/minimum values, and the maximal tidal excursion, as it was observed at Guadiana low estuary (Garel and Ferreira, 2011).

At a fortnightly scale the tide has caused important variations in all the studied parameters, but especially in turbidity (Figure 3.14 G), DO (%) (Figure 3.13 D), pH, (Figure 3.14 E) and Chl *a* (Figure 3.14 F), with a higher magnitude of variation than on the semidiurnal scale. It was depicted that turbidity (Figure 3.25 G), DO (Figures 3.21 C, C1 3.22 D,D1), pH (Figure 3.23 E, E1) and Chl *a* (Figure 3.24 F) had the highest values at spring tidal conditions and the lowest at neap tidal conditions. During neap tidal conditions, turbidity and Chl *a* were very low, recorded as less than zero which were considered unrealistic and removed from the record, as referred in the Material and Methods chapter. Temperature (Figure 3.13 A) and salinity (Figure 3.13 B) showed an important peak at the fortnightly frequency, but with lower magnitude than in the semidiurnal scale. Differently from the others, these parameters had the highest values during neap tidal conditions and the lowest during spring tidal conditions (Figures 3.19 A, A1 and 3.20 B, B1), as also reported in the Ria Formosa (Cravo *et al*., 2014) and in the Guadina estuary (Garel and Ferreira, 2011). Part of the differences can be explained by the different water residence time within Ria Formosa that is critical to control the variability of the study parameters. For instance, the water volume input through Faro-Olhão inlet, magnified during spring tides, is responsible for a relative short residence time in areas close to the inlets, about 0.5–2 days in spring and neap tides, respectively (Tett *et al*., 2003). In consequence, the higher tidal range and intensity of currents in spring tidal conditions may have re-suspended part of the sediment from the seabed (Dronkers, 1986; Silva and Santos, 2003), increasing the water turbidity but also as said before at high water, an import of Chl *a* with the consequent DO and pH increase may be occured (Cravo *et al*., 2014). At neap tidal condition, under low tidal flushing, as said before the increase of the residence time within Ria Formosa may intensify the biological processes, promoting the respiration which may limit the oxygen availability in the system, and have negatively affected marine life as it is confirmed for the same study area by Cravo *et al.* (2020).

4.4 Contribution to environmental policy and management

To develop policies that will help maintain a good to high Ecological Quality Status of the Ria Formosa, long term monitoring and management of water parameters are crucial. The Water Framework Directive (WFD 2000/60/EC) sets the legal requirements for the classification of ecological status of water bodies, including shallow water ecosystems such as coastal lagoons that in the case of Ria Formosa due to the negligible river contribution is considered coastal

waters (Newton *et al.*, 2003; Nobre *et al.*, 2005; Rodrigues *et al*., 2017). The monitoring of the water quality at a high frequency (sample interval lower than 1 h) is also relevant to contribute for the water management, by fast detection and identification of water quality issues such as hypoxia, eutrophication, etc. Ultimately, this may contribute for the protection of marine biodiversity that represents a major objective of WFD. The WFD requires that the ecological status classification reflects changes in the structure of the biological communities and in the overall ecosystem functioning as a consequence of anthropogenic pressures (e.g. acidification, toxic and hazardous contaminants, physical habitat alterations, etc.; Netwon *et al.*, 2013). Therefore, the development of systems for observation/monitoring, assessment and classification of ecological status is a priority to rapidly inform management strategies to ensure the sustainable use of Ria Formosa water bodies (indicated in Figure 2.1) and avoid water quality problems. One step to set the ecological status is to define the Ecological Quality Ratios (EQR) or the ratio between the type specific reference value and the observed value for a given biological metric.

Phytoplankton metrics in Ria Formosa were divided into five quality classes, from High to Bad (ASSETS score) (Nobre *et al.*, 2005; Loureiro *et al.*, 2006, Brito *et al*., 2012). The output from that research model (Bricker *et al.*, 1999; Bricker *et al.*, 2003) permitted to evaluate symptoms of eutrophication such as the increase in chlorophyll *a* and low concentrations of dissolved oxygen (Nobre *et al*., 2005, Brito *et al*., 2012). The Ria Formosa has a short water residence time in the main channels and eutrophication symptoms are not apparent in the water column (Ferreira *et al*., 2003). It is worth remark that the inner areas of Ria Formosa are classified as eutrophication-sensitive areas (DL 149/2004; Diário da República, 2004) where elevated Chl *a* and low DO may easily exceed the boundary concentrations (Gamito *et al.* 2005; Newton *et al.*, 2013) by attaining bad/poor status classification. For two years of observation, the Chl *a* 90^{th} percentile value was 1.66 µg/L (Table 3.2), below 5.3 µg/L which is a reference for the High status in the classification of ecological quality, where 8 µg/L is for the boundary High/Good, and 12 µg/L for the boundary Good/Moderate (Brito *et al*., 2012). It is showing that the score of High quality is mantained in the present work.

The mean salinity around 36 showed that Ria Formosa is euryhaline, confirming the inclusion of Ria Formosa in the category of coastal water as stated before. Moreover, relative to pH, the mean value (*ca*. 8), is within the range (8.0 to 8.2) characteristic of coastal waters (Alcântara *et al*., 2012). Globally, the measured range of percentage of oxygen saturation (*ca.* 30-130 %; Table 3.2) is in accordance with the range previously reported by Benoliel (1984) in the early

80's. The mean value for DO recorded in this work (92%), is above the minimum available value for shellfish waters (80 %; Directive 2006/113/EC) (EU, 2006). This value, despite not problematic, being slightly lower that 100% reveal that in the study area the influence of benthic organic matter remineralization processes near the monitoring station or the lateral transport over the close extensive salt marsh area (as it possible to see in Figure 2.2) can decrease the DO below 100% saturation.

The highly intense observation with the multiparametric probe allowed to record values during 24 h a day over 7 days a week along a period of two years, providing the "real picture" in terms of environmental conditions variability in the study area within Ria Formosa. With this approach it was possible to capture episodes of storms, upwelling and countercurrent events and their impact in terms of temperature, salinity, pH, chlorophyll *a*, turbidity as well as the DO that is a key parameter in terms of water quality and for survival of marine biota. The lowest DO undersaturation values below the mean threshold for shellfish waters (80 %) were recorded mainly in summer (Figure 3.10 D), due to temperature increase, specially at low water at neap tide during the night (Figure 3.22 D1), with consequent increase of oxygen demand by respiration (Cravo *et al*., 2020). The same pattern is detected after a period of heavy precipitation in March 2018 (Annex 2), confirmed by a salinity decrease, and turbidity increase (Figures 3.9 B, 3.12 G), which may be associated with the organic matter runoff and higher rates of bacterial degradation (Pereira *et al.*, 2007; Newton *et al*., 2010; Cravo *et al.*, 2020). Nevertheless, just the 0.6% of the occurrences were recorded with values < 60%, not accomplishing the imposed minimum individual benchmark value for Shellfish Waters (EU, 2006), as is reported in the same study area by Cravo *et al.* (2020).

Hypoxia, representing concentrations < 2 mg/L, only occurred once (1.89 mg/L), representing a negligible percentage (< 1%) of the data set. The DO mean lethal (LC_{50}) for all organisms has been pointed out in literature as 2.05 mg/L (Vaquer-Sunyer and Duarte, 2008), meaning that these waters corresponds to relatively well-oxygenated waters, like found by Nobre *et al*. (2005) in Ria Formosa. In fact, the 10^{th} percentile found in this work was 5.7 mg/L (Table 3), in accordance with the range pointed by Ferreira *et al*. (2006) despite that, very close to the threshold considered the minimum for aquatic life in seawater (5 mg/L) (EPA, 2000).

Vaquer-Sunyer and Duarte (2008) reported median sublethal oxygen concentrations below 5.00 mg/L. Thus, the conventional 2 mg/L for hypoxia may lead to some fisheries collapses, and probably is an inadequate threshold to conserve coastal biodiversity, because significant

mortality have already been experienced by many, such as fish and crustaceans. It is important to remark the fact that global warming is predicted due to the increase in mean global temperature by the end of the 21st century (IPCC, 2014). Decreases in DO would have important consequences on climate, hydrology, biodiversity, and biogeochemical cycles in the marine ecosystem (Vaquer-Sunyer and Duarte, 2011). The impacts of global warming along with excessive nutrient inputs are the major drivers of the proliferation of hypoxia in the coastal ocean (Cloern, 2001; Kemp *et al*., 2009). Increasing temperature may intensify coastal upwelling, which may lead to lower sea-surface temperature and a subsequent decline in oxygen in the associated bottom waters (Bakun, 1990; Bakun and Weeks, 2004). The combined effects of elevated seawater temperatures, deoxygenation and acidification are expected to have negative effects on entire marine ecosystems with result in natural and socio-economic consequences (Vaquer-Sunyer and Duarte, 2008; Newton *et al.*, 2013).

Climate change is already affecting the marine environment and will continue to trigger changes in biological, chemical, and physical processes. Such changes can reduce the ecosystem resilience to other man-induced pressures, leaving ecosystems increasingly sensitive to disruption (IPCC, 2014). Marine strategies in some coastal areas like coastal lagoons is needed to identify ways of adapting to the effects of global warming and to reduce the vulnerability of natural and human systems to climate change effects. The advantages of acquire environmental data at high frequency is effective to rapidly act, manage and protect these productive ecosystems. Coastal lagoons are very sensitive ecosystem and fixed monitoring are indispensable, since can guide assessments of the current state of the ecosystems, and elucidate the ongoing trends and shifts, which should anticipate management policies. Despite significant progress in the establishment of coastal water monitoring networks, associated capacity development and improved modeling and reporting processes, there are still fundamental gaps in observations and significant limitations in accessing comprehensive and timely coastal water information.

Data from continuos acquisition on fixed monitoring station are useful for mathematical models which are powerful tools to explore ecosystems under different scenarios and to investigate the potential alterations due to climate changes, in terms of physical and biochemical processes. Therefore, the joint use of real time measurements and mathematical modelling approaches is priceless inside an environment such as Ria Formosa. An important point, when computing long term measurements is the consistency of the data quality over time.

5 Conclusions

This work was focused on the temporal variability of temperature, salinity, DO, pH, chlorophyll *a* and turbidity along the period of study, from July 2017 to June 2019, using real time data recorded by the multiparametric probe installed in the scope of the UBEST project.

Globally, the observations got along the period of study were essential to discriminate data at different time scales of physical, chemical and biological processes occuring within Ria Formosa around the study area, in WB2.

Complementary data of metereological time series and satellite images revealed to be fundamental to characterize the mesoscale processes, which were key factors on regulating the variability of the studied parameters. This highlighs the importance of having environmental data-bases which may be readily available to the scientific community and environmental and ocean sciences managers.

The data obtained through the fixed monitoring station are highly valuable and were able to capture rapidly changing environmental conditions and episodic events. Phytoplankton enhancement occurred mainly in summer, the subsaturation in DO during the night, at low water, during neap tidal condition, and mesoscale events, such as storms and upwelling, were all examples of temporary events which can not be detected without a fixed monitoring station.

Considering the objectives of the MSFD, the deployment of such station represents an added value. Thanks to the high frequency sampling rate, it was possible to define an informative value for Chl *a* 90^{th} percentile and 10^{th} percentile value for dissolved oxygen for two years of observations, taken every 15 minutes.

The definition of a detailed maintenance programme for inspection, cleaning and calibration, is imperative to improve the data quality over a long term monitoring and get accurate data sets. It will be very interesting to continue this kind of observation/monitoring to get long term series, assess temporal evolution and changes of the environmental conditions, particularly in Ria Fiormosa WB2, where the antropogenic pressure is relevant and inform managers with responsability in this important ecosystem.

6 References

Alcântara, P., Cravo, A., Jacob, J. (2012). Variability of nutrients and Chlorophyll. Ciencias Marinas, 38, 161–176.

Alvarez-Borrego, S. (2004). Nutrient and phytoplankton dynamics in a coastal lagoon strongly affected by coastal upwelling. Ciencias Marinas, *30*(1A), 1–19.

Anthony, A., Atwood, J., August, P., Byron, C., Cobb, S., Foster, C., Fry, C., Gold, A., Hagos, K., Heffner, L., Kellogg, D. Q., Dibble, K., Opaluch, J., Oviatt, C., Herbert, A., Rohr, R., Smith, L., Smythe, T., Swift, J., Vinhateiro, N., (2009). Coastal Lagoons and Climate Change: Ecological and Social Ramifications in U.S. Atlantic and Gulf Coast Ecosystems.

Agência Portuguesa do Ambiente, APA. (2012d). Plano de Gestão das Bacias Hidrográficas que integram a Região Hidrográfica das Ribeiras do Algarve (RH8), Volume 1, Parte 2, TOMO 5. Ministério da Agricultura, do Mar, do Ambiente e do Ordenamento do Território.

Agência Portuguesa do Ambiente, APA. (2015). Plano de Gestão da Região Hidrográfica das Ribeiras do Algarve (RH8), Parte 2, Caracterização e Diagnóstico. Plano de Gestão da Região Hidrográfica 2016/2021.

Aubrey, D. G., and Speer, P. E. (1985). A study of Non-linear Tidal Propagation in shallow Inlet/Estuarine Systems, Part I: Observations. Estuarine, Coastal and Shelf Science (1985) 21, 185-205.

Bakun, A. (1990). Global climate change and intensification of coastal ocean upwelling. Science, 247, 198–201.

Bakun, A., Weeks, S. J. (2004). Greenhouse gas buildup, sardines, submarine eruptions and the possibility of abrupt degradation of intense marine upwelling ecosystems. Ecology Letters, 7, 1015–1023.

Baptista, A. M. (2006). CORIE: the first decade of a coastal-margin collaborative observatory. Oceans'06, MTS/ IEEE, Boston, MA.

Barbosa, A. B. (2010). Seasonal and interannual variability of Planktonic Microbes in a Mesotidal Coastal Lagoon (Ria Formosa, SE Portugal): Impact of Climatic Changes and Local Human Influences. In: Paerl HW and Kennish MJ (Eds.). Coastal Lagoons: Critical Habitats of Environmental Change, 335–366. Boca Raton, Florida. CRC Press.

Babier., E. B., Hacker, S. D., Kennedy, C., Koch, E. W., Stier, A. C., Silliman, B. R. (2011). The value of estuarine and coastal ecosystem services. Ecological Monographs, 81(2), 169-193.

Barnes, R. S. K. (1980). Coastal lagoons. Cambridge University Press, Cambridge, UK.

Bebianno, M. J. (1995). Effects of pollutants in the Ria Formosa Lagoon, Portugal. Science of the Total Environment 171:107–115.

Benoliel, M. J. (1984). Vigilância em contínuo da qualidade da água da Ria Formosa (Ria de Faro-Olhão) 1980. Relatório Técnico Final REL-TF-QP-3/84, Divisão de Química e Poluição, Instituto Hidrográfico, Lisboa, Portugal.

Benazzouz, A., Mordane, S., Orbi, A., Chagdali, M., Hilmi, K., Atillah, A., Lluís Pelegrí, J., & Hervé, D. (2014). An improved coastal upwelling index from sea surface temperature using satellite-based approach – The case of the Canary Current upwelling system. *Continental Shelf Research*, *81*, 38–54.

Bird, E. C. F. (1994). Physical setting and geomorphology of coastal lagoons. Kjerfve, editor. Coastal lagoon processes.

Borja, A., Marques, C., Quintino, C. (2013). Marine research in the Iberian Peninsula: A pledge for better times after an economic crisis.

Bricker, S. B., Clement, C. G., Pirhalla, D. E., Orlando, S. P., Farrow, D. R. G. (1999). National Estuarine Eutrophication Assessment. Effects of Nutrient Enrichment in the Nation's Estuaries. NOAA–NOS Special Projects Office, 1999.

Bricker, S. B., Ferreira, J. G., Simas, T. (2003). An integrated methodology for assessment of estuarine trophic status. Ecological Modelling 169, 39 – 60.

Brito, A., Newton, A., Tett, P., Fernandes, T. F. (2010). Sediment and water nutrients and microalgae in a coastal shallow lagoon, Ria Formosa (Portugal): implications for the Water Framework Directive. Journal of Environmental Monitoring, 12(1), 318–328.

Brito, A. C., Quental, T., Coutinho, T. P., Branco, M. A. C., Falcão, M., Newton, A., Icely, J., Moita, T. (2012). Phytoplankton dynamics in southern Portuguese coastal lagoons during a discontinuous period of 40 years: An overview. Estuarine, Coastal and Shelf Science, 110, 147–156.

Cañedo-Argüelles, M., Rieradevall, M., Farrés-Corell, R., & Newton, A. (2012). Annual characterisation of four Mediterranean coastal lagoons subjected to intense human activity. *Estuarine, Coastal and Shelf Science*, *114*, 59–69.

Cardeira, S., Rita, F., Relvas, P. and Cravo, A. (2013). Chlorophyll *a* and chemical signatures during an upwelling event off the South Portuguese coast (SW Iberia). *Continental Shelf Research*, 52, pp.133-149.

Carrasco, A. R., Ferreira, Ó., Freire, P., Dias, J. A. (2009). Morphological changes in a low energy backbarrier. Journal of Coastal Research, Special Issue 56, 173-177.

Ceia, F. R. (2009). Vulnerabilidade das ilhas-barreira e dinâmica da Ria Formosa na óptica da gestão. Gestão Costeira Integrada, 9(1), 57–77.

CEPASA. (1980). Observac¸o˜es de varia´veis quı´micas e fı´sicas na a´gua da Ria de Faro (la, fase, Fev.–Dez. 1977) Vol. 68 (pp. 1–31). CEPASA.

Cervantes-Duarte, R., Prego, R., López-López, S., Aguirre-Bahena, F., Ospina-Alvarez, N. (2013). Annual patterns of nutrients and Chlorophyll in a subtropical coastal lagoon under the upwelling influence (SW of Baja-California Peninsula). Estuarine, Coastal and Shelf Science, 120, 54–63.

Chatfield, C. (2004). The analysis of time series. Texts in Statistical Science. USA: Chapman & Hall, sixth edition.

Cloern, J. E. (2001). Our evolving conceptual model of the coastal eutrophication problem. Marine Ecology-Progress Series, 210, 223–253.

Cloern, J., and Dufford, R. (2005). Phytoplankton community ecology: principles applied in San Francisco Bay. US Geological Survey, MS496, 345 Middlefield Road, Menlo Park, California 94025, USA 21845 Orchard Place, Fort Collins, Colorado 80521, USA.

Comissão Coordenação e Desenvolvimento Regional do Algarve, CCDRA. (2003). Relatório do Estado do Ambiente [Algarve]. Ministério do Ambiente, do Ordenamento do Território e do Desenvolvimento Regional.

Costa, M., Silva, R., Vitorino, J. (2001). Contribuição para o estudo do clima de agitação marítima na costa portuguesa. 2ªs Jornadas Portuguesas de Engenharia Costeira e Portuária, Associação Internacional de Navegação, 20.

Cravo, A., Cardeira, S., Pereira, C., Rosa, M., Madureira, M., Rita, F., Luís, J., Jacob, J. (2013 b). Nutrients and particulate matter exchanges through the Ria Formosa coastal lagoon, Portugal. Journal of Coastal Research, Special Issue 65, 1999–2004.

Cravo, A., Cardeira, S., Pereira, C., Rosa, M., Alcântara, P., Madureira, M., Rita, F., Luís, J., Jacob, J. (2014). Exchanges of nutrients and Chlorophyll a through two inlets of Ria Formosa, South of Portugal, during coastal upwelling events. Journal of Sea Research, 93, 63–74.

Cravo, A., Fernandes, D., Damião, T., Pereira, C., Reis, M. P. (2015). Determining the footprint of sewage discharges in a coastal lagoon in South-Western Europe. Marine Pollution Bulletin, 96 (1-2), 197209.

Cravo, A., Cardeira, S., Pereira, C., Rosa, M., Alcântara, P., Madureira, M., Rita, F., Correia, C., Rosa, A., Jacob, J. (2019). Nutrients and Chlorophyll-a exchanges through an inlet of the Ria Formosa Lagoon, SW Iberia during the productive season –Unravelling the role of the driving forces.

Cravo, A., Rosa, A., Jacob, J., and Correia, C. (2020). Dissolved oxygen dynamics in Ria Formosa Lagoon (South Portugal) - A real time monitoring station observatory. *Marine Chemistry*, 223, p.103806.

Danchenko, S., Fragoso, B., Guillebault, D., Icely, J., Berzano, M., and Newton, A. (2019). Harmful phytoplankton diversity and dynamics in an upwelling region (Sagres, SW Portugal) revealed by ribosomal RNA microarray combined with microscopy. *Harmful Algae*, 82, pp.52-71.D'Avanzo, C., and J. N. Kremer. (1994). Diel oxygen dynamics and anoxic events in an eutrophic estuary of Waquoit Bay, Massachusetts. Estuaries 17:131-139.

Dias, J. M., Sousa, M. C., Bertin, X., Fortunato, A. B., Oliveira, A. (2009). Numerical modeling of the impact of the Ancão Inlet relocation (Ria Formosa, Portugal). Environmental Modelling and Software, 24(6), 711–725.

Dias, J. M., Sousa, M. C. (2009). Numerical modeling of Ria Formosa tidal dynamics. Journal of Coastal Research, Special Issue 56, 1345–1349.

Dronkers, J. (1986). Tidal asymmetry and estuarine morphology. Neth J Sea Res 20(2–3):117–131.

Duarte, P., Azevedo, B., Guerreiro, M., Ribeiro, C., Bandeira, R., Pereira, A., Falcão, M., Serpa, D., Reia, J. (2007). Biogeochemical modelling of Ria Formosa (South Portugal). Hydrobiologia, 611 (1), 115–132.

Emery, W. J., and Thomson, R.E. (2001). Elsevier Science. Data Analysis Methods in Physical Oceanography. 2nd Edition.

EPA (U.S. Environmental Protection Agency). (2000). Ambient Aquatic Life Water Quality Criteria for Dissolved Oxygen (Saltwater): Cape Cod to Cape Hatteras. (140 pp.).

Erena, M., Domínguez, J., Giménez, F., Soria, J., Galiano, S. (2019). Monitoring Coastal Lagoon Water Quality through Remote Sensing: The Mar Menor as a Case Study. Water 2019, 11, 1468.

European Community, EU. (2000). Directive of the European Parliament and of the Council 2000/60/EC, Establishing a Framework for Community Action in the Field of Water Policy. 62 pp.

European Community, EU (2006). Official Journal of the European Union. Directive 2006/113/EC of the European Parliament and of the Council of 12 December 2006.

Evans, G. W. (2019). Projected Behavioural Impacts of Global Climate Change. Annual Review of Psychology Vol. 70:449-474 (Volume publication date January 2019) https://doi.org/10.1146/annurev-psych-010418-103023

Fabião, J., Rodrigues, M., Fortunato, A., Jacob, J., Cravo, A. (2016). Water exchanges between a multi-inlet lagoon and the ocean: the role of forcing mechanisms. Ocean Dynamics, 66(2), 173–194.

Falcão, M., and Vale, C. (1990). Study of the Ria Formosa ecosystem: benthic nutrient remineralization and tidal variability of nutrients in the water. Hydrobiologia, 207(1), 137–146.

Falcão, M., and Vale, C. (1998). Sediment–water exchanges of ammonium and phosphate in intertidal and subtidal areas of a mesotidal coastal lagoon (Ria Formosa). Hydrobiologia 373:193–201.

Falcão, M., and Vale, C. (2003). Nutrient dynamics in a coastal lagoon (Ria Formosa, Portugal): the importance of lagoon-sea water exchanges on the biological productivity. Ciencias Marinas, 29(4), 425-433

Ferreira, J. G., Simas, T., Nobre, A., Silva, M. C., Shifferegger, K., Lencart-Silva, J. (2003). Identification of sensitive areas and vulnerable zones in transitional and coastal Portuguese systems. Application of the United States National Estuarine Eutrophication Assessment to the Minho, Lima, Douro, Ria de Aveiro, Mondego, Tagus, Sado, Mira, Ria Formosa and Guadiana systems. INAG and IMAR.

Ferreira, J. G., Abreu, P. F., Bettencourt, A. M., Bricker, S. B., Marques, J. C., Melo, J. J., Newton, A., Nobre, A., Patricio, J., Rocha, F., Rodrigues, R., Sais, F., Silva, M. C., Simas, T., Soares, C. V., Stacey, P. E., Vale, C., de Wit, M., Wolff, W. J. (2005). Monitoring plan for water quality and ecology of Portuguese transitional and coastal waters (MONAE), 164 pp.

Ferreira, J. G., Nobre, A. M., Simas, T. C., Silva, M. C., Newton, A., Bricker, S. B., Wolff, W. J., Stacey, P. E., Sequeira, A. (2006). A methodology for defining homogeneous water bodies in estuaries - application to the transitional systems of the EU Water Framework Directive. Estuar. Coast. Shelf Sci. 66 (3–4), 468–482.

Fiúza, A. F. G., Macedo, M. E., and Guerreiro, M. R. (1982). Climatological space and time variation of the Portuguese coastal upwelling: Oceanologica Acta, v. 5, p. 31- 40.

Flemming, B. W. (2011). Siliciclastic Back-Barrier Tidal Flats. Principles of Tidal Sedimentology, 231–267.

Gamito, S., J. Gilabert, C. M. Diego, and A. Pérez-Ruzafa. 2005. Effects of changing environmental conditions on lagoon ecology. Pp. 193–230, In: I. E. Gonenç and J. P. Wolfin (eds.), Coastal lagoons: Ecosystem processes and modeling for sustainable use and development. Boca Raton, Florida: CRC Press.

Gamito, S. (2008). Three main stressors acting on the Ria Formosa lagoonal system (Southern Portugal): Physical stress, organic matter pollution and the land–ocean gradient. Estuarine, Coastal and Shelf Science 77, 710–720.

García-Lafuente, J., Delgado, J., Criado-Aldeanueva, F., Bruno, M., del Río, J., Miguel Vargas, J. (2006). Water mass circulation on the continental shelf of the Gulf of Cádiz. Deep-Sea Res. Part II Top. Stud. Oceanogr. 53 (11–13), 1182–1197.

Garel, E., Pinto, L., Santos, A., Ferreira, Ó. (2009a). Tidal and river discharge forcing upon water and sediment circulation at a rockbound estuary (Guadiana estuary, Portugal). Estuary Coast Shelf Sci 84(2):269–281

Garel, E., Nunes, S., Neto, J. M., Fernandes, R., Neves, R., Marques, J.C, Ferreira, Ó. (2009b). The autonomous Simpatico system for real time continuous water-quality and current velocity monitoring: examples of application in three Portuguese estuaries. Geo Mar Lett 29:331–341.

Garel, E., and Ferreira, O. (2011). Monitoring estuaries using non-permanent stations: practical aspects and data examples. Ocean Dynamics (2011) 61:891–902.

Garel, E., Laiz, I., Drago, T., Relvas, P. (2016). Characterisation of coastal counter-currents on the inner shelf of the Gulf of Cadiz. J. Mar. Syst. 155, 19–34.

Gasol, J., Pinhassi, J., Alonso-Sáez, L., Ducklow, H., Herndl, G., Koblízek, M., Labrenz, M., Luo, Y., Morán, X., Reinthaler, T., & Simon, M. (2008). Towards a better understanding of microbial carbon flux in the sea. Aquatic Microbial Ecology, 53, 21–38.

Gilbert, J. D., Guerrero, F., & de Vicente, I. (2014). Sediment desiccation as a driver of phosphate availability in the water column of Mediterranean wetlands. Science of The Total Environment, 466–467, 965–975.

Glaeser, J. D. (1978). Global distribution of barrier islands in terms of tectonic setting. J Geol 86:283–297.

Glasgow, H. B., Burkholder, J. M., Reed, R.E, Lewitus, A. J., Kleinman, J. E. (2004). Real-time remote monitoring of water quality: a review of current applications, and advancements in sensor, telemetry, and computer technologies. J Exp Mar Biol Ecol 300:409–448.

Goela, P. C., Cordeiro, C., Danchenko, S., Icely, J., Cristina, S., & Newton, A. (2016). Time series analysis of data for sea surface temperature and upwelling components from the southwest coast of Portugal. Journal of Marine Systems, 163, 12–22.

Gonzalez-Nuevo, G., Gago, J., and Cabanas, J. M. (2014). Upwelling index: a powerful tool for marine research in the NW Iberian upwelling system, Journal of Operational Oceanography, 7:1, 47-57.

Intergovernmental Panel on Climate Change, IPCC. (2014). Climate Change 2014: Synthesis Report. Contribution of Working Groups I, II and III to the Fifth Assessment Report of the Intergovernmental Panel on Climate Change [Core Writing Team, R.K. Pachauri and L.A. Meyer (eds.)]. IPCC, Geneva, Switzerland, 151 pp.

Jacob, J., Cardeira, S., Rodrigues, M., Bruneau, N., Azevedo, A., Fortunato, A. B., Cravo, A. (2013). Experimental and numerical study of the hydrodynamics of the western sector of Ria Formosa. Journal of Coastal Research, Special Issue 65, 2011-2016.

Jacob, J., Simoes, N., Cravo, A. (2014). Influencia e propagaçao no interior da Ria Formosa dos processos oceanograficos de mesoscale na costa sul de Portugal.

Jacob, J., Cravo, A., Rosa, A., Rodrigues, M., Rogeiro, J. (2018). One Year Monitoring of Water Characteristics Inside Ria Formosa. 5as Jornadas de Engenharia Hidrográfica.

Jacob, J., & Cravo, A. (2019). Recent evolution of the tidal prisms at the inlets of the western sector of the Ria Formosa, south coast of Portugal. Regional Studies in Marine Science, 31, 100767.

Kemp, W. M., Testa, J. M., Conley, D. J., Gilbert, D., Hagy, J. D. (2009) Temporal responses of coastal hypoxia to nutrient loading and physical controls. Biogeosciences, 6, 2985–3008.

Ketchum, B.H. (1954). Relation between circulation and planktonic populations in estuaries. Ecology 35 (2), 191 – 200.

Kjerfve, B., Magill, K. E. (1989). Geographic and hydrodynamic characteristics of shallow coastal lagoons. Marine Geology, 88(3–4), 187–199.

Kjerfve, B. (1994). Coastal lagoons. In: Kjerfve B (Ed.). Coastal lagoons processes. Elsevier Oceanography Series, 60, 1–8.

Koch, E. W, (2001). Beyond light: physical, geological and geochemical parameters as possible submersed aquatic vegetation habitat requirements. Estuaries 24:1–17

Koslow, A., and Couture, J. (2015). Pacific Ocean observation programs: Gaps in ecological time series 1 Scripps Institution of Oceanography, 9500 Gilman Drive, University of California, SD, La Jolla, CA 92093-0218, USA.

Lloret, J., Marín, A., and Marín-Guirao, L. (2008). Is coastal lagoon eutrophication likely to be aggravated by global climate change? Estuarine, Coastal and Shelf Science, 78(2), 403-412.

Luis, J. F. (2007). Mirone: A multi-purpose tool for exploring grid data. Computers & Geosciences, 33, 31-41.

Loureiro, S., Newton, A., Icely, J. (2005). Effects of nutrient enrichments on primary production in the Ria Formosa coastal lagoon (Southern Portugal). Hydrobiology, 550(1), 29–45.

Loureiro, S., Newton, A., Icely, J. (2006). Boundary conditions for the European Water Framework Directive in the Ria Formosa lagoon, Portugal (physico-chemical and phytoplankton quality elements). Estuarine, Coastal and Shelf Science, 67(3), 382–398.

Machás, R., & Santos, R. (1999). Sources of organic matter in Ria Formosa revealed by stable isotope analysis. Acta Oecologica, *20*(4), 463–469.

Mudge, S. M., Icely, J. D., Newton, A. (2007). Oxygen depletion in relation to water residence times. Journal of Environmental Monitoring, 9, 1194-1198.

Mudge, S. M., Icely, J. D., Newton, A. (2008). Residence times in a hypersaline lagoon: Using salinity as a tracer. Estuarine, Coastal and Shelf Science, 77(2), 278–28.

Navarro, G., Ruiz, J., Huertas, I.E., García, C.M., Criado-Aldeanueva, F., Echevarría, F., (2006). Basin-scale structures governing the position of the deep fluorescence maximum in the Gulf of Cádiz. Deep Sea Res. Part II Top. Stud. Oceanogr. 53 (11), 1261–1281.

Newton, A. (1995). The water quality of the Ria Formosa lagoon, Portugal. PhD Thesis, University of Wales, UK.

Newton, A., Icely, J. D., Falcao, M., Nobre, A., Nunes, J. P., Ferreira, J. G., Vale, C. (2003). Evaluation of eutrophication in the Ria Formosa coastal lagoon, Portugal. Continental Shelf Research, 23 (1719), 1945-1961.

Newton, A., Mudge, S. M. (2003). Temperature and salinity regimes in a shallow, mesotidal lagoon, the Ria Formosa, Portugal. Estuarine, Coastal and Shelf Science, 57(1-2), 73-85.

Newton, A., Mudge, S. M. (2005). Lagoon-sea exchanges, nutrient dynamics and water quality management of the Ria Formosa (Portugal). Estuarine, Coastal and Shelf Science, 62(3), 405–414.

Newton, A., Oliveira, P. S., Icely, J. D., Foster, P. A. (2010). Monitoring of oxygen condition in the Ria Formosa coastal lagoon, Portugal. Journal of Environmental Monitoring, 12(1), 355-60.

Newton, A., et al. (2013)An overview of ecological status, vulnerability and future perspectives of European large shallow, semi-enclosed coastal systems, lagoons and transitional waters, Estuarine, Coastal and Shelf Science (2013), http://dx.doi.org/10.1016/ j.ecss.2013.05.023.

Nobre, A.M., Ferreira, J.G., Newton, A., Simas, T., Icely, J.D., Neves, R. (2005). Management of coastal eutrophication: integration of field data, ecosystem-scale simulations and screening models. Journal of Marine Systems 56, 375e390.

Nogueira, E., Pérez, F., Ríos, F., Aida, F. (1997). Modelling Thermohaline Properties in an Estuarine Upwelling Ecosystem (Ría de Vigo: NW Spain) Using Box-Jenkins Transfer Function Models. Ríos Instituto de Investigacións Mariñas, C.S.I.C., Eduardo Cabello, 6. 36208 Vigo, Spain.

Pacheco, A., Ferreira, Ó., Williams, J. J., Garel, E., Vila-Concejo, A., Dias, J.A. (2010). Hydrodynamics and equilibrium of a multiple-inlet system. Marine Geology, 274(1-4), 32-42.

Palma, A.S., Mouriño, H., Silva, A., Barão, M.I., Moita, M.T. (2010). Can Pseudo-nitzschia blooms be modeled by coastal upwelling in Lisbon Bay? Harmful Algae 9, 294e303.

Pereira, M. G., Icely, J., Mudge, S., Newton, A., Rodrigues, R. (2007). Temporal and spatial variation of phytoplankton pigments in the western part of Ria Formosa lagoon, Southern Portugal. Environmental Forensics, 8(781714560), 205–220.

Pérez-Ruzafa, A., Campillo, S., Fernández-Palacios, J. M., García-Lacunza, A., García-Oliva, M., Ibañez, H., Navarro-Martínez, P. C., Pérez-Marcos, M., Pérez-Ruzafa, I. M., Quispe-Becerra, J. I., Sala-Mirete, A., Sánchez, O., and Marcos, C. (2019). Long-Term Dynamic in

Nutrients, Chlorophyll *a*, and Water Quality Parameters in a Coastal Lagoon During a Process of Eutrophication for Decades, a Sudden Break and a Relatively Rapid Recovery. *Front. Mar. Sci* 6:26.

PROCESL, HIDRO4 & PROSISTEMAS, PH&P. (2000a). Plano de Bacia Hidrográfica das Ribeiras do Algarve – Caracterização Geral da Bacia Hidrográfica, 1ª Fase – Análise e Diagnóstico da Situação de Referência, Vol. I – Síntese, 186 p.

Pilkey, O. H. (2003). A celebration of the world's barrier islands. Columbia University Press, New York.

Platt, T. (1972). Local phytoplankton abundance and turbulence. Deep-Sea Research 19, 183-187.

Pugh, D. (1987). Tides, surges and mean sea level. United States 01 01.

Raven, J., Caldeira, K., Elderfield, H., Hoegh-Guldberg, O. (2005). Ocean acidification due to increasing atmospheric carbon dioxide. Royal Society, London, UK. Available online at: http://royalsociety. org/document.asp?id=3249.

Relvas, P., Barton, E. D. (2002). Mesoscale patterns in the Cape San Vincente (Iberian Peninsula) upwelling region. Journal of Geophysical Research 107 (C10), 3164.

Ryabinin, V., Barbière, J., Haugan, P., Kullenberg, G., Smith, N., McLean, C., Troisi, A., Fischer, A., Aricò, S., Aarup, T., Pissierssens, P., Visbeck, M., Enevoldsen, H. O. and Rigaud, J. (2019). The UN Decade of Ocean Science for Sustainable Development. Front. Mar. Sci. 6:470.

Rosa, A., Cravo, A., Jacob, J. (2016). Is there a seasonal fingerprint in the mass exchanges between the main inlet of Ria Formosa and the Atlantic Ocean? 4 as Jornadas de Engenharia Hidrográfica, Instituto Hidrográfico, Lisboa, 287–290.

Rosa, A., Cardeira, S., Pereira, C., Rosa, M., Madureira, M., Rita, F., Jacob, J., Cravo, A. (2019). Temporal variability of the mass exchanges between the main inlet of Ria Formosa lagoon (southwestern Iberia) and the Atlantic Ocean. Estuarine, Coastal and Shelf Science Volume 228, 15 November 2019, 106349

Rodrigues, M., Rosa A, Cravo A, Fortunato AB, Jacob J (2017). Understanding the biogeochemical buffering capacity of estuaries relative to climate change and anthropogenic inputs. Report 1. Characterization of the study areas: Tagus estuary and Ria Formosa.

Salles, P., Voulgaris, G., Aubrey, D. G. (2005). Contribution of nonlinear mechanisms in the persistence of multiple tidal inlet systems. Estuarine, Coastal and Shelf Science, 65(3), 475–491.

Sánchez, R.F., Mason, E., Relvas, P., da Silva, A.J., and Peliz, Á. (2006). On the inner-shelf circulation in the northern Gulf of Cádiz, southern Portuguese shelf: Deep Sea Research Part II: Topical Studies in Oceanography, v. 53, p. 1198-1218.

Serpa, D.; Jesus, D.; Falcao, M.; Cancela da Fonseca, L. (2005). Ria Formosa ecosystem: socioeconomic approach. Relat. Cient. Téc. IPIMAR, Série digital (http://ipimar-iniap.ipimar.pt) n.º 28, 50p.

Serpa, D., Falcão, M., Duarte, P., da Fonseca, L. C., & Vale, C. (2007). Evaluation of ammonium and phosphate release from intertidal and subtidal sediments of a shallow coastal lagoon (Ria Formosa – Portugal): a modelling approach. Biogeochemistry, 82(3), 291–304

Silva, J., & Santos, R. (2003). Daily variation patterns in seagrass photosynthesis along a vertical gradient. *Marine Ecology Progress Series*, *257*, 37–44.

Smakhtin, V., Revenga, C., Döll, P., Tharme, R., Nackoney, J., Yumiko Kura, & Agriculture, I. (2004). Taking into account environmental water requirements in global-scale water resources assessments. Comprehensive Assessment Secretariat.

Sousa, A. I., Lillebø, A. I., Pardal, M. A., & Caçador, I. (2010). Productivity and nutrient cycling in salt marshes: Contribution to ecosystem health. Estuarine, Coastal and Shelf Science, 87(4), 640–646.

Tett, P., Gilpin, L., Svendsen, H., Erlandsson, C. P., Larsson, U., Kratzer, S., Fouilland, E., Janzen, C., Lee, J., Grenz, C., Newton, A., Ferreira, J. G., Fernandes, T., Scory, S. (2003). Eutrophication and some European waters of restricted exchange. Continental Shelf Research, 23(17-19), 1635-1671.

Tett, P., Gowen, R. J., Painting, S. J., Elliott, M. and others (2013) Framework for understanding marine ecosystem health. Mar Ecol Prog Ser 494:1-27.

Valiela, I., McClelland, J., Hauxwell, J., Behr, P.J., Hersh, D., Foreman, K. (1997). Macroalgal blooms in shallow estuaries: controls and ecophysiological and ecosystem consequences. Limnology and Oceanography 42 (5), 1105 – 1118.

Valença, M., Cardoso, A., Borges, C., Palma, C., Santos, P. (2011). Vigilância da Qualidade do Meio Marinho - 25 anos de estudo. Instituto Hidrográfico.

Vaquer-Sunyer, R., Duarte, C. M. (2008). Thresholds of hypoxia for marine biodiversity. Proceedings of the National Academy of Sciences of the United States of America, 105, 15452–15457.

Vaquer-Sunyer, R., Duarte, C. M. (2010). Temperature effects on oxygen thresholds for hypoxia in marine benthic organisms. Global Change Biology, 17(5), pp.1788-1797.

Vila-Concejo, A., Ferreira, Ó., Matias, A., Dias, J. M. A. (2003). The first two years of an inlet: Sedimentary dynamics. Continental Shelf Research, 23(14-15), 1425-1445.

Zaytsev, O., & Cervantes-Duarte, R. (2018). Nutrient flux estimates in a tidal basin: A case study of Magdalena lagoon, Mexican Pacific coast. *Estuarine, Coastal and Shelf Science*, *207*, 16–29.

Zhang, L., Thomas, S., & Mitsch, W. J. (2017). Design of real-time and long-term hydrologic and water quality wetland monitoring stations in South Florida, USA. *Ecological Engineering*, *108*, 446–455.

Annexes

Annex 1

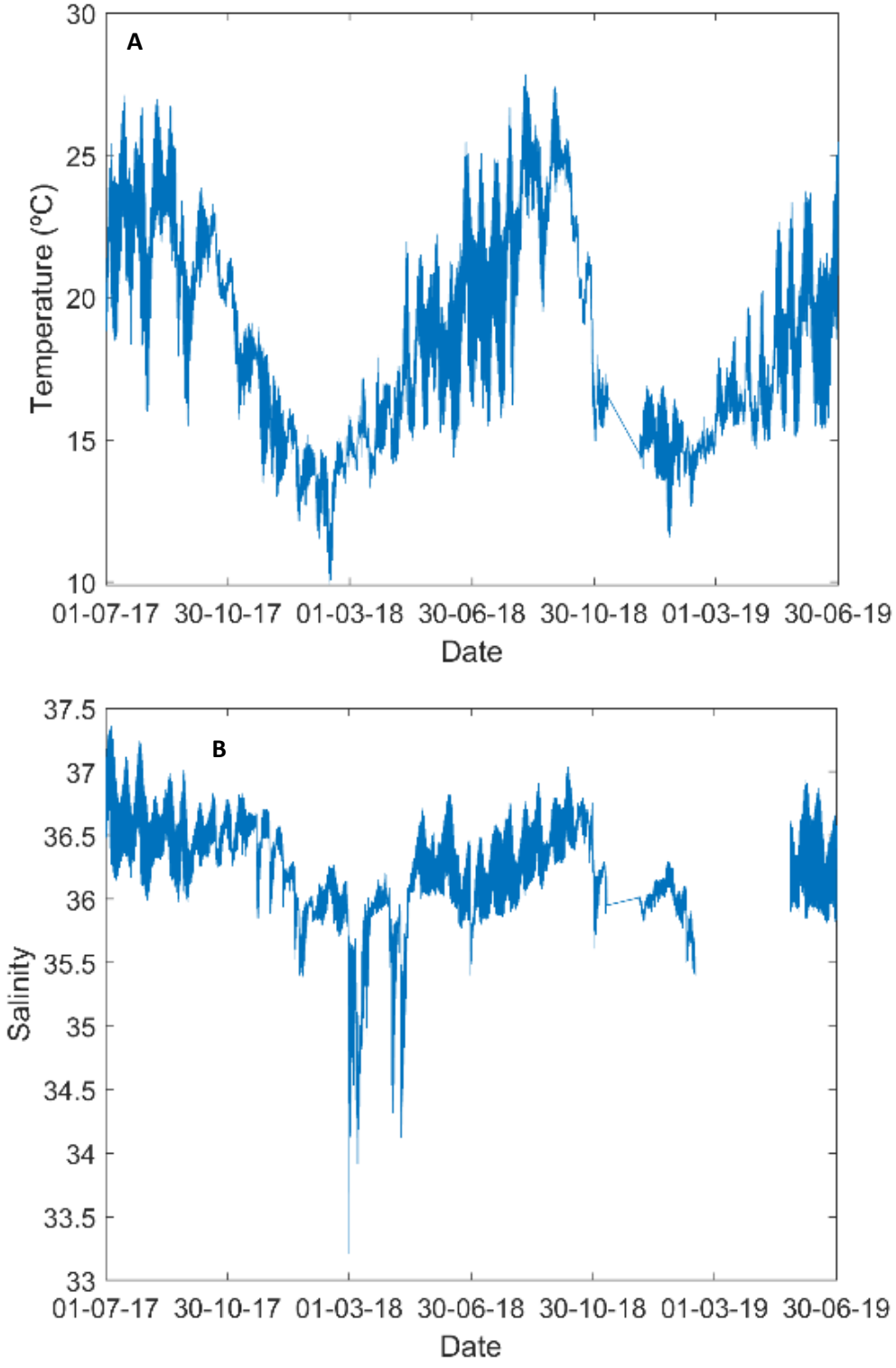

Annex 1: Raw time series A) temperature (ºC); B) salinity

Annex 1 (Cont.)

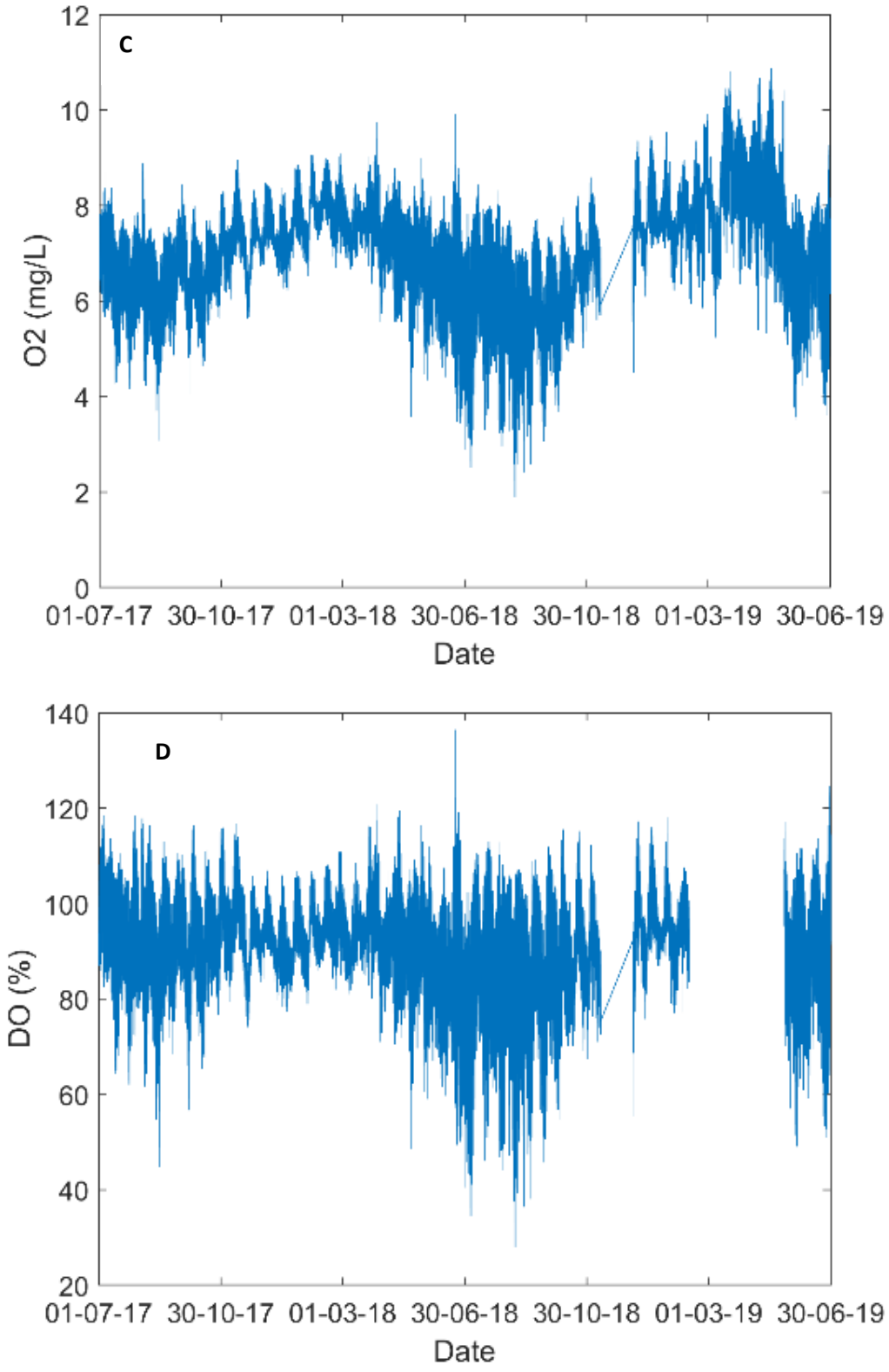

Annex 1: Raw time series C) DO (mg/L); D) DO (%)

Annex 1 (Cont.)

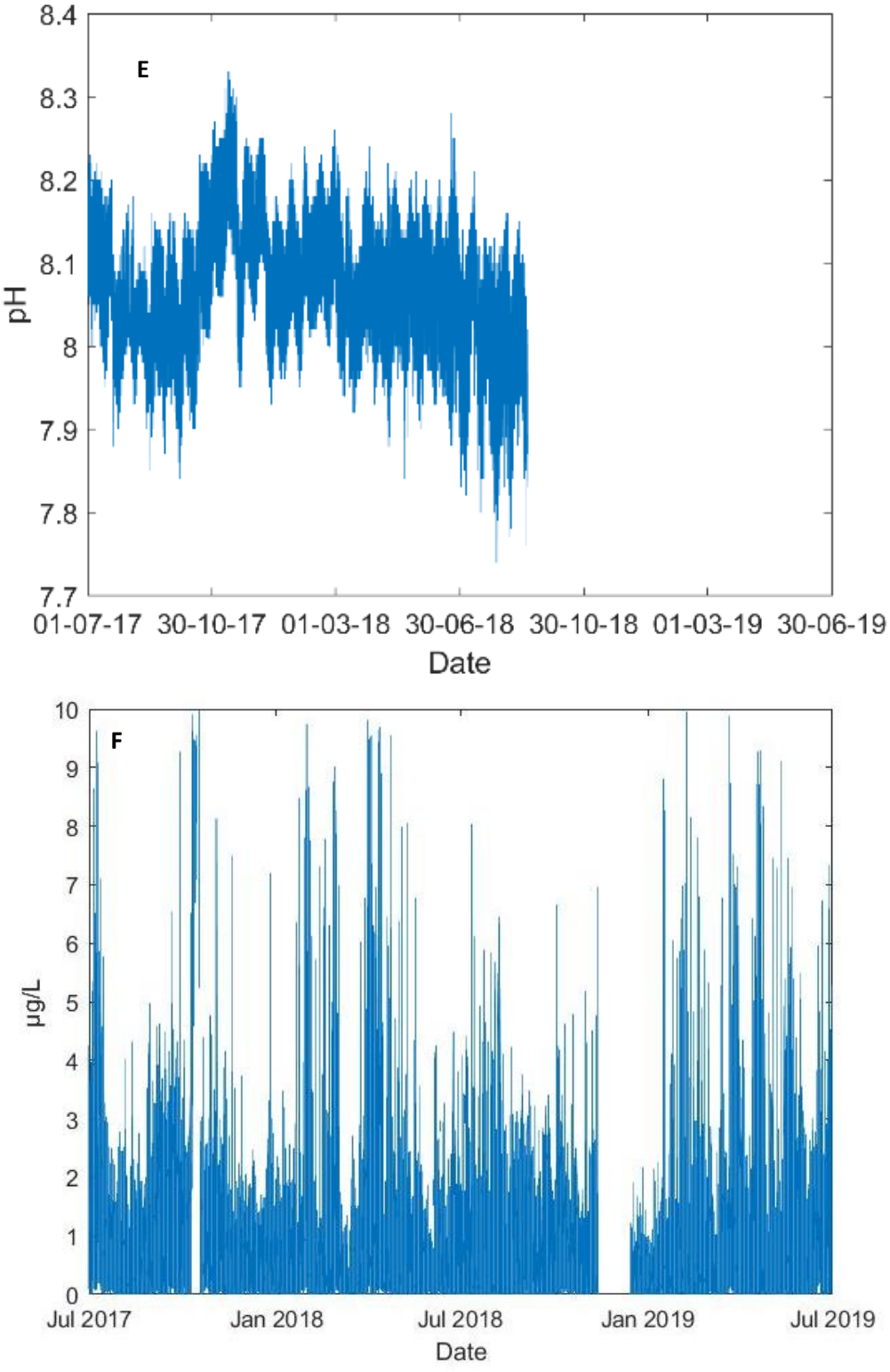

Annex 1: Raw time series E) pH; F) Chlorophyll a (µg/L)

Annex 1 (Cont.)

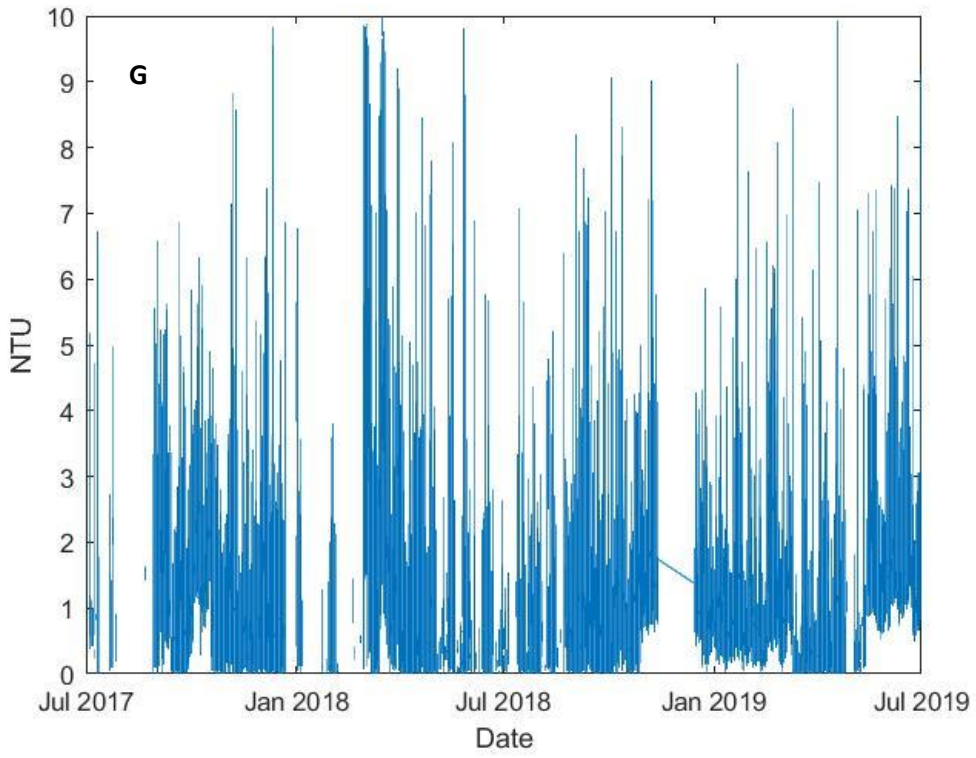

Annex 1: raw timeseries G) turbidity (NTU)

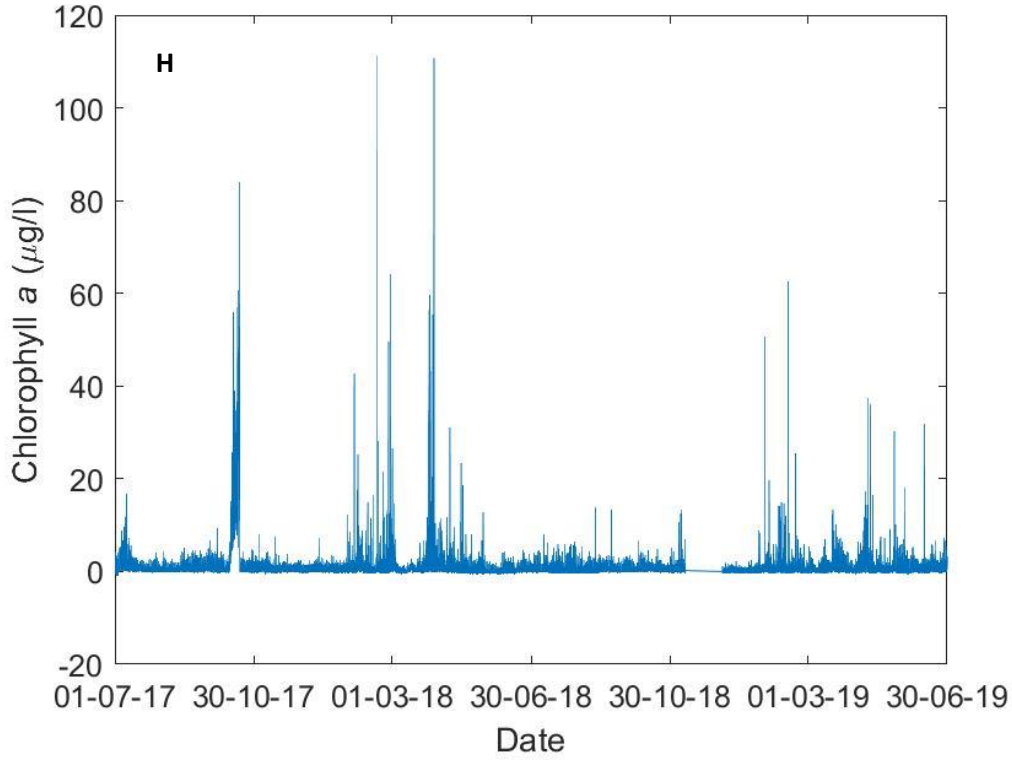

Annex 1: raw timeseries H) Chlorophyll a with unrealistic values

Annex 1 (Cont.)

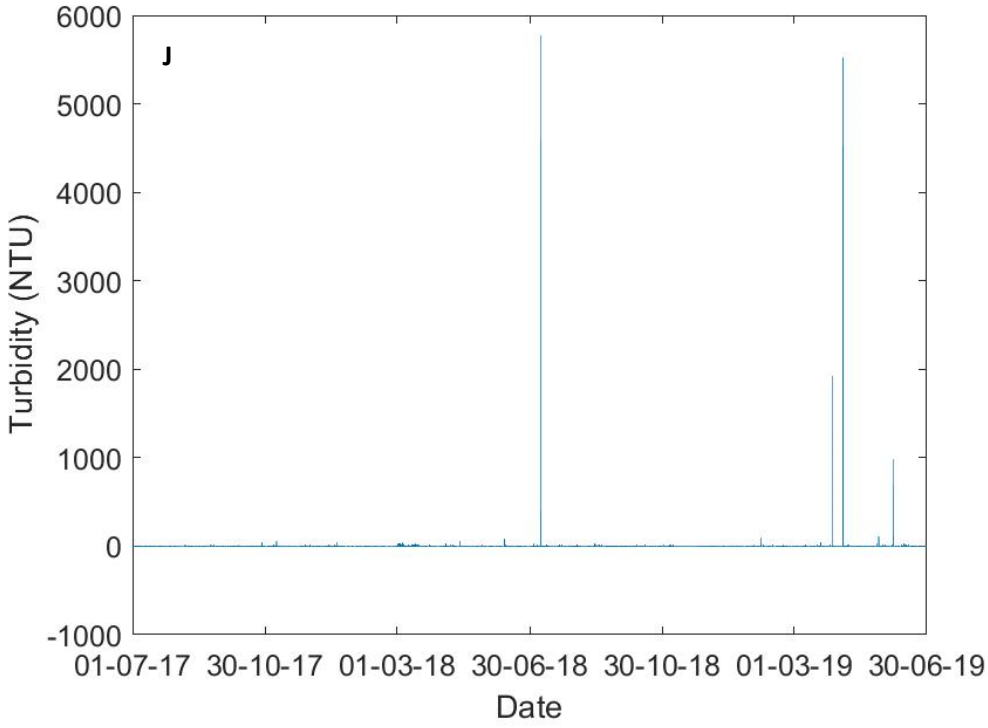

Annex 1: raw timeseries J) turbidity with unrealistic values

Annex 2

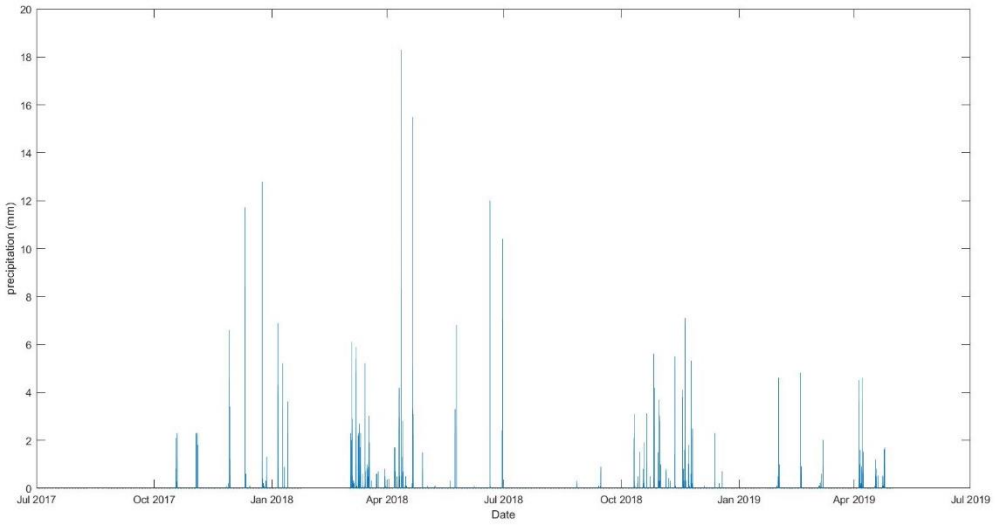

Annex 2: Precipitation along the period of study